(2)

# NAVAL POSTGRADUATE SCHOOL

## Monterey, California






# THESIS

INVESTIGATION OF SYSTEMATIC EFFECTS IN ATMOSPHERIC MICROTHERMAL PROBE DATA

by

Daniel S. Roper

December, 1992

Thesis Advisor: Donald L. Walters

# REPORT DOCUMENTATION PAGE

| | |
|---|---|
| 1a. REPORT SECURITY CLASSIFICATION<br>Unclassified | 1b. RESTRICTIVE MARKINGS |
| 2a. SECURITY CLASSIFICATION AUTHORITY | 3. DISTRIBUTION/AVAILABILITY OF REPORT<br>Approved for public release; distribution is unlimited. |
| 2b. DECLASSIFICATION/DOWNGRADING SCHEDULE | |
| 4. PERFORMING ORGANIZATION REPORT NUMBER(S) | 5. MONITORING ORGANIZATION REPORT NUMBER(S) |
| 6a. NAME OF PERFORMING ORGANIZATION<br>Naval Postgraduate School<br>6b. OFFICE SYMBOL (*If applicable*)<br>33 | 7a. NAME OF MONITORING ORGANIZATION<br>Naval Postgraduate School |
| 6c. ADDRESS (*City, State, and ZIP Code*)<br>Monterey, CA 93943-5000 | 7b. ADDRESS (*City, State, and ZIP Code*)<br>Monterey, CA 93943-5000 |
| 8a. NAME OF FUNDING/SPONSORING ORGANIZATION<br>8b. OFFICE SYMBOL (*If applicable*) | 9. PROCUREMENT INSTRUMENT IDENTIFICATION NUMBER |
| 8c. ADDRESS (*City, State, and ZIP Code*) | 10. SOURCE OF FUNDING NUMBERS<br>Program Element No. / Project No. / Task No. / Work Unit Accession Number |

11. TITLE (*Include Security Classification*)
INVESTIGATION OF SYSTEMATIC EFFECTS IN ATMOSPHERIC MICROTHERMAL PROBE DATA

12. PERSONAL AUTHOR(S) Daniel S. Roper

| 13a. TYPE OF REPORT | 13b. TIME COVERED | 14. DATE OF REPORT (*year, month, day*) | 15. PAGE COUNT |
|---|---|---|---|
| Master's Thesis | From To | December 1992 | 106 |

16. SUPPLEMENTARY NOTATION
The views expressed in this thesis are those of the author and do not reflect the official policy or position of the Department of Defense or the U.S. Government.

| 17. COSATI CODES | | | 18. SUBJECT TERMS (*continue on reverse if necessary and identify by block number*) |
|---|---|---|---|
| FIELD | GROUP | SUBGROUP | optical turbulence, diurnal variation, thermocouple response , microthermal probes, thermosonde, propagation |
| | | | |
| | | | |

19. ABSTRACT (*continue on reverse if necessary and identify by block number*)

The propagation of electromagnetic radiation through the atmosphere is a crucial aspect of laser target acquisition and surveillance systems and is vital to the effective implementation of some Theater Missile Defense systems. Atmospheric turbulence degrades the image or laser beam quality along an optical path. During the past decade, the U.S. Air Force's Geophysics Directorate of Phillips Laboratory collected high speed differential temperature measurements of the atmospheric temperature structure parameter, $C_T^2$, and the related index of refraction structure parameter , $C_n^2$. The stratospheric results show a 1-2 order of magnitude increase in day turbulence values compared to night. Resolving whether these results were real or an artifact of solar contamination is a critical Theater Missile Defense issue.

This thesis analyzed the thermosonde data from an experimental program conducted by the Geophysics Directorate in December 1990 and found strong evidence of solar induced artifacts in the daytime thermal probe data. In addition, this thesis performed a theoretical analysis of the thermal response versus altitude of fine wire probes being used in a new thermosonde system under development at the Naval Postgraduate School. Experimental wind tunnel measurements were conducted to validate the analytical predictions.

| 20. DISTRIBUTION/AVAILABILITY OF ABSTRACT | 21. ABSTRACT SECURITY CLASSIFICATION | |
|---|---|---|
| ☒ UNCLASSIFIED/UNLIMITED ☐ SAME AS REPORT ☐ OTIC USERS | Unclassified | |
| 22a. NAME OF RESPONSIBLE INDIVIDUAL<br>Donald L. Walters | 22b. TELEPHONE (*Include Area code*)<br>(408)-656-2267 | 22c. OFFICE SYMBOL<br>PH/We |

Approved for public release; distribution is unlimited.

Investigation of Systematic Effects in
Atmospheric Microthermal Probe Data

by

Daniel S. Roper
Captain, United States Army
B.S., United States Military Academy, 1982

Submitted in partial fulfillment
of the requirements for the degree of

MASTER OF SCIENCE IN PHYSICS

from the

NAVAL POSTGRADUATE SCHOOL
December 1992

Author: 

Daniel S. Roper

Approved by: 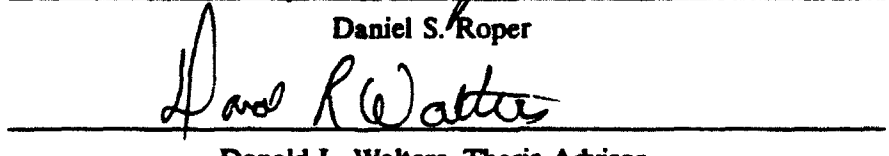

Donald L. Walters, Thesis Advisor

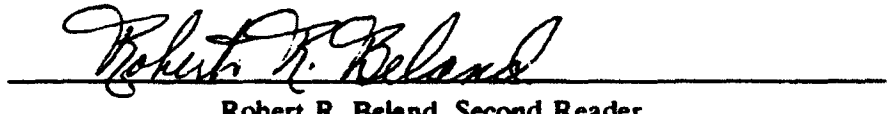

Robert R. Beland, Second Reader

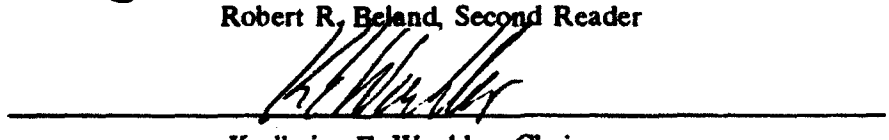

Karlheinz E. Woehler, Chairman
Department of Physics

## ABSTRACT

The propagation of electromagnetic radiation through the atmosphere is a crucial aspect of laser target acquisition and surveillance systems and is vital to the effective implementation of some Theater Missile Defense systems. Atmospheric turbulence degrades the image or laser beam quality along an optical path. During the past decade, the U.S. Air Force's Geophysics Directorate of Phillips Laboratory collected high speed differential temperature measurements of the atmospheric temperature structure parameter, $C_T^2$, and the related index of refraction structure parameter, $C_n^2$. The stratospheric results show a 1-2 order of magnitude increase in day turbulence values compared to night. Resolving whether these results were real or an artifact of solar contamination is a critical Theater Missile Defense issue.

This thesis analyzed the thermosonde data from an experimental program conducted by the Geophysics Directorate in December 1990 and found strong evidence of solar induced artifacts in the daytime thermal probe data. In addition, this thesis performed a theoretical analysis of the thermal response versus altitude of fine wire probes being used in a new thermosonde system under development at the Naval Postgraduate School. Experimental wind tunnel measurements were conducted to validate the analytical predictions.

## TABLE OF CONTENTS

# I. INTRODUCTION

The propagation of electromagnetic radiation through the atmosphere is a crucial aspect of many laser target acquisition and surveillance systems and is vital to the effective implementation of the Theater Missile Defense System (TMD). Turbulence degrades the quality of atmospheric propagation along the optical path of the radiation. Random fluctuations in the atmospheric index of refraction produce optical turbulence and distort the phase front of the beam [Ref. 1:p. 6-6]. The index of refraction structure parameter, $C_n^2$, which is a function of atmospheric wind shear, pressure, and temperature, quantifies optical turbulence. Nearly three decades of measurements show that $C_n^2$ varies both horizontally, vertically, and with time. What is not well-known is the fine-scale spatial distribution and the intensity of turbulence in the upper troposphere and the stratosphere. Atmospheric temperature fluctuations characterized by the temperature structure parameter, $C_T^2$, produce index of refraction variations by altering the air density. During the past decade, the U.S. Air Force Geophysics Directorate of Phillips Laboratory (PL/GP) has collected measurements of this quantity using balloon-borne, high-speed, differential temperature thermosondes [Ref. 2:p.30]. Recently, the Naval Postgraduate School (NPS) has used both fine thermistors as well as fine wire differential thermocouples to measure $C_T^2$ in both

day and night conditions [Ref. 3] and [Ref. 4]. The GP experiments have shown a 1-2 order of magnitude increase in day turbulence values compared to night. Attempts to explain this result have followed two lines of reasoning: 1) either there is a real increase in optical atmospheric turbulence in the day, or 2) the data (collected by two 3.8 $\mu$m platinum-coated tungsten wire probes for GP and 12.4 $\mu$m chromel-constantan thermocouples for the NPS Group) are unreliable in the day due to systematic effects such as the solar heating of the probes coupled with package rotation, pendulum motion, and probe vibration.[Ref. 2:p. 55]

This thesis investigated two systematic error effects in balloon thermosonde systems used by NPS and GP. This was accomplished in two phases. The first was to look for solar induced artifacts in the daytime thermal probe data. The second phase was to predict then measure the thermal probe response time of the NPS probes as a function of altitude. The initial phase of this investigation consisted of a statistical evaluation of a December 1990 experiment conducted by GP at Holloman Air Force Base, New Mexico, that focused on the cross-correlation of measurements taken from adjacent pairs of probes under day and night conditions. The second phase was an analytical development and measurement of the probe response time versus altitude, focusing on thermodynamic and fluid dynamic factors. These calculations were compared with wind tunnel measurements to validate and improve current probe response models. The underlying motivation of this investigation was to investigate

systematic error sources in critical atmospheric turbulence measurements needed for effective deployment of theater missile defense systems.

# II. BACKGROUND

## A. THEORY

Lasers emit radiation in a highly directional, collimated beam with a very low angle of divergence. The beam divergence angle $\theta$ can be "diffraction limited," i.e., limited by the wave characteristics of light. Under vacuum propagation conditions the divergence angle $\theta$ is

$$\theta \sim \frac{\lambda}{D}, \tag{1}$$

where $\lambda$ is the light wavelength and D is the diameter of the aperture. [Ref. 5:p. 21] Atmospheric turbulence degrades the spatial coherence of a beam of electromagnetic radiation. The Navier-Stokes equations govern the fine-scale random fluctuations of turbulent flow [Ref. 6:p. 262]. At high Reynolds numbers, $Re \sim 10^5$, the Navier-Stokes equations do not have unique solutions. Consequently we must use statistical models based on semi-empirical, dimensional analysis and physical reasoning. These focus on the mean flow properties of the fluid and on second order statistics of the fluctuations (correlations, spectra, and structure functions) [Ref. 7: p. 311]. A collimated laser beam initially propagates with a uniform wave front until it encounters a turbulent

medium (the atmosphere). Atmospheric temperature inhomogeneities cause random fluctuations in the atmospheric index of refraction, n, [Ref. 1:p. 6-6] which distort the phase of the wave. The result of this distortion on an initially collimated laser beam is to induce centroid wander, broadening, and break-up (in strong turbulence) which are caused by a general reduction in the spatial coherence of the original beam (Figure 1).

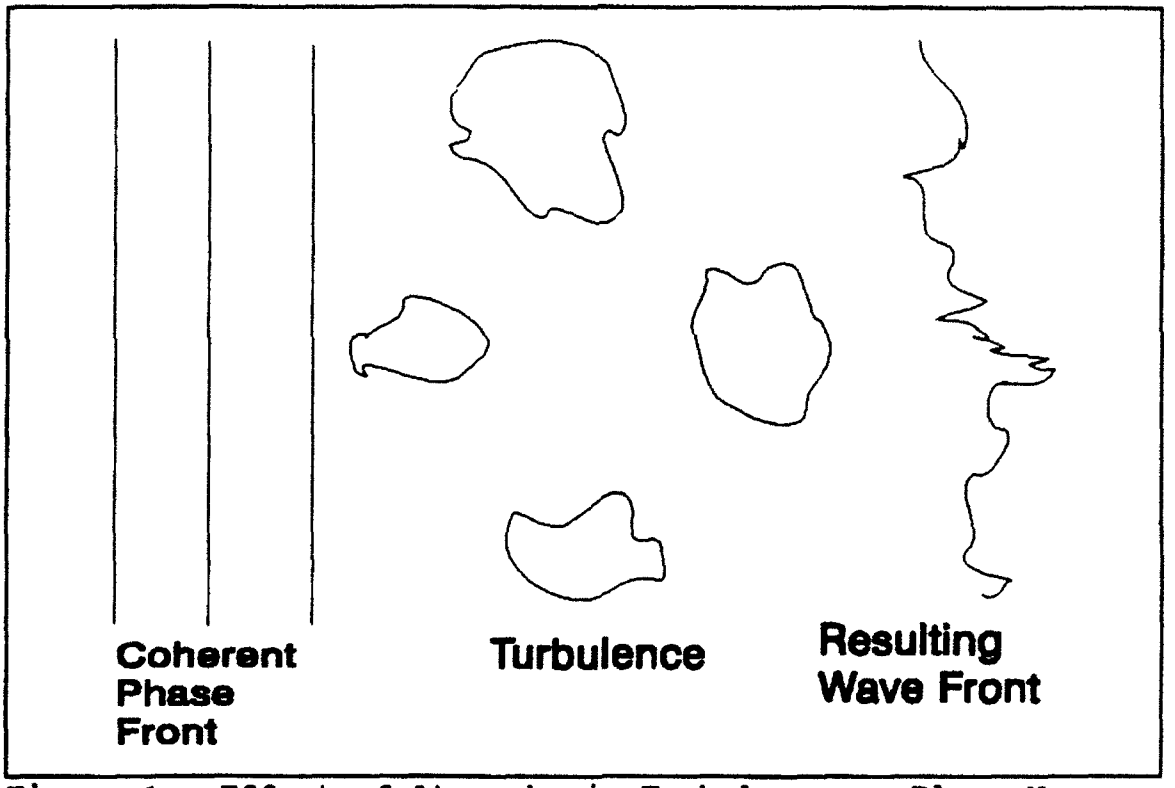


**Figure 1.** Effect of Atmospheric Turbulence on Plane Wave.

## B. STRUCTURE FUNCTIONS AND PARAMETERS

The mean square difference between two arbitrary measurements X such as temperature is defined as a structure function

$$D_x(\overline{r_1}, \overline{r_2}) = \langle (X(\overline{r_1}) - X(\overline{r_2}))^2 \rangle , \tag{2}$$

where $D_x$ depends on the separation distance [Ref. 8:p. 19]. If we assume homogeneous, isotropic turbulence, then Kolmogorov and Tatarski [Ref. 8:p. 46] have shown that

$$D_x = C_x^2 r^{2/3}, \tag{3}$$

where

$$r = |\overline{r}_1 - \overline{r}_2| = r_{12} . \tag{4}$$

This $r^{2/3}$ dependence depicts Kolmogorov turbulence represented by the structure parameter $C_x^2$.

The index of refraction structure parameter, $C_n^2$ describes the fluctuations in the index of refraction over a given distance. It is the mean-square statistical average of the difference in the index of refraction, *n*, between two points separated by a distance $r_{12}$ [Ref. 9:p. 397]

$$C_n^2 = \frac{\langle (n_1 - n_2)^2 \rangle}{r_{12}^{2/3}} . \tag{5}$$

Similarly, the temperature structure parameter, $C_T^2$ is

$$C_T^2 = \frac{\langle (T_1 - T_2)^2 \rangle}{r_{12}^{2/3}}, \tag{6}$$

where $T_1$ and $T_2$ are the ambient atmospheric temperatures measured along a horizontal path of length r. According to Kolmogorov, this relation is only valid in the inertial sub range described by $l_0 << r << L_0$, where $l_0$ and $L_0$ depend on the kinetic energy and boundary conditions. The inner scale, $l_0$, where energy dissipation by viscosity and diffusion takes place, is typically on the order of millimeters near the ground and perhaps centimeters in the troposphere. The outer scale, $L_0$, the largest scale of isotropy, is usually on the order of meters or 10s of meters [Ref. 1:p. 6-9] and depends on the boundary conditions.

The index of refraction, n, is a function of atmospheric pressure, humidity, temperature, and optical wavelength. We may neglect the effects of humidity in all but the most humid atmospheric environments and can disregard the wavelength dependence at optical wavelengths. For optical/IR wavelengths, a simplified form of this critical parameter is

$$n - 1 = 79 x 10^{-6} \frac{P}{T}, \tag{7}$$

where P is atmospheric pressure (millibars) and T is the atmospheric temperature (Kelvin) [Ref. 10:p. 232]. Taking the partial derivative of Eq. (7) and assuming isobaric turbulence, $C_n^2$ depends on $C_T^2$ by

$$C_n^2 = (79 \times 10^{-6} \frac{P}{T^2})^2 C_T^2 . \qquad (8)$$

The effects that turbulence produces on a laser beam are seen by measuring the amplitude or phase fluctuations of the final image at the target. A common measure of image quality is the Strehl ratio which is the relative intensity of the point spread function measured at the mean centroid location relative to an ideal, diffraction limited optical system. The Strehl ratio depends on the spatial coherence of the laser radiation after passing through the atmosphere which in turn depends on the atmospheric modulation transfer function. The atmospheric modulation transfer function (MTF) characterized by the transverse coherent path length, $r_0$, is a measure of the electric field transverse autocorrelation length, the distance over which the electromagnetic field remains coherent [Ref. 1:p. 6-29]. Fried showed that, for plane waves,

$$r_0 = 2.1 [1.46 k^2 \int_0^L C_n^2(z)\, dz]^{-3/5}, \qquad (9)$$

where k is the optical wave number ($2\pi/\lambda$) and L is the optical path length [Ref. 9:p. 397]. Typical values of $r_0$ range from centimeters in regions of high

turbulence, to tens of centimeters at good astronomical sites, to meters and perhaps larger in low turbulence regions.

## C. CURRENT APPLICATIONS

Some alternatives to the TMD scenario involve near horizontal atmospheric propagation at altitudes of 10-20 km. One initiative, the Airborne Laser Program (ABL), involves mounting a laser in an aircraft flown above the tropopause into the stratosphere to avoid clouds, sub-visual cirrus (ice crystals), and tropospheric turbulence [Ref. 11]. The upper altitude limit arises from aircraft altitude constraints although other platforms such as low orbit satellites are also being considered (space-based alternatives are subject to more restrictive political constraints). The lower altitude limit essentially is the bottom of the stratosphere. The reason for this is that beam propagation in the troposphere encounters higher turbulence, particularly near the jet stream, and has higher absorption and scattering from atmospheric aerosols, water vapor, ice crystals, and clouds.

With adequate phase information, adaptive optics can pre-distort the wavefront of the beam to correct for turbulence that is along the propagation path. This is necessary to achieve a 30 cm - 1.0 m diameter spot size on a target at a range of 400 km (0.8 $\mu$rad). The Airborne Laser Program needs an accurate assessment of the atmospheric turbulence along stratospheric optical paths to complete a systems analysis. This was the driving force for this investigation.

## D. PREVIOUS RESULTS

GP and NPS have conducted numerous experiments to measure the temperature structure parameter using balloon-borne thermosondes and single-point temperature probes. Thermosondes measure differential temperature fluctuations across a horizontal path, commonly one meter [Ref. 12:p. 14]. The mean square fluctuation in temperature between two 3.8 $\mu$m platinum-coated, tungsten probes separated by one meter gives a measurement of $C_T^2$ which, in turn, gives $C_n^2$ using Eq. (8) [Ref. 13:p. 2]. The NPS single-point temperature probes measure temperature using 100 $\mu$m thermistors along both the ascending and descending trajectories of the balloon.

Previous experiments and analyses have found a clear increase in the index of refraction structure parameter $C_n^2$ above ~8 km during daylight hours. In June 1990, GP conducted a series of thermosonde launches, in conjunction with NPS optical measurements. Figures 2 and 3 show plots of $C_n^2$ from both day and night launches. The raw data minima in Figure 2, a night flight, approach the sonde noise level (solid curve) for much of the flight. The raw data in the daytime flight (Figure 3), almost never approach the sonde noise level [Ref. 3:p. 55]. This anomaly has been characteristic of all day flights and is suspicious.

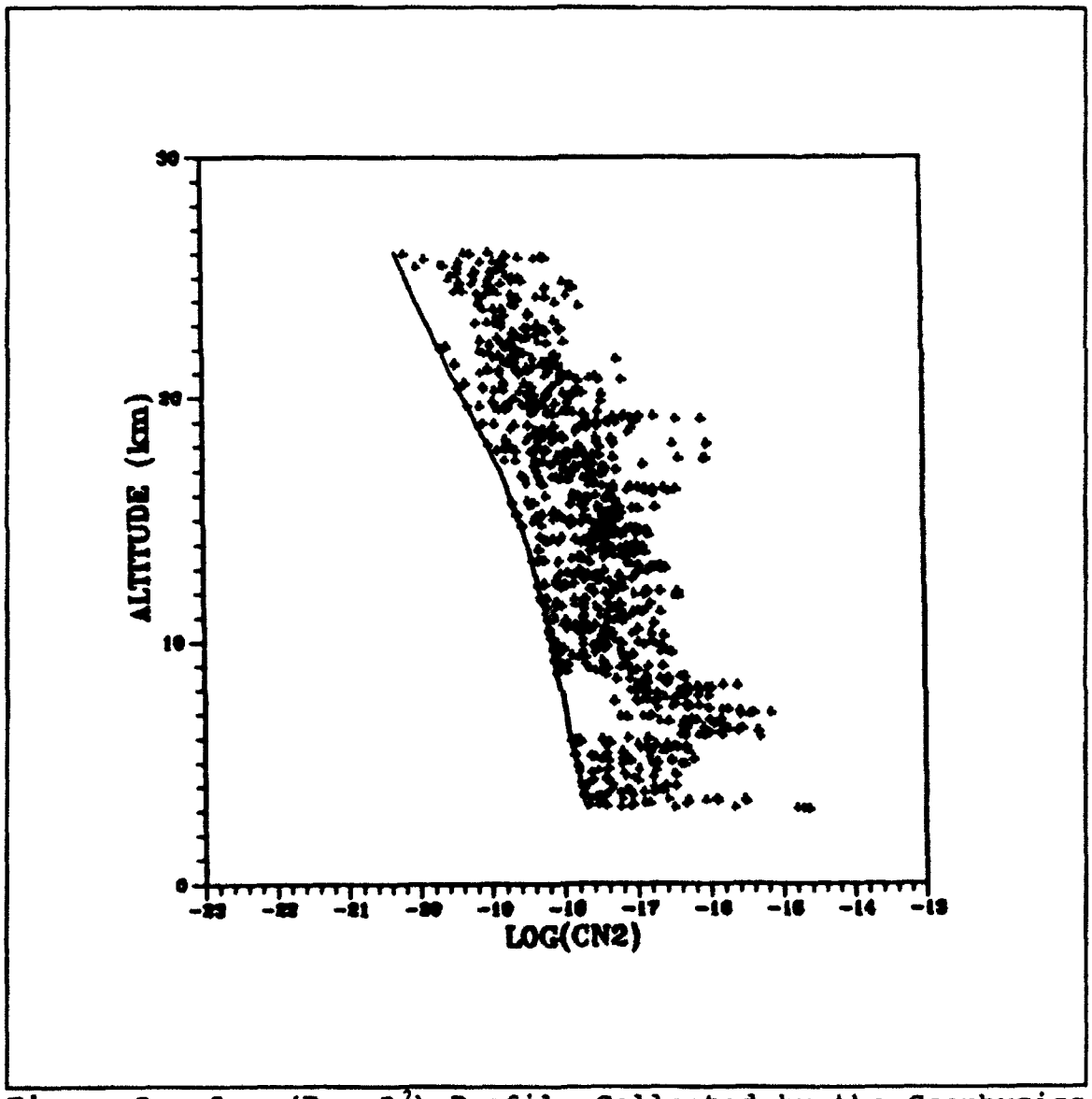


**Figure 2.** Log (Raw $C_n^2$) Profile Collected by the Geophysics Directorate on Maui, 2 June 1990 (Night) [Ref. 3:p. 55].

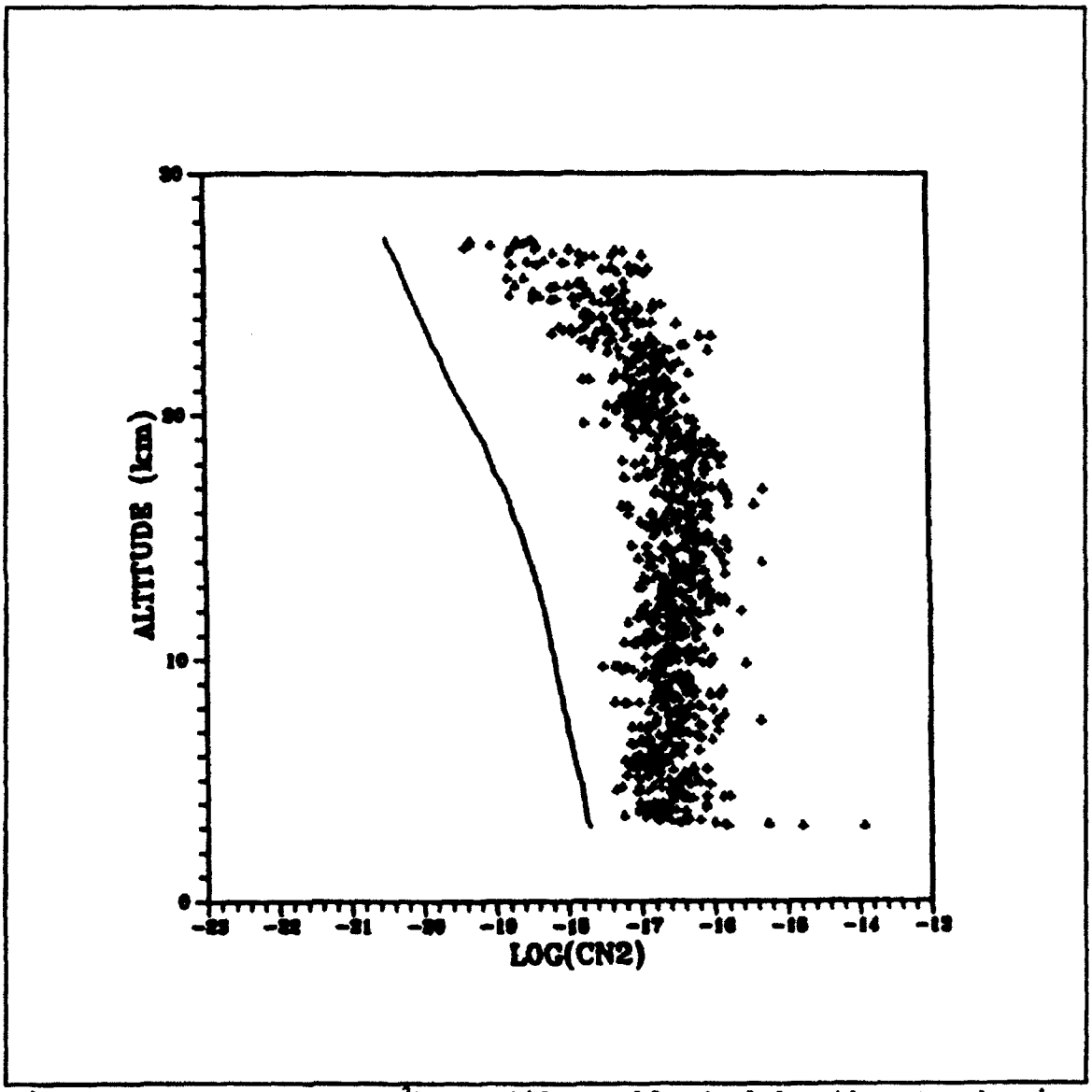


**Figure 3.** Log (Raw $C_n^2$) Profile Collected by the Geophysics Directorate on Maui, 3 June 1990 (Day) [Ref. 3:p.55].

GP and Sparta, Inc., published a scientific report in August 1990 addressing temperature perturbations from solar heating of thin layers of aerosol and ozone. They found that there was some evidence to support the postulate of temperature perturbations due to solar heating of ozone, although this could not be proven due to the low vertical resolution nature of $O_3$. GP concluded that it was not probable that variations in $C_T^2$ were due to perturbations in background stratospheric aerosols. [Ref. 13:p. 14] GP also investigated the possibility that solar radiation heating of the probe support wires caused instrumental effects but concluded that this was not responsible for the prevalent diurnal variation [Ref. 2:p. 55].

Previous work at NPS suggested that solar heating and probe wire vibrations, caused by the wind from the balloon's ascent coupled with the probe package's oscillating motion, produced an AC signal that seriously degraded the daytime data [Ref. 3]. An actual increase in daytime turbulence was extremely unlikely since the day-night change in turbulence occurred within minutes of sunrise or sunset. It is unlikely that this rapid onset and decay is a real phenomena because large-scale molecular diffusion of energy throughout the atmosphere should not be possible on such small time scales. Optical measurements collected in July of 1990 showed no indication of a change in isoplanatic angles between day and night whereas thermosonde results collected during the same period showed persistent day-night differences. Optical isoplanatic angles are sensitive to $C_n^2$ weighted by altitude $z^{5/3}$ [Ref. 3:p. 9].

Consequently, turbulence in the 5-15 km region has the dominant contribution. Weitekamp showed that simulated solar heating of a GP 3.8 $\mu$m tungsten probe in the laboratory produced a 0.1 to 0.2 C temperature increase. This was sufficient to account for the observed increase in the day $C_T^2$ values when coupled with probe vibration and sonde rotary and pendulum motion.

# III. DIURNAL VARIATION

## A. DIURNAL VARIATION EXPERIMENT 2

### 1. Purpose

The Geophysics Directorate group conducted a series of thermosonde launches from 4 to 9 December 1990 at Holloman Air Force Base, New Mexico, to study the diurnal variation in turbulence measurements of $C_n^2$. The purpose was to validate or disprove the existence of measurement artifacts that were responsible for the diurnal variations observed by both NPS and GP in previous experiments. [Ref. 14] These artifacts include:

1. Balloon thermal wake in combination with payload motion (pendulum and rotation).

2. Differential solar heating of the probes due to misalignment in combination with payload motion (pendulum and rotation).

3. Differential solar heating of the probes due to different wire geometry or emissivity/reflectivity in combination with payload motion (pendulum and rotation).

4. Differential solar heating of the probes due to probe wire oscillation, possibly exacerbated by payload motion (pendulum and rotation).

### 2. Experimental Procedure

The GP thermosonde system measured the temperature difference between two 3.8 $\mu$m platinum-coated tungsten wire probes exposed to the

ambient atmosphere. The probe wires were flexible s-shaped or u-shaped wires approximately 0.45 cm long connected to two probe supports. The probes formed elements of an AC Wheatstone bridge which measured the difference in resistance between them. High and low pass filters restricted the system bandwidth to the range .2 Hz to 1000 Hz at the -3dB level. The thermosonde passed the temperature difference $T_2$ - $T_1$ through a root mean square (RMS) module with a 4-second time constant to ground-based monitoring equipment every four seconds which logged the data and calculated $C_n^2$ [Ref. 12:p. 15]. The sondes ascended at an average rate of approximately 5 meters per second. An ascent to 30 km required approximately 95 minutes. Historically, a GP thermosonde launch consisted of a thermosonde package with a single pair of probes with a 1 m spacing connected to a VIZ MICROSONDE 1 telemetry package. The December 1990 launches were unique since they used two separate thermosonde packages strapped together with a single VIZ telemetry package. The two pairs of probes were arranged in 1 m differential pairs on a single 50 x 50 mm styrofoam boom, so that each sensor element was approximately 8 cm from the corresponding member of the other pair. There were two probe configurations for the experiment. On most flights, both pairs of probes were parallel. One flight had one pair of probes parallel and the second set perpendicular to each other.

## 3. Experimental Conditions

In all, five successful balloon launches occurred during December 1990. Four were day launches and one was a night launch. Local sunset occurred around 1653 hours. Difficulties in controlling the heavier dropsonde packages precluded any data taking during descent. Table I contains a summary of the individual sonde launches.

### *a. 4 December 1990*

Time of launch of DVE9465 was 1450 hours local and both sets of probes were parallel. The last good data were obtained at 29.03 km.

### *b. 5 December 1990*

The time of launch of DVE9460 was 1407 hours local on 5 December 1990 and both sets of probes were parallel. Good data were obtained up to 26.48 km.

### *c. 6 December 1990*

The time of launch of DVE9454 was 1330 hours local on 6 December 1990. Both sets of probes were oriented in a parallel fashion. The maximum altitude providing useful data was 20.5 km.

### *d. 7 December 1990*

The time of launch of DVE9448 was 1357 hours local on 7 December 1990. One set of probes was in a parallel configuration while the

second set was perpendicular. This was the only launch in which this was the case. The maximum altitude that provided useful data was 28.86 km.

e. ***8 December 1990***

DVE9462 was the only night launch. Time of launch was 1837 hours local. Both sets of probes were parallel. Good data were taken up to 30.02 km.

**TABLE I.** Diurnal Variation Experiment 2 Launch Summary, Conducted by the Geophysics Directorate at Holloman, Air Force Base, NM from 4-8 December 1990.

| DATE | 4DEC 90 | 5DEC 90 | 6DEC 90 | 7DEC 90 | 8DEC90 |
|---|---|---|---|---|---|
| FLIGHT | DVE9465 | DVF9460 | DVE9454 | DVE9448 | DVE9462 |
| TIME (Local) | 1450 | 1407 | 1330 | 1357 | 1837 |
| PROBES | par/par | par/par | par/par | par/perp | par/par |
| MAX ALT (km) | 29.03 | 26.48 | 20.5 | 28.86 | 30.02 |

## B. RESULTS AND ANALYSIS OF DIURNAL VARIATION EXPERIMENT 2

### 1. Data Reduction

The telemetry package continuously transmitted data, at four second intervals, to the ground-based monitoring equipment, resulting in data sets of approximately 1450 lines for a 90 minute flight. The data were a succession of independent 4 second, RMS temperature differences in the form

$$[<(T_2-T_1)^2>]^{1/2} \qquad (10)$$

Eq. (6), the temperature structure function equation, along with the temperature difference data and the r=1 m spacing of the probes gave a $C_T^2$ value for each altitude at which measurements were made, approximately every 20 m. Combining these data with measured pressure and temperature yielded $C_n^2$ values at each altitude.

### 2. Statistical Methodology

To determine if any measurement artifacts contaminated the data, we performed three statistical analyses of the data taken from the two pairs of probes. The first involved examining plots of the individual data points vs. altitude. This can reveal major inconsistencies. The second involved an examination of x-y cross-correlation plots between data from pairs of probes. The third involved computation of the correlation coefficient between probe pairs. The temperature differences measured at each successive altitude should have

a high correlation, since both sets of probes were essentially passing through the same air mass. If there were independent measurement artifacts, however; inconsistencies in the x-y cross-correlation plots and the correlation between data could possibly provide some insight as to the source of the error.

This thesis used the *Microsoft EXCEL* spreadsheet to compute the statistical correlation between both pairs of RMS temperature fluctuations. The correlation coefficient, *r*, was computed according to the standard statistical expression

$$r(CT_1, CT_2) = \frac{\sigma_{CT1,\,CT2}}{\sqrt{\sigma_{CT1}\sigma_{CT2}}}, \qquad (11)$$

where

$$\sigma_{C_{T_1},\,C_{T_2}} = \frac{1}{N}\sum (C_{T_1} - \overline{C_{T_1}})\,(C_{T_2} - \overline{C_{T_2}}), \qquad (12)$$

and CT1 was the RMS temperature difference for one pair of probes and CT2 was the difference for the second pair. Values of $r \sim 1$ indicate a high degree of correlation; values of $r \sim 0$ indicate little or no correlation.

For analyses, the 30 km data sets were divided into 5 km segments. We also computed a single r coefficient for each flight that contained all the data points. Applying Eq. (12) to each vertical 5 km region (or to the complete flight in the case of the total data set) gave the standard deviation needed in Eq. (11),

which in turn, yielded the correlation coefficient between each pair of measurements.

The measured noise level of the $C_T^2$ instrument packages was .002K. Consequently, $(\Delta T)_{rms}$ is undefined for values less than .002K [Ref. 12:p. 14]. All data taken that produced a reading of $\leq$.002K were discarded as being statistically invalid because it would not be possible to discriminate between the signal and the noise.

## 3. Results

### *a. Diurnal Variation*

Plots of Log (Raw $C_n^2$) vs. altitude show the typical order of magnitude increase in optical turbulence in the day compared to night in the 10-20 km region. Figures 4 and 5 of the 7 December flight represent a daytime flight and are also the only plots obtained using the parallel/perpendicular configuration (Appendix A contains the other daytime plots). Figures 6 and 7 show the data taken by the two sets of probes on the 8 December night flight.

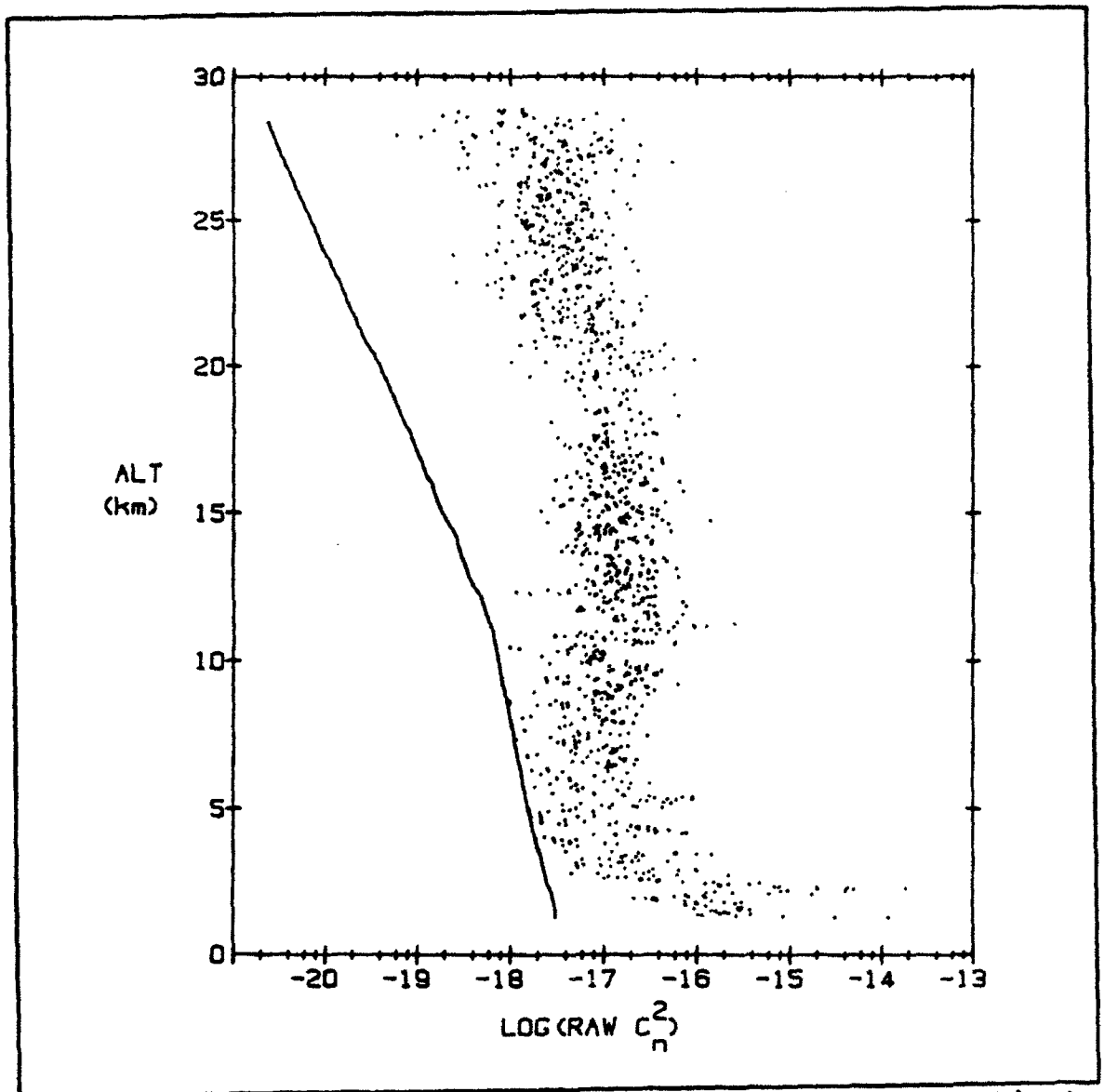


**Figure 4.** Log (Raw $C_n^2$) vs. Altitude Profile (Daytime), Collected by the Geophysics Directorate, from 1.2 to 30 km, Holloman Air Force Base, NM, 7 December 1990 (Probe Set 1).

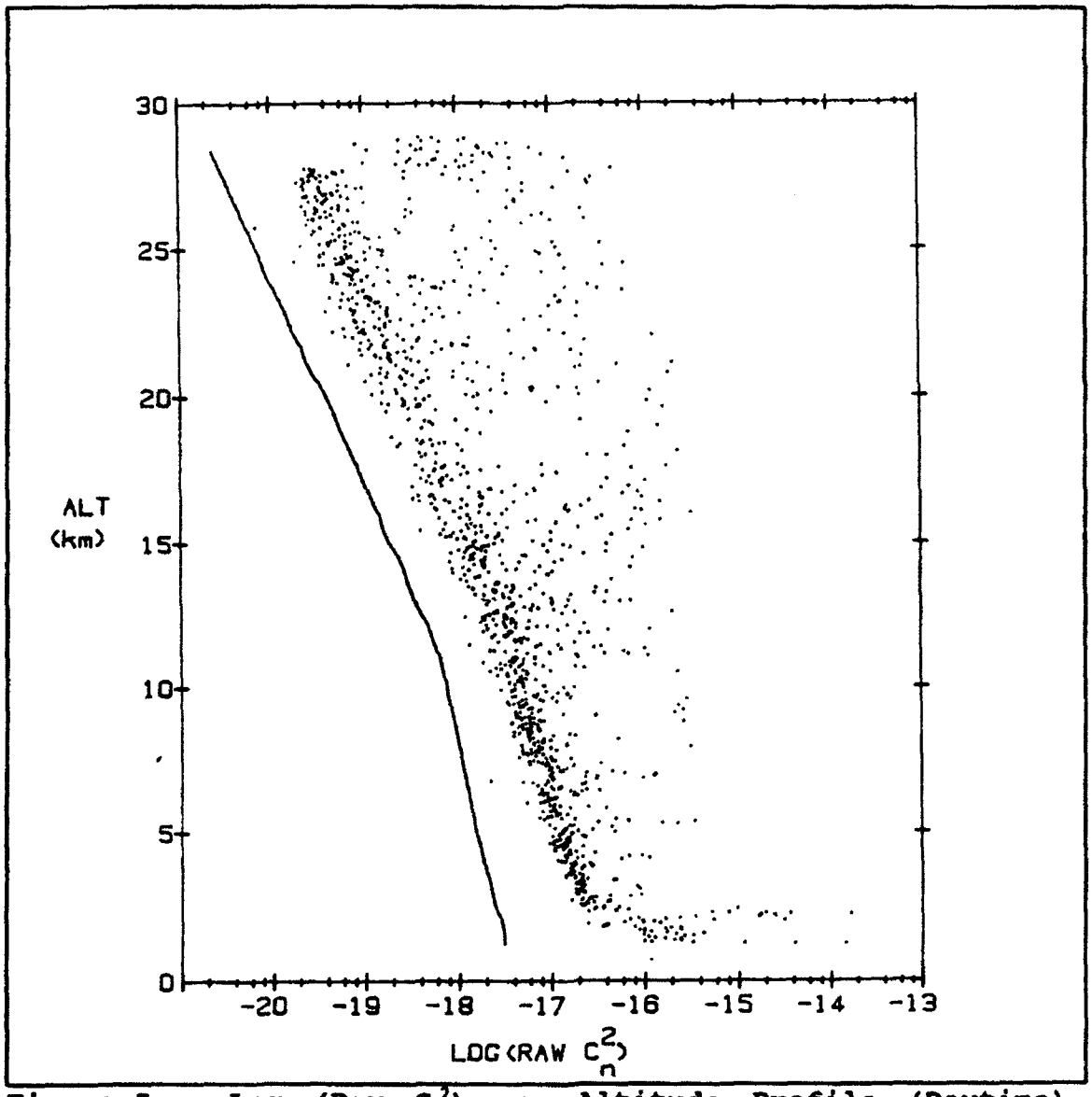


**Figure 5.** Log (Raw $C_n^2$) vs. Altitude Profile (Daytime), Collected by the Geophysics Directorate, from 1.2 to 30 km, Holloman Air Force Base, NM, 7 December 1990 (Probe Set 2).

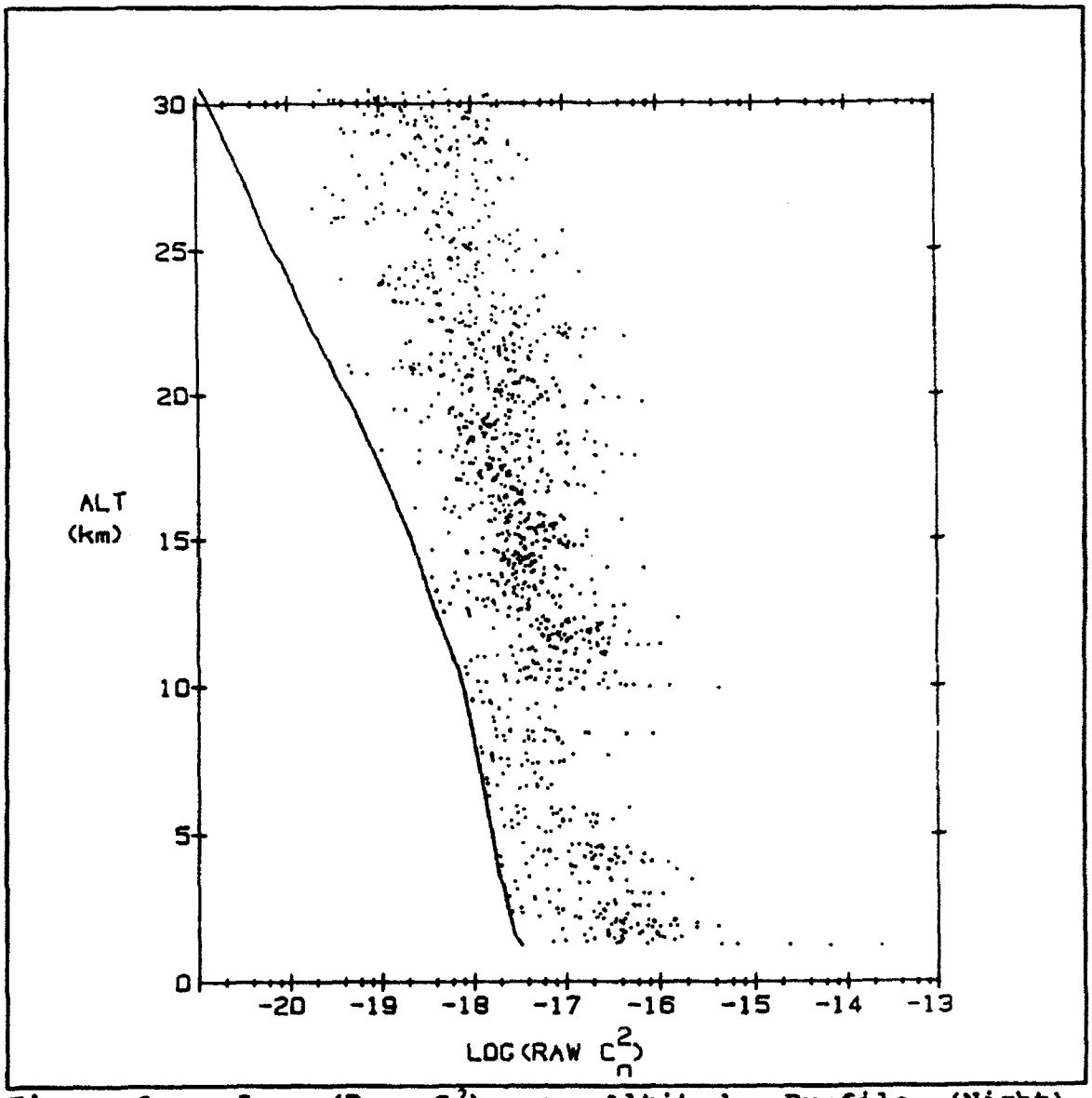


**Figure 6.** Log (Raw $C_n^2$) vs. Altitude Profile (Night), Collected by the Geophysics Directorate, from 1.2 to 30 km, Holloman Air Force Base, NM, 8 December 1990 (Probe Set 1).

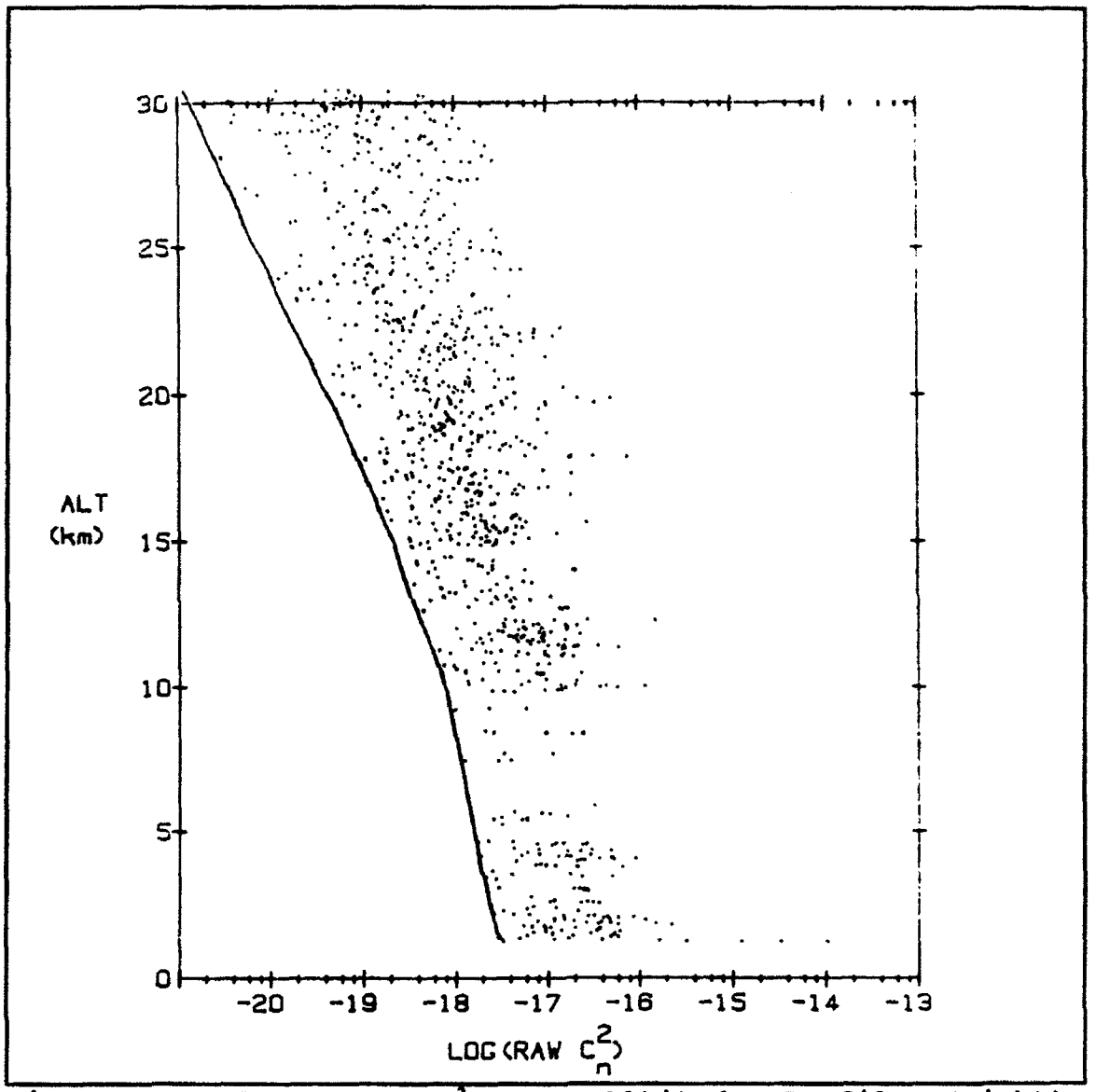


**Figure 7. Log (Raw $C_n^2$) vs. Altitude Profile (Night), Collected by the Geophysics Directorate, from 1.2 to 30 km, Holloman Air Force Base, NM, 8 December 1990 (Probe Set 2).**

### *b. 7 December 1990*

On 7 December 1990, a day flight with both parallel and perpendicular probe configurations, the two different sets of probes behaved differently. The set of parallel probes exhibited a trend common to the other day flights. At low altitudes, up to approximately 8-12 km, some of the data points closely approached the baseline temperature-pressure curve. As the probe continued to ascend, the log (Raw $C_n^2$) values increased and moved away from the system noise level curve by an order of magnitude (Figure 4). The perpendicular set of probes exhibited enhanced differences. These log (Raw $C_n^2$) values consistently were an order of magnitude higher than the noise level throughout the entire flight (Figure 5). This indicates that there was a constant source of error, or contamination, throughout the entire flight.

Figures 8 thru 11 show the x-y correlation between the two values (CT1 and CT2) measured at each altitude. These figures show the effect of noise or some constant signal with a value of approximately 0.006 K that affects the data in channel 2. Examination of 10 km increments of the atmosphere reveals that this signal first became apparent between 10-20 km (Figure 10) and became very pronounced at 20-30 km (Figure 11). The dense spike in the data at CT1 $\approx$ 0.006 K illustrates this effect.

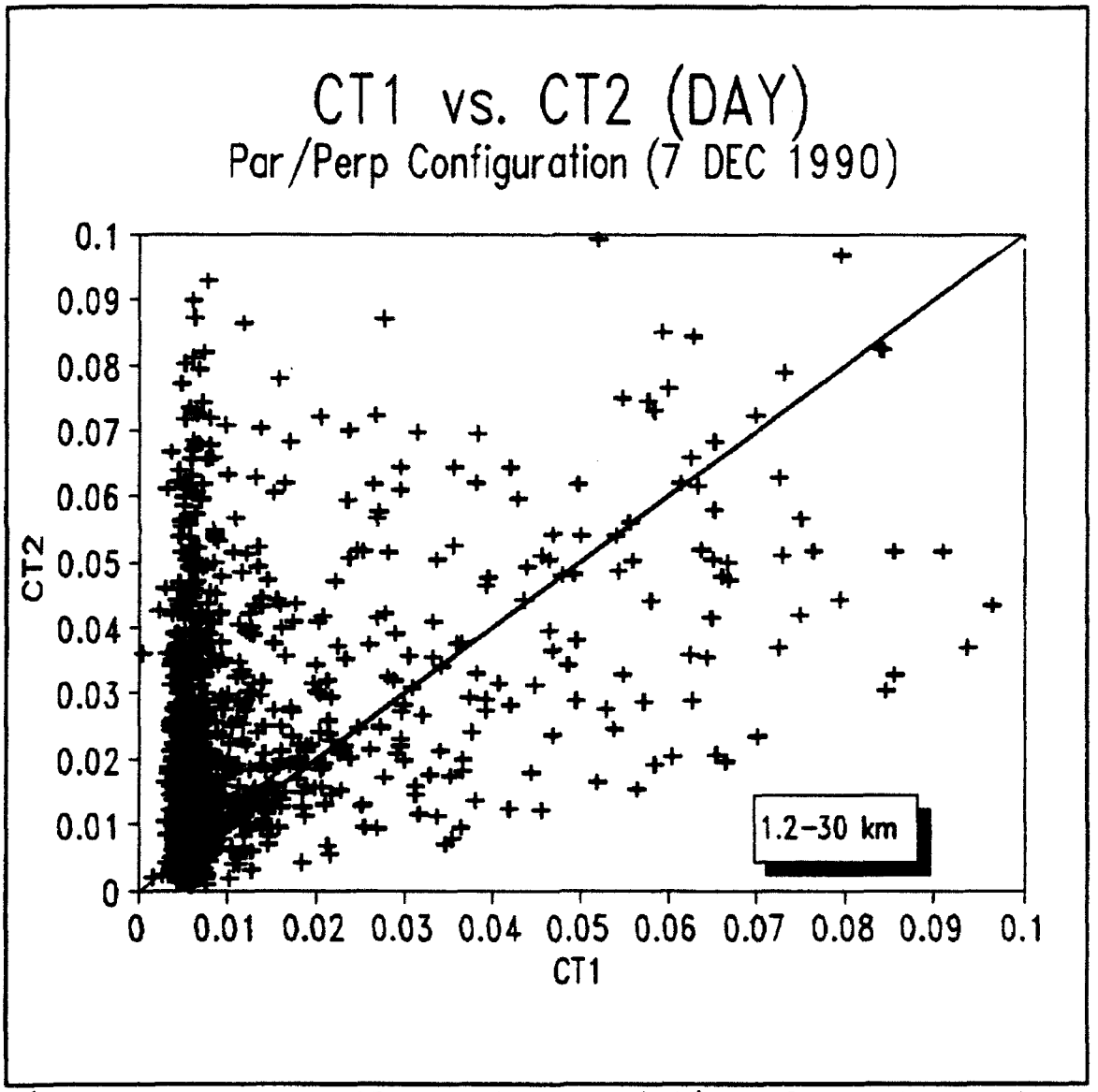


**Figure 8.** CT1 vs. CT2 (Day), Correlation of RMS Temperature Fluctuations Between Two Pairs of Probes (Parallel/Perpendicular Configuration) Collected Between 1.2 and 30 km, Holloman Air Force Base, NM, 7 December 1990.

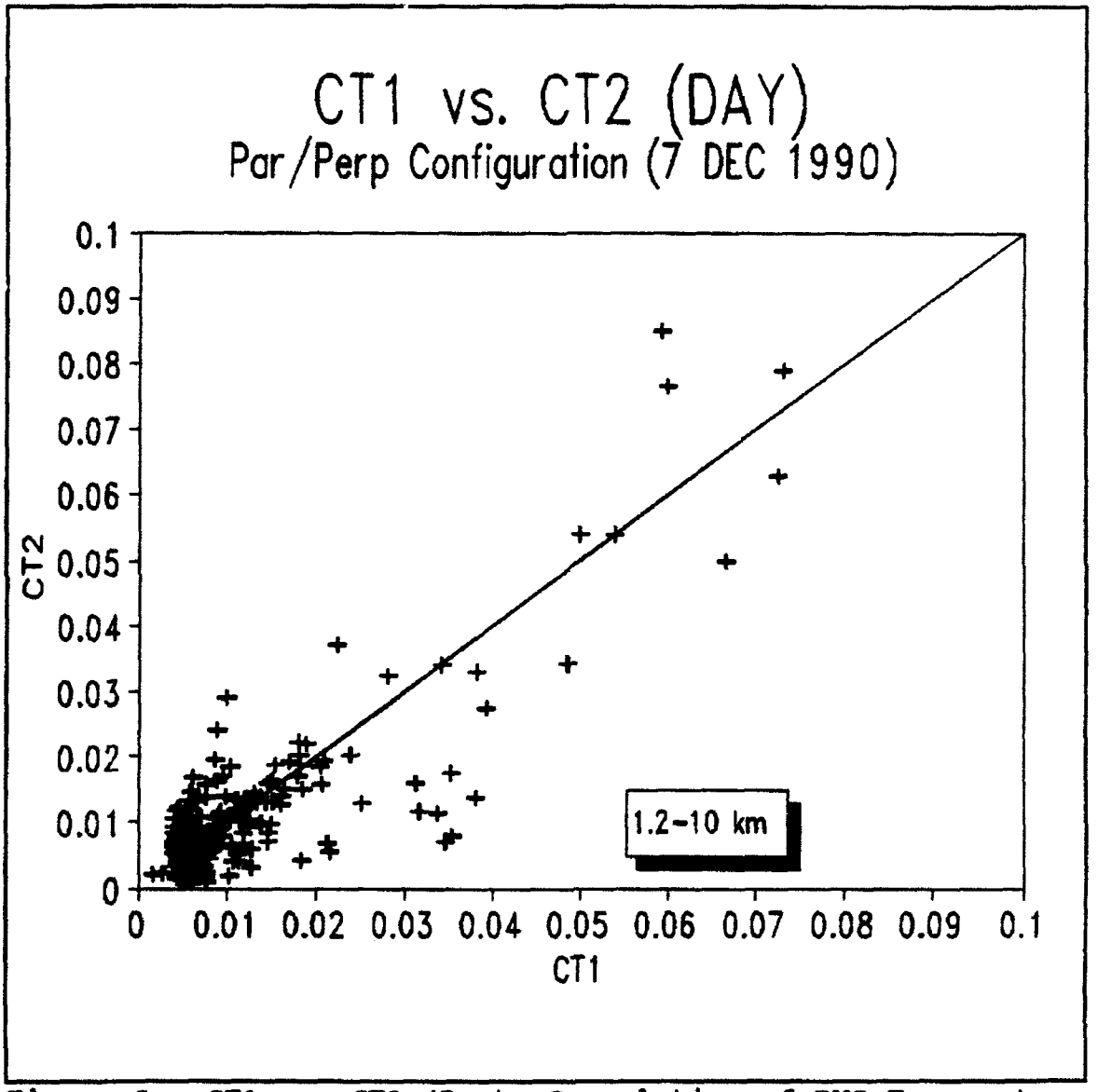


**Figure 9.** CT1 vs. CT2 (Day), Correlation of RMS Temperature Fluctuations Between Two Pairs of Probes (Parallel/Perpendicular Configuration) Collected Between 1.2 and 10 km, Holloman Air Force Base, NM, 7 December 1990.

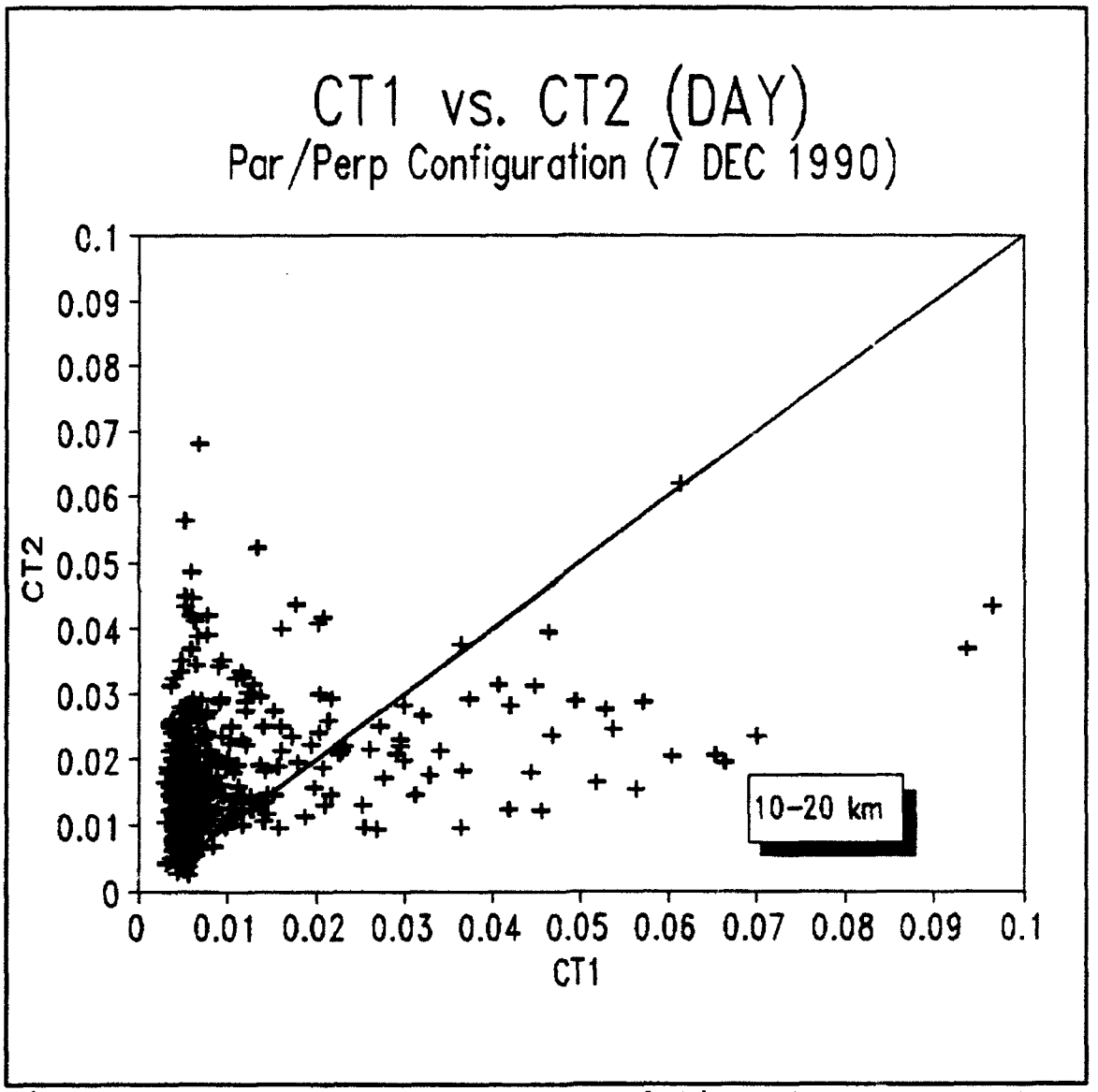


**Figure 10.** CT1 vs. CT2 (Day), Correlation of RMS Temperature Fluctuations Between Two Pairs of Probes (Parallel/Perpendicular Configuration) Collected Between 10 and 20 km, Holloman Air Force Base, NM, 7 December 1990.

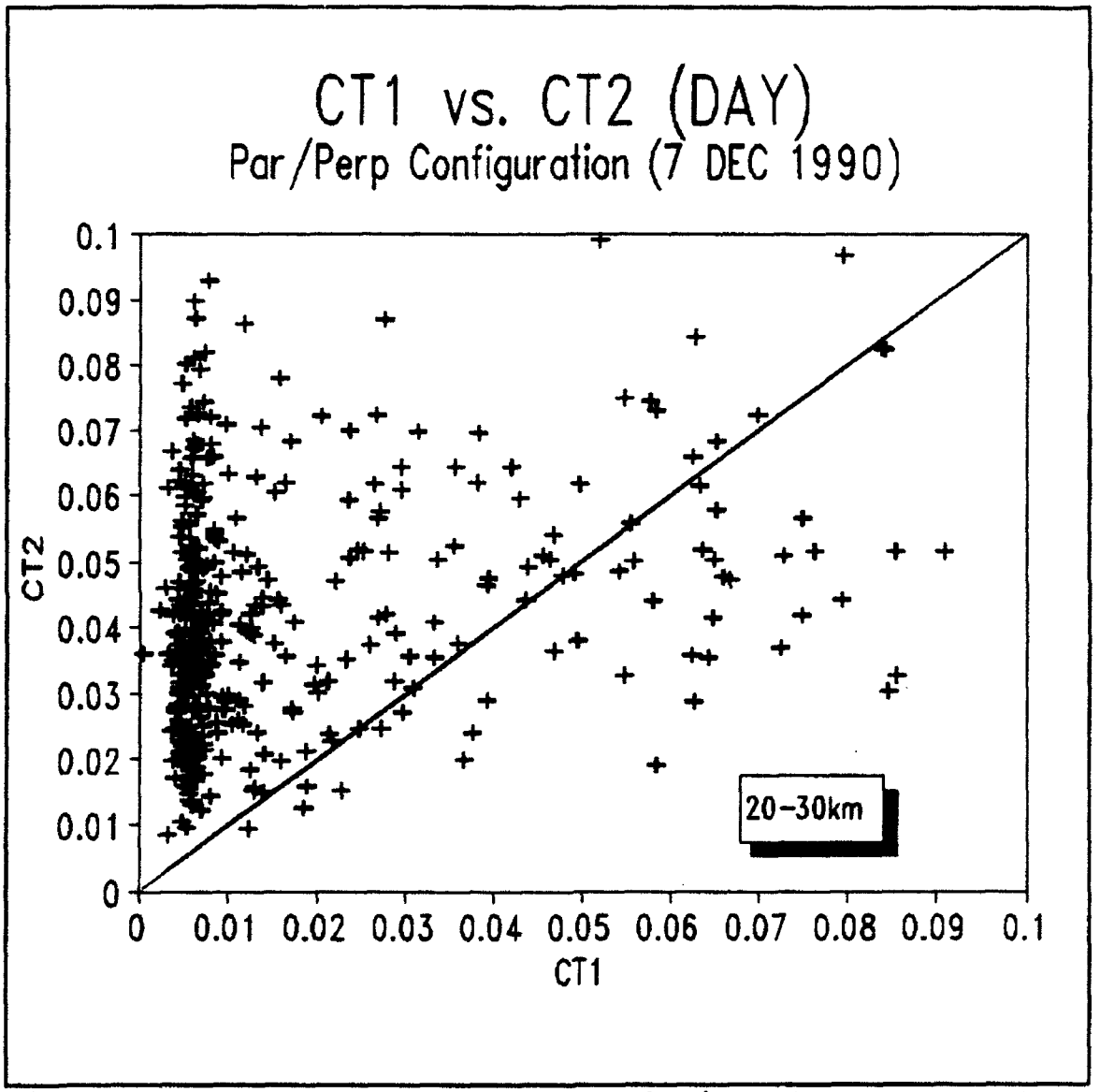


**Figure 11.** CT1 vs. CT2 (Day), Correlation of RMS Temperature Fluctuations Between Two Pairs of Probes (Parallel/Perpendicular Configuration) Collected Between 20 and 30 km, Holloman Air Force Base, NM, 7 December 1990.

The correlation coefficient for the entire flight was 50%, the lowest of the five successful flights. Table II shows that r was high, 96%, in the first 5 km interval and was below 50% for the rest of the flight.

**Table II.** CT1 vs. CT2 Correlation for 7 December 1990 Daytime Launch with Parallel/Perpendicular Probe Configuration at Holloman Air Force Base, NM.

| ALTITUDE (km) | CORRELATION, r | Data points |
|---|---|---|
| 1.2-5 | .96 | 155 |
| 5-10 | .42 | 220 |
| 10-15 | .32 | 252 |
| 15-20 | .27 | 174 |
| 20-25 | .34 | 240 |
| 25-30 | .40 | 176 |
| TOTAL | .50 | 1217 |

### *c. 8 December 1990*

The plots of log (Raw $C_n^2$) values for the 8 December 1990 flight followed the characteristic nighttime behavior. Some of the data consistently approached the noise level up to approximately 15-20 km, at which point they showed a slight shift to the higher values. Figures 6 and 7 show these results.

Figures 12 thru 15 plot the CT1 vs. CT2 correlation vs. altitude. These figures show the effect of a small but relatively constant offset. The CT2 values are consistently greater than the CT1 values. This could not occur without a signal, instrument, or calibration error since the probes passed through essentially the same air mass up to 30 km and took 893 independent measurements. Table III shows that the correlation coefficient was high in all intervals with the exception of the 5-10 km region which had an insufficient number of data points above the noise.

**TABLE III.** CT1 vs. CT2 Correlation for Geophysics Directorate 8 December 1990 Night Launch with Dual-Parallel Probe Configuration at Holloman Air Force Base, NM.

| ALTITUDE (km) | CORRELATION, r | Data Points |
|---|---|---|
| 1.2-5 | .98 | 115 |
| 5-10 | .58 | 29 * |
| 10-15 | .90 | 161 |
| 15-20 | .92 | 240 |
| 20-25 | .86 | 199 |
| 25-30 | .86 | 148 |
| TOTAL | .91 | 893 |

* statistically insufficient

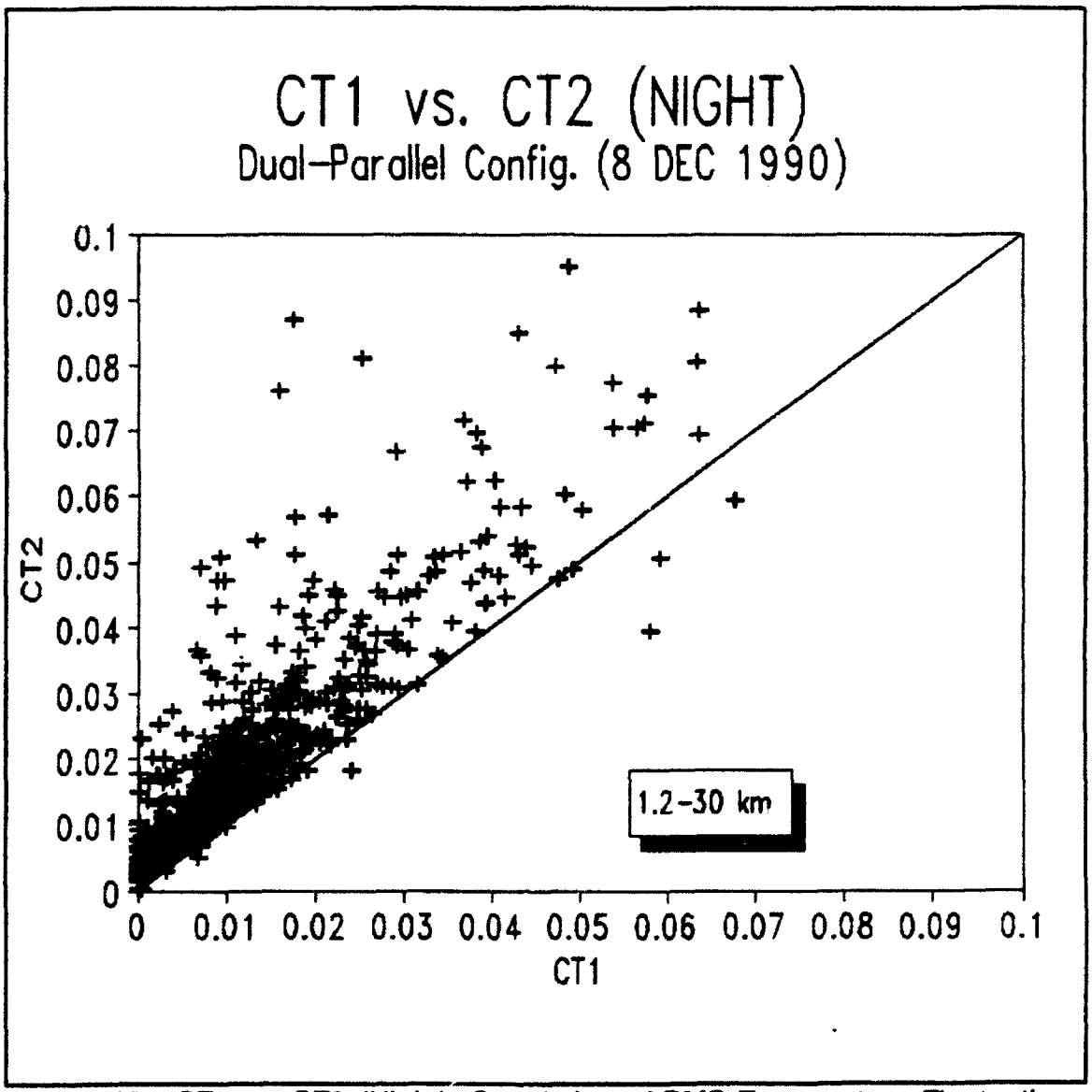


**Figure 12.** CT1 vs. CT2 (Night), Correlation of RMS Temperature Fluctuations Between Two Pairs of Probes (Dual-Parallel Configuration) Collected Between 1.2 and 30 km, Holloman Air Force Base, NM, 8 December 1990.

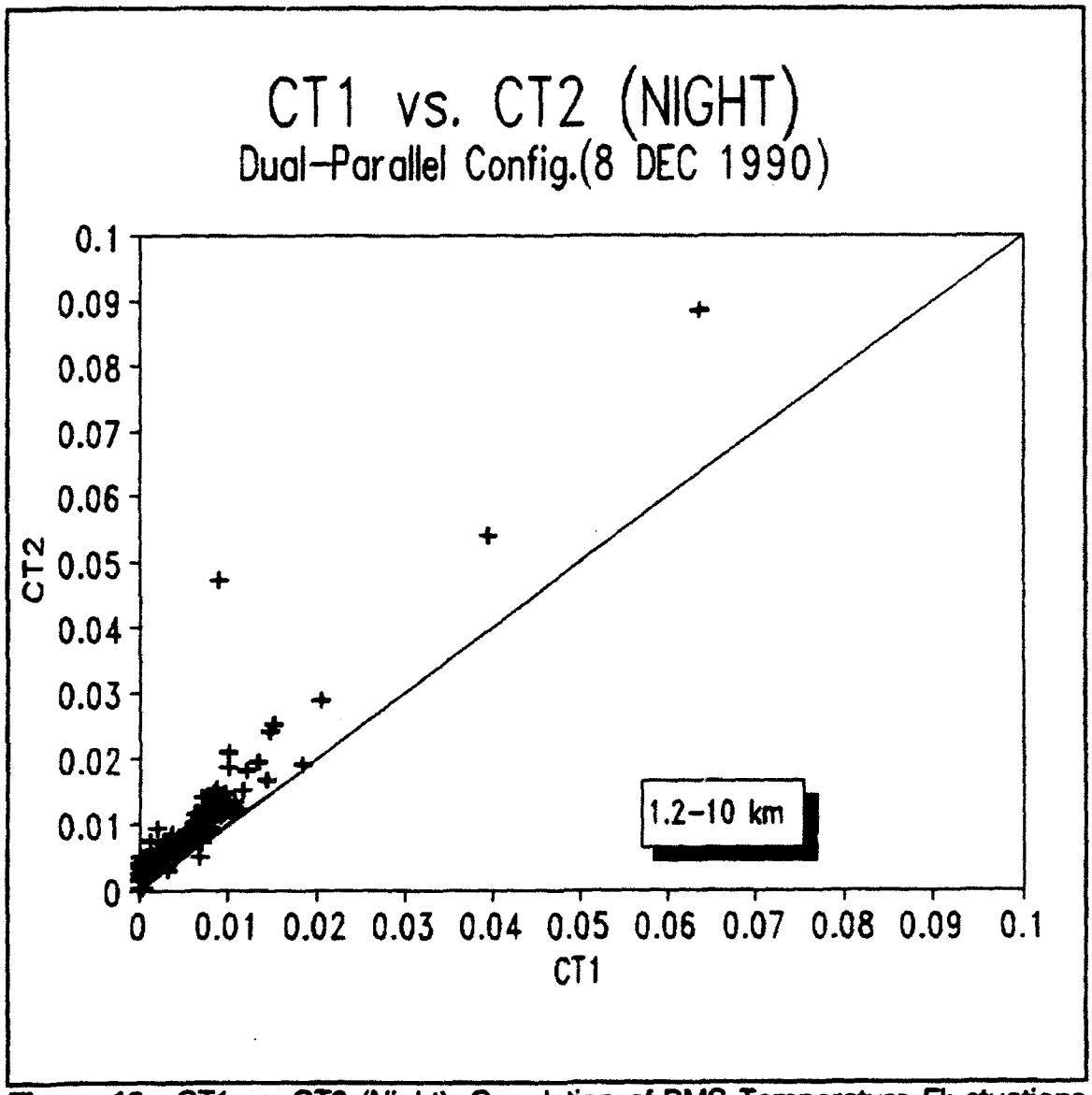


**Figure 13.** CT1 vs. CT2 (Night), Correlation of RMS Temperature Fluctuations Between Two Pairs of Probes (Dual-Parallel Configuration) Collected Between 1.2 and 10 km, Holloman Air Force Base, NM, 8 December 1990.

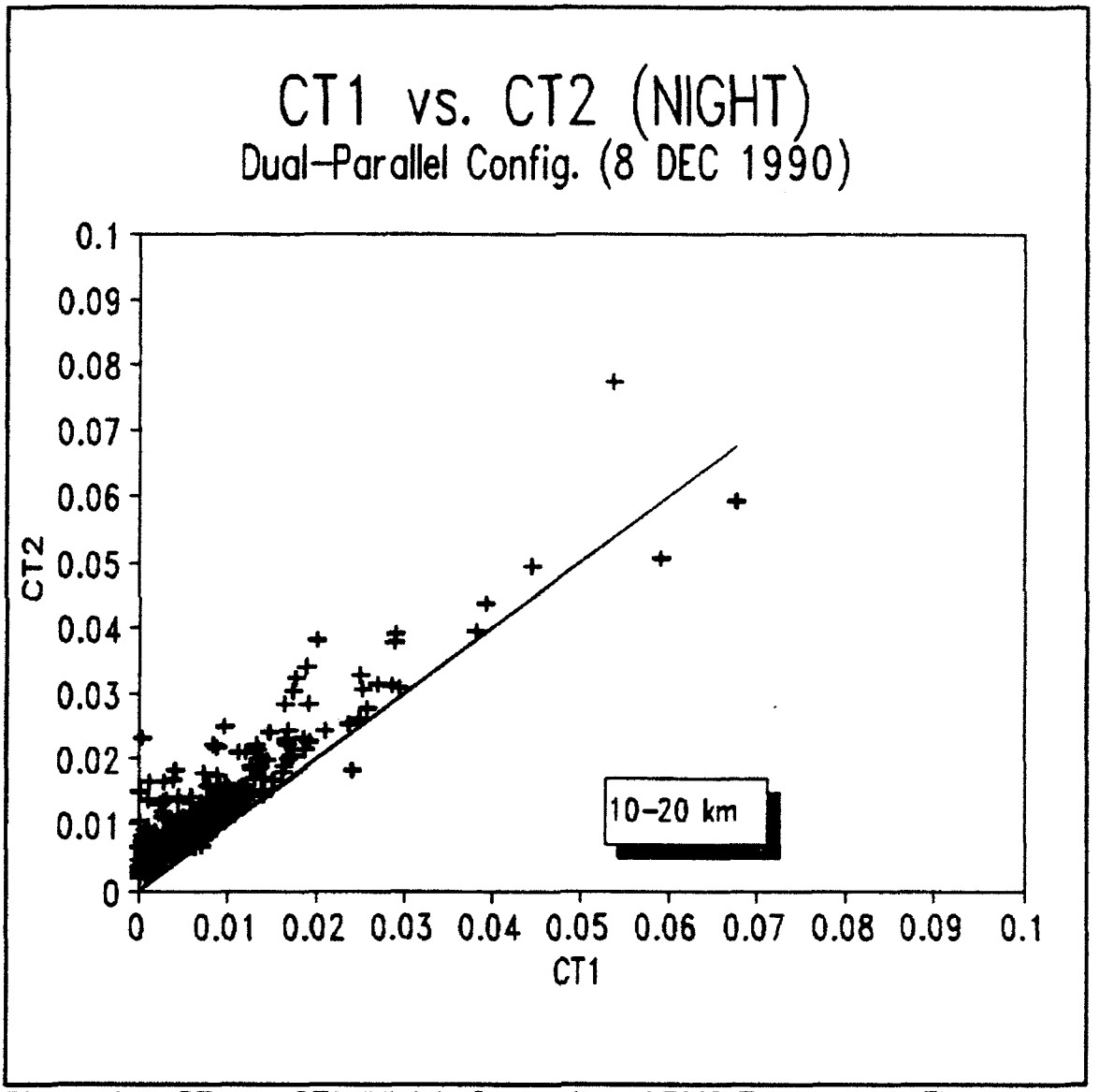


**Figure 14.** CT1 vs. CT2 (Night), Correlation of RMS Temperature Fluctuations Between Two Pairs of Probes (Dual-Parallel Configuration) Collected Between 10 and 20 km, Holloman Air Force Base, NM, 8 December 1990.

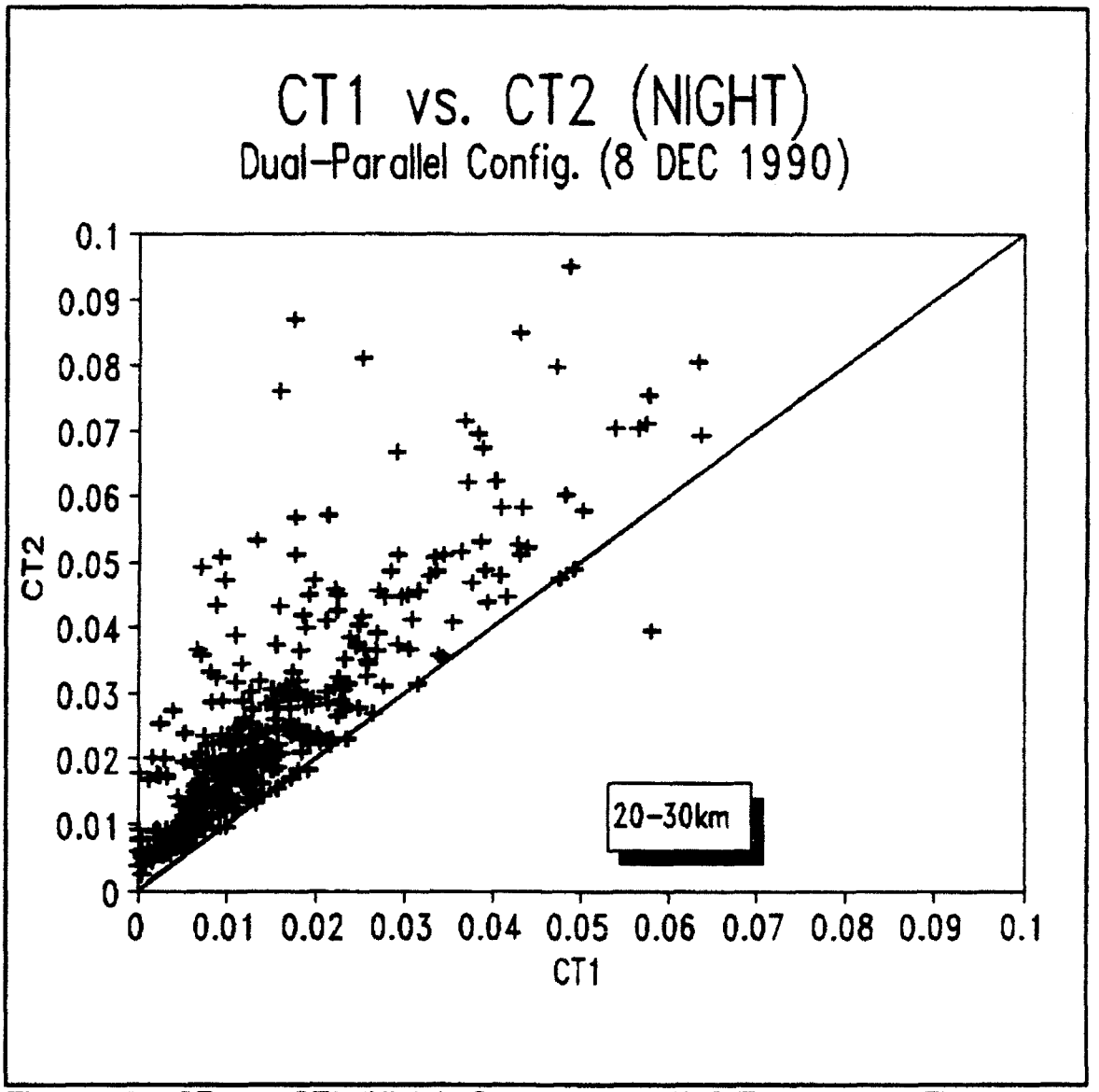


**Figure 15.** CT1 vs. CT2 (Night), Correlation of RMS Temperature Fluctuations Between Two Pairs of Probes (Dual-Parallel Configuration) Collected Between 20 and 30 km, Holloman Air Force Base, NM, 8 December 1990.

The plots of the 4, 5, and 6 December flights followed the typical daytime trend and are in Appendix A. The data collection during the descent phase of the experiment was not successful due to difficulties in using the heavier than standard package.

## 4. Analysis

The high degree of correlation of all flights in the 1-5 km region is due in part to the turbulent boundary layer which produces high $C_n^2$ in the daytime. Following Weitekamp, solar induced temperature differences due to insolation are smallest at ground level and are the largest at the tropopause when the probe is at a temperature of approximately 200 K. During the day, solar energy raises the probe surface temperature above the ambient air temperature. This difference increases as the probe's temperature declines. This increase mimics turbulent fluctuations when it varies rapidly with time. At night, however, the surface temperature drops below that of the air as it cools by radiation. The decrease in correlation in the 5-10 km region appears to be the result of the decline in the boundary layer contribution coupled with the increase in the solar induced probe-atmosphere temperature differences.

The only flight with the parallel/perpendicular configuration of the two sets of probes, launched on 7 December, had by far the lowest correlation (total average *r* of 50 %). This indicates that the probe orientation with respect to the sun influenced the differences in the measured temperatures [Ref. 3]. The motion of the ascending sonde package continuously changed the orientation,

and hence the projected surface area, of the probes with respect to the incident solar radiation resulting in uneven thermodynamic heating and cooling of the probes [Ref. 3:p. 33]. The results of the 7 December 1990 flight further support his findings.

The most significant results occurred in the region of most pressing interest, namely 10 to 20 km. The nighttime data correlation was approximately 91 %, markedly higher than any of the daytime data (Figures 10 and 14). This indicated that solar contamination of the daytime data is a real effect.

The 4 December 1990 flight had very low correlation in the 15 km to 25 km region; much lower than even the 7 December flight (see Table IV). This could have been due to instrument error, calibration, or perhaps the probes actually measured an increase in turbulence. Some sort of instrument malfunction was most likely the case. The fact that the correlation of this flight jumped to 77% from 25 km to 30 km, compared to 16% in the 20 to 25 km altitude region indicates a systematic error. This marked increase was the most dramatic data discontinuity between any altitude regions in any of the five flights in Diurnal Variation Experiment 2 and should be considered skeptically prior to making any inferences from it.

Figure 16 is a plot of the results of the correlation analysis of each flight. Table IV summarizes the data for the 4, 5, and 6 December flights.

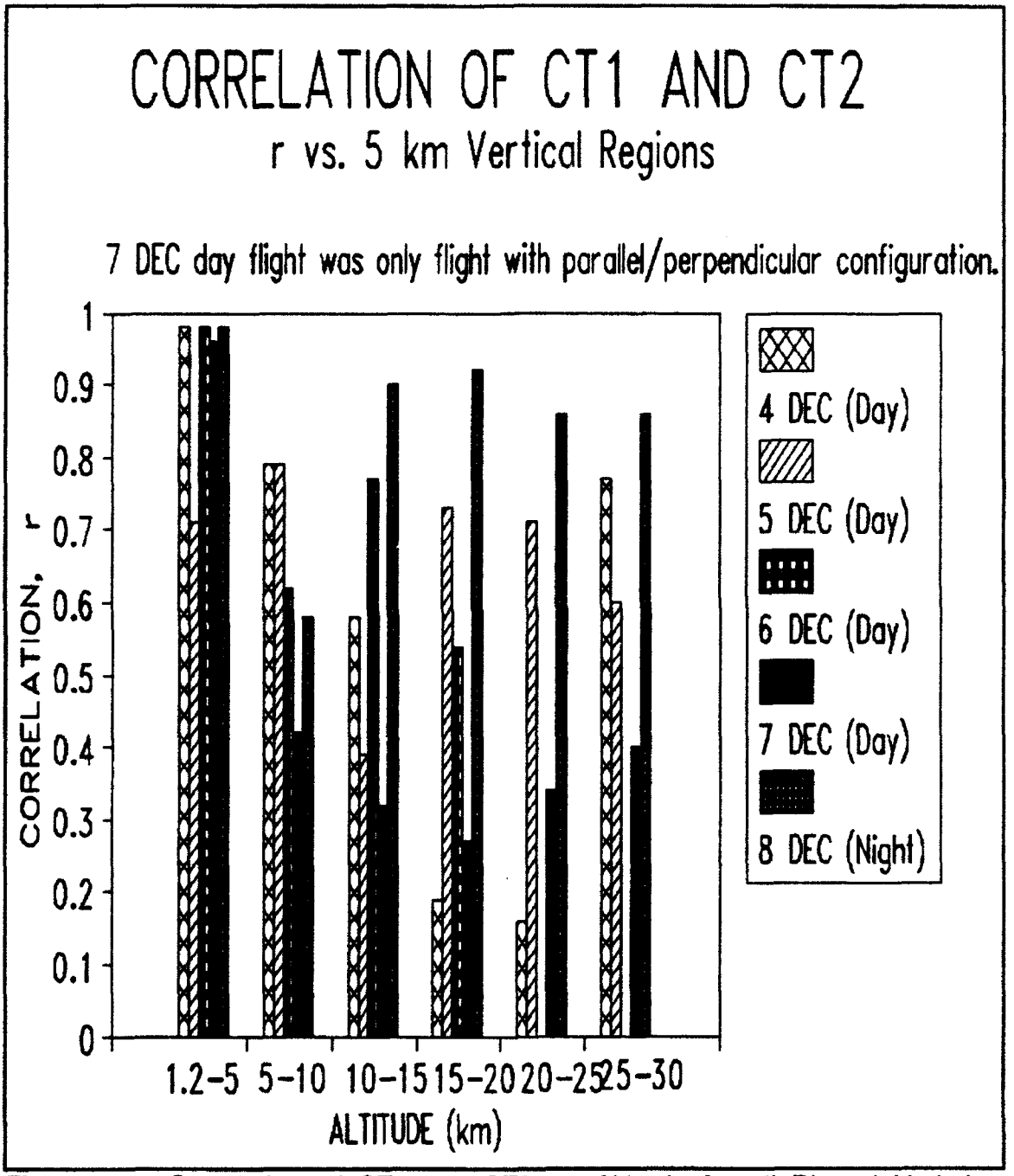


**Figure 16.** Correlation of CT1 and CT2 vs. Altitude for all Diurnal Variation Experiment Flights Conducted by the Geophysics Directorate at Holloman, Air Force Base, NM, from 4-8 December 1990.

**TABLE IV.** CT1 and CT2 Correlation vs. Altitude for Probe Pairs for Remaining Flights in Diurnal Variation Experiment 2.

| DATE | ALT (km) | CORRELATION (r) | # of POINTS |
|---|---|---|---|
| **4 DEC 90** | 1.2-5 | .98 | 148 |
| | 5-10 | .79 | 52 |
| | 10-15 | .58 | 262 |
| | 15-20 | .19 | 241 |
| | 20-25 | .16 | 229 |
| | 25-30 | .77 | 165 |
| | **TOTAL** | **.63** | **1285** |
| | | | |
| **5 DEC 90** | 1.2-5 | .71 | 11 |
| | 5-10 | .79 | 52 |
| | 10-15 | .39 | 155 |
| | 15-20 | .73 | 154 |
| | 20-25 | .71 | 107 |
| | 25-30 | .60 | 9 |
| | **TOTAL** | **.82** | **488** |
| | | | |
| **6 DEC 90** | 1.2-5 | .97 | 232 |
| | 5-10 | .62 | 217 |
| | 10-15 | .77 | 60 |
| | 15-20 | .54 | 41 |
| | **TOTAL** | **.78** | **550** |

## C. DVE SUMMARY

The high correlation obtained for the temperature differences (CT1 and CT2) for the sets of probes in the night-time flight on 8 December 1990 and the low correlation obtained during day-time flights particularly near the tropopause support the hypothesis that the apparent order of magnitude increase in optical turbulence is an instrument effect attributable to solar heating of the probes. This is consistent with previous work that shows that the solar induced, probe-air temperature differences are largest at low temperatures [Ref. 3:p. 19]. The fact that the only flight that had the parallel/perpendicular configuration of the two sets of probes, the 7 December launch, had the largest overall variations (smallest correlation coefficient, r), indicates that the probe orientation with respect to the sun contributed to the differences in the measured temperatures.

The motion of the package (rotation or pendulum-like oscillations), could produce a low frequency signal. The parallel/perpendicular configuration would correlate more poorly than the double parallel configuration because the probes would move through the air masses with different orientations and be exposed to different conditions. Differential solar heating of the probes from probe wire oscillation, possibly exacerbated by payload motion (pendulum and rotation) could produce a higher frequency signal which could mask the data [Ref. 3:pp. 16,46]. The flexible probe wires, which oscillate from the cross flow of air, would continuously present differing cross-sectional areas to the sun and induce a signal. If probe vibrations were the cause of these differing results, then both the

parallel/perpendicular configuration and the dual parallel configuration would have exhibited uneven heating behavior. The daytime data currently available are only reliable, meaning consistent, with nighttime data up to approximately 8-10 km, which is an altitude that is clearly beneath the tropopause. Daytime microthermal probe data beyond this are highly questionable. Although the number of flights in this series of launches was limited, these results are consistent with those of many previous day launches and support the hypothesis that solar heating of the probes contaminates the daytime data. Although the exact mechanism of this contamination is not readily apparent, the evidence confirming its existence is convincing.

If balloon wake (thermal shedding) was responsible for the diurnal variation in the $C_T^2$ measurements, the correlation of the nighttime flights should be poorer than the day. The balloon, which is cooler than its surroundings at night, creates a cooled wake beneath it as it rises. The wake effect should be worse at night since the temperature difference between the balloon and the surrounding air is larger than in the day. Weitekamp showed that this effect was small at the distances that the thermosonde packages were suspended beneath the balloon [Ref. 3:p. 25].

## D. SONDE STABILIZATION FOR SUBSEQUENT EXPERIMENTS

To eliminate solar effects apparent in the daytime launches due to rotation and oscillation of the sonde, it is necessary to stabilize the sonde as much as

possible. The most reliable and consistent data will occur when the probes maintain a consistent alignment with respect to the sun. Possible solutions to this may include the use of a gyro mechanism to stabilize the platform, vertical baffles or fin stabilizers, solar cells to determine relative solar angle, and weights/anchors to hold the apparatus steady. To reduce the effects of probe vibration, the tungsten wire probes must be attached straight across the probe supports rather than with a flexible configuration. This will involve a delicate compromise to avoid thermal stress and strain on the wire and its contacts and yet suppress vibration.

# IV. PROBE RESPONSE

## A. PROBE RESPONSE TIME AS A FUNCTION OF DECREASING TEMPERATURE AND AIR DENSITY

### 1. Thermocouple Measurement Limitations Due to Probe Response Time

A second systematic issue that impacts the performance of the thermal probe turbulence measurements involves estimating the probe response time vs. altitude. When a thermocouple measures the temperature of its atmospheric surroundings, the value that it provides is its own temperature, not that of the surrounding air. This occurs because of the finite heat transfer mechanisms occurring at the surface-air interface. The thermal mass of the probe and the convective air-surface interface limit the rate of heat transfer producing a delayed probe response. This limits the high frequency components of the signal used to compute structure functions. [Ref. 15:p. 15] This becomes increasingly important for structure function measurements with small separation distances. A 10 cm separation requires a probe response time of 1-2 ms. This problem increases at higher altitudes. The low density environment in the 10 to 20 km (10 mb) region offers less effective heat transport (primarily forced convection) by which the probes adjust to the temperature of their surroundings, consequently

measurements underestimate the corresponding structure functions as altitudes increase.

## 2. Fluid Characteristics and Heat Transfer

### *a. Forced Convection*

Forced convection is the dominant (albeit, still a weak) heat transfer mechanism in regions where the mean free path of the surrounding molecules is comparable to the dimensions of the heat transfer surface (the cylindrical wire probe). The physical mechanism of forced convection which removes heat (energy) from the probes is the collisional momentum transfer to surrounding air molecules when these molecules impact the probe [Ref. 16:p. 631]. The mean free path of atmospheric molecules increases from 0.06 $\mu$m at sea level to approximately 4.4 $\mu$m at 30 km [Ref. 17:p. 14-13]. This is comparable to the dimensions of a 12.4 $\mu$m diameter cylindrical wire probe. These are the dimensions of the ANSI Type E chromel-constantan thermocouples that the NPS group used in the summer and fall 1992 experiments; the thermocouples were manufactured by Omega Engineering, Inc. [Ref. 18:p. A-33]. Above 30 km, as the molecular mean free path length continues to increase, forced convection is no longer the dominant heat transfer mechanism for probes of this size.

### *b. Viscosity*

The thermodynamic transport property that characterizes the fluid-mechanical behavior of the medium is the viscosity, $\mu$, also known as the dynamic viscosity. It exists as a point function in a flowing fluid, the air, and follows all of the laws and state relations of ordinary equilibrium thermodynamics [Ref. 7:p. 20]. Viscosity is a measure of the diffusion of momentum parallel to the flow velocity and transverse to the gradient of the flow velocity [Ref. 16:p. 219] and has the dimensions of $(kg/m \cdot s)$. It relates the local stresses in a moving fluid to the rate of strain in the fluid element by

$$\tau = \mu \frac{du}{dy}, \tag{13}$$

where $\tau$ is the shear stress and du/dy is the local fluid velocity gradient [Ref. 7:p. 26].

Prandtl showed that low viscosity fluid flows such as airflow are divided into a thin viscous boundary layer near a solid surface which borders a nearly inviscid outer layer which is still governed by the Euler and Bernoulli Equations [Ref. 19:p. 46] Under shearing, a fluid begins to move at a strain rate inversely proportional to the coefficient of viscosity. Viscosity depends primarily on temperature at low altitudes by

$$\mu = \frac{\beta \cdot T^{2/3}}{T+S}, \tag{14}$$

where $\beta$ is a constant equal to 1.458 x $10^{-6}$ $kgs^{-1}m^{-1}K^{-1/2}$ and S, Sutherland's constant, is equal to 110.4 K [Ref. 20:p. 14-5].

### c. *Kinematic Viscosity*

The kinematic viscosity, $\nu$, is the ratio of the dynamic viscosity of a gas to its density by

$$\nu = \frac{\mu}{\rho}, \tag{15}$$

where $\rho$ is the atmospheric density in ($kg/m^3$) [Ref. 20:p. 14-6]. The dimensions of $\nu$ are ($m^2/s$). Figure 17 shows how kinematic viscosity increases with altitude.

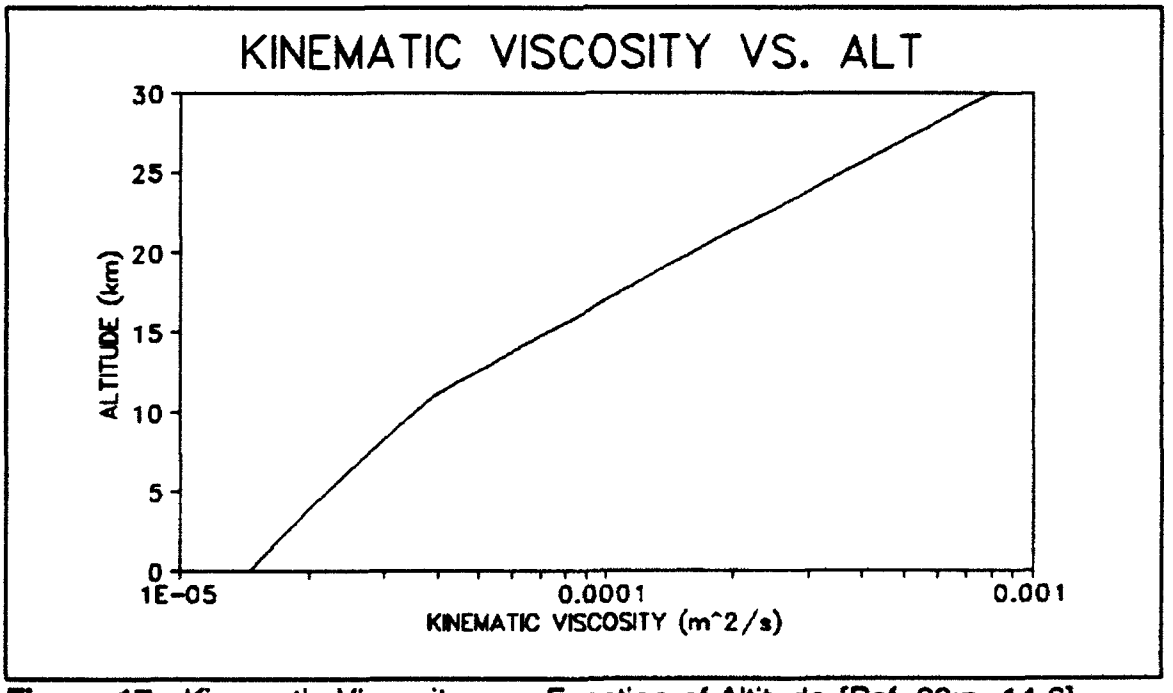


**Figure 17.** Kinematic Viscosity as a Function of Altitude [Ref. 20:p. 14-6].

### *d. No-Slip Condition*

When a fluid flow encounters a solid surface, molecular interactions cause the fluid and the surface to seek energy and momentum equilibrium with each other; all liquids are essentially in equilibrium with the surface with which they are in contact; fluids in contact with a solid take on the velocity and temperature of the surface. These are the no-slip and no-temperature-jump conditions which are only valid when the molecular mean free path is less than the surface dimensions of the solid. [Ref. 7:p. 35]

### *e. Reynolds Number, Re*

The parameter that describes the viscous behavior of a Newtonian fluid such as air is the dimensionless Reynolds number Re

$$Re = \frac{\rho VL}{\mu} = \frac{VL}{\nu}, \tag{16}$$

where $\rho$ is the atmospheric density, $\mu$ is the dynamic viscosity, V is the characteristic velocity, and L is the characteristic length scale of the flow. The Reynolds number is a ratio of the dynamic forces of mass flow (inertia) to the viscous forces within the atmosphere. For a 12.4 $\mu$m chromel-constantan probe, the value of the Reynolds number varies from 3.75 at sea level to 0.07 at 30 km for windspeeds of 4.4 m/s. Figure 18 is a plot of the Reynolds number for the 12.4 $\mu$m probe. The plot includes Reynolds numbers computed using both the maximum and minimum probable diameters of a 12.4 $\mu$m wire in accordance with

the manufacturer's manufacturing tolerances (a 12.4 $\mu$m AWG No. 56 thermocouple wire can vary from 11.4 to 13.4 $\mu$m [Ref. 21]). These values represent two regimes of the Reynolds number: $0<Re<1.0$ describes a region of highly viscous laminar creeping motion, and the range $1.0<Re<100$ describes a region of laminar motion with strong Reynolds number dependence [Ref. 7: p. 309]. Table V summarizes Reynolds numbers for the probe as a function of altitude where the probe velocity is 4.4 m/s.

**TABLE V.** Reynolds Number for NPS 12.4 +/- 1.0 $\mu$m Chromel-Constantan Probes from 0 to 30 km at v=4.4 m/s.

| ALT (km) | 11.4 $\mu$m Probe | 12.4 $\mu$m Probe | 13.4 $\mu$m Probe |
|---|---|---|---|
| 0 | 3.44 | 3.75 | 4.05 |
| 10 | 1.43 | 1.55 | 1.68 |
| 20* | 0.32 | 0.34 | 0.37 |
| 30 | 0.06 | 0.07 | 0.07 |

* above 19 km, where Re <0.4, the equation for Re begins to lose its accuracy; however, empirical fits to the data by Holman [Ref. 16:p. 303] have shown that Re values follow approximately the same trend in this regime.

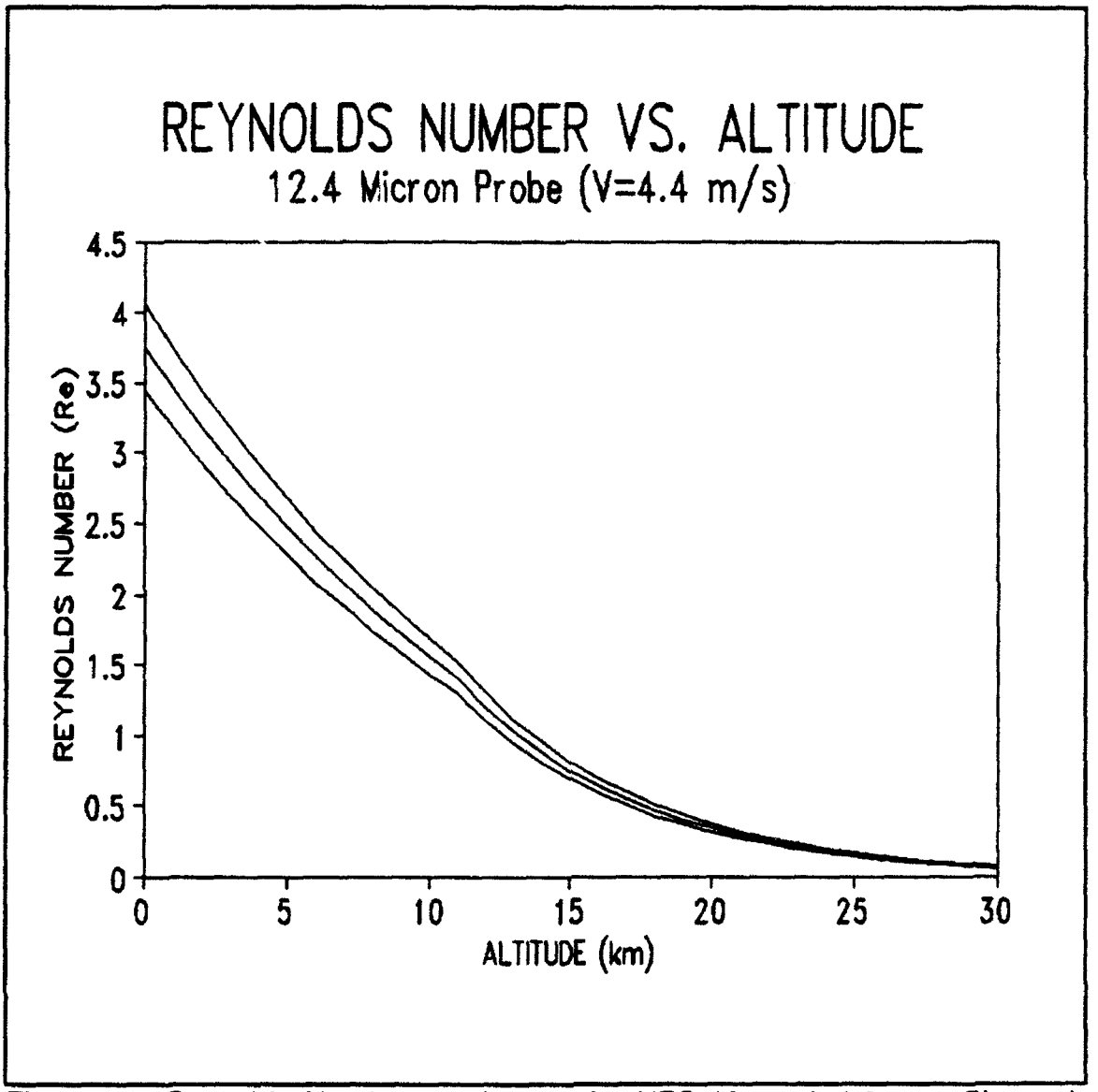


**Figure 18**: Reynolds Number vs. Altitude for NPS 12.4 +/- 1.0 $\mu$m Chromel-Constantan Thermocouple Probe.

### *f. Nusselt Number*

From Kothandaraman and Subramanyan the Nusselt number for a cylinder in a cross-flow is [Ref. 22:p. 91]

$$Nu = C\left(\frac{u\_d}{\nu}\right)^n, \tag{17}$$

where C and n are empirically developed constants based upon the local Reynolds number where

$$Re = \left(\frac{u\_d}{\nu}\right). \tag{18}$$

Table VI contains the values of the constants C and n. Figure 19 is a plot of Nu vs. altitude for the NPS probe based on the Reynolds numbers shown in Table V. Table VII summarizes the Nusselt number values.

**TABLE VI.** Constants for Determination of Nusselt Number for Eq. (16).

| Re | C | n |
|---|---|---|
| < 0.4 | 0.891* | 0.330* |
| 0.4 -4.0 | 0.891 | 0.330 |
| > 4.0 | 0.821 | 0.385 |

* empirically fit

**TABLE VII.** Nusselt Number vs. Altitude for NPS 12.4 +/- 1.0 $\mu$m Chromel-Constantan Thermocouple Probes.

| ALT (km) | 11.4 $\mu$m Probe | 12.4 $\mu$m Probe | 13.4 $\mu$m Probe |
|---|---|---|---|
| 0 | 1.34 | 1.38 | 1.41 |
| 10 | 1.00 | 1.03 | 1.06 |
| 20 | 0.61 | 0.63 | 0.64 |
| 30 | 0.35 | 0.37 | 0.38 |

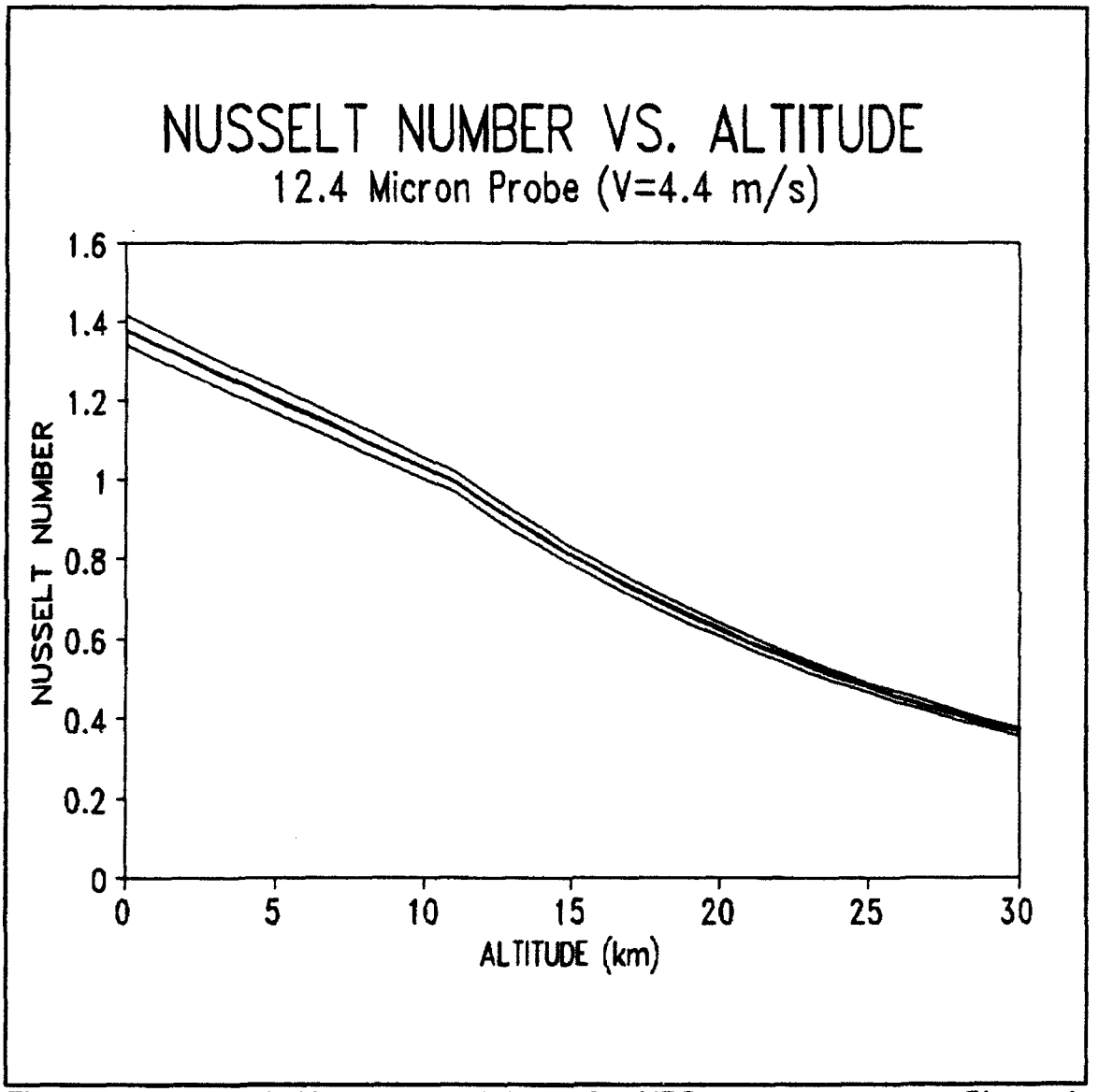


**Figure 19.** Nusselt Number vs. Altitude for NPS 12.4 +/- 1.0 $\mu$m Chromel-Constantan Thermocouple Probe.

### *g. Rate of Convective Heat Flow*

Newton's Law of Cooling governs the rate of convective heat flow between a solid and its environment by [Ref. 19:p. 89]

$$q=hA\Delta T, \tag{19}$$

where

q = rate of heat transfer

h = convective heat transfer coefficient

A = solid surface area

$\Delta T$ = temperature difference between the solid and its environment.

### *h. Convective Heat Transfer Coefficient, $h_c$*

The convective heat transfer coefficient, $h_c$, is a parameter that describes the energy transport (both thermodynamic and mass) between the probe and the surrounding atmosphere. It is a fluid property that conveniently groups terms that are a complex function of fluid flow and geometric conditions of the probe and the environment [Ref. 19:p. 44]. It is generally expressed as an empirical form of the Nusselt number, Nu, by

$$Nu=\frac{h_c d}{k}, \tag{20}$$

where d is the characteristic length (wire diameter) and k is the thermal conductivity of the surrounding air in (kcal/m-hr K) [Ref. 23:p. 6-3]. The convective heat transfer coefficient, $h_c$, has dimensions of $W/m^2K$.

Previous work by Brown [Ref 12:p. 19] and Weitekamp [Ref. 3:p. 38] has shown that there is approximately a factor of four decrease in the convective heat transfer coefficient, $h_c$, from the ground to an altitude of 30 km. The value of $h_c$ for the NPS 12.4 $\mu$m chromel-constantan probe exhibited similar behavior; the actual values of $h_c$ were different due to the different sizes and composition of the respective probes, but the trend was the same as shown in Figure 20 for the NPS probes ascending at 4.4 m/s. Table VIII summarizes these data.

**TABLE VIII.** Convective Heat Transfer Coefficient, $h_c$, vs. Altitude for NPS 12.4 +/- 1.0 $\mu$m Chromel-Constantan Thermocouple Probes.

| ALT (km) | $h_c$ for 11.4 $\mu$m Probe ($W/m^2K$) | $h_c$ for 12.4$\mu$m Probe ($W/m^2K$) | $h_c$ for 13.4 $\mu$m Probe ($W/m^2K$) |
|---|---|---|---|
| 0 | 2973 | 2808 | 2665 |
| 10 | 1760 | 1662 | 1577 |
| 20 | 1040 | 982 | 932 |
| 30 | 637 | 602 | 571 |

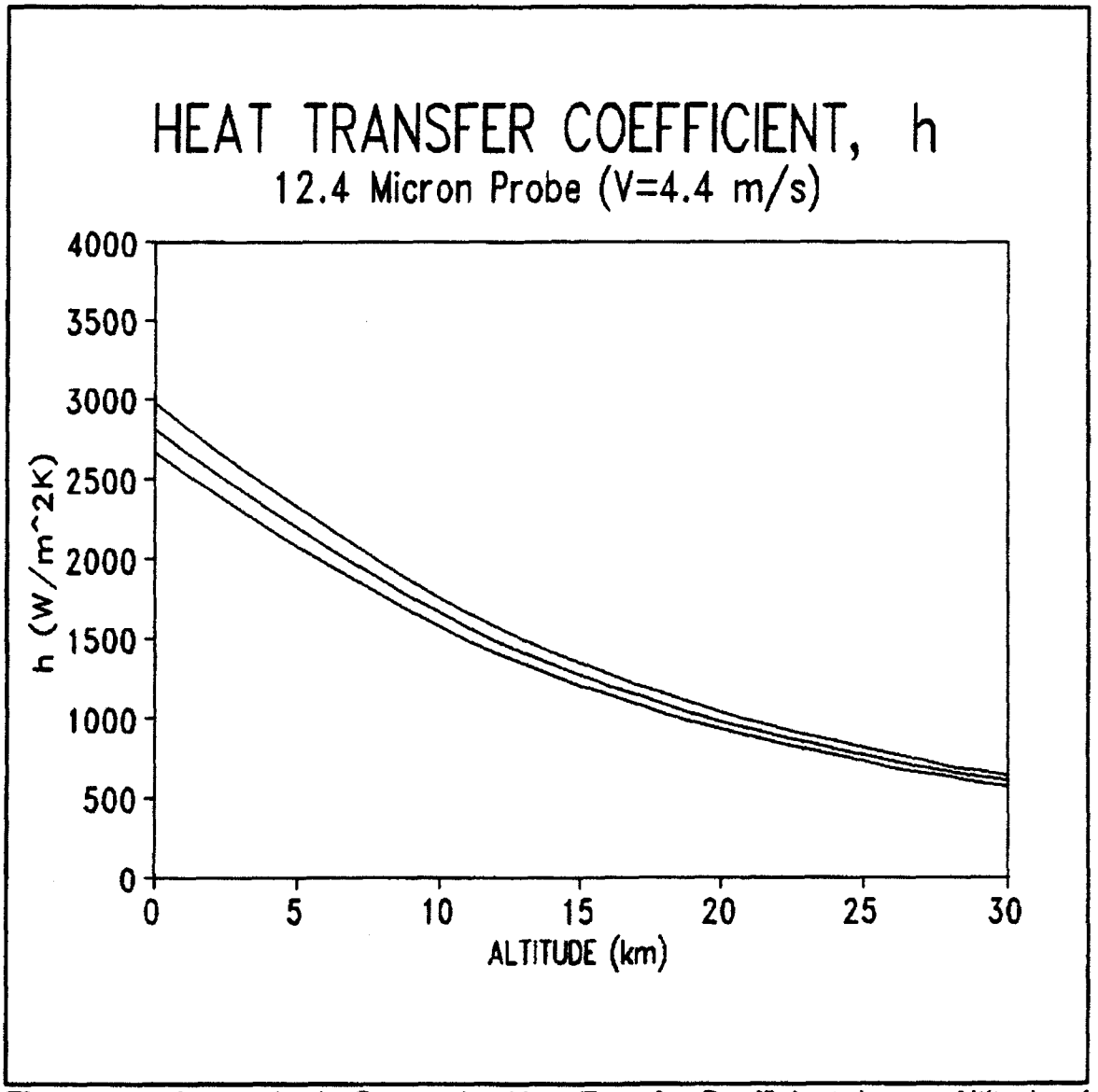


**Figure 20.** Atmospheric Convective Heat Transfer Coefficient, $h_c$, vs. Altitude of NPS 12.4 +/- 1.0 $\mu$m Chromel-Constantan Thermocouple Probe with Wind Velocity of 4.4 m/s.

## B. TIME CONSTANT, $\tau$

### 1. Theoretical Probe Response

The time for the thermocouple to complete 63.2 % of its response to a step change in the temperature of the air around it is the characteristic time, $\tau$ [Ref. 24:p. 566]. The characteristic time is

$$\tau = \frac{\rho c d}{4 h_c}, \tag{21}$$

where $\rho$ is the thermocouple density in (gm/cm$^3$), $c$ is the thermocouple specific heat capacity in (J/g$\cdot$K), $d$ is the diameter of the thermocouple in (cm), and $h_c$ is the convective heat transfer coefficient in (J$\cdot$s)/(cm$^2\cdot$K) Hence, the characteristic time is the ratio of the probe thermal storage capacity to the heat input per degree of temperature difference. [Ref. 24:p. 555]

Eq. (21) shows that the response time of a particular probe varies only with the convective heat transfer coefficient, $h_c$; the other quantities depend on the structure of the thermocouple and do not change appreciably under experimental conditions. Several factors affect the accuracy of this equation. Manufacturing tolerances in wire diameter coupled with the presence of a welded junction bead that connects the thermocouple wires near the center (Figure 21) contribute to an imprecise prediction of probe response.

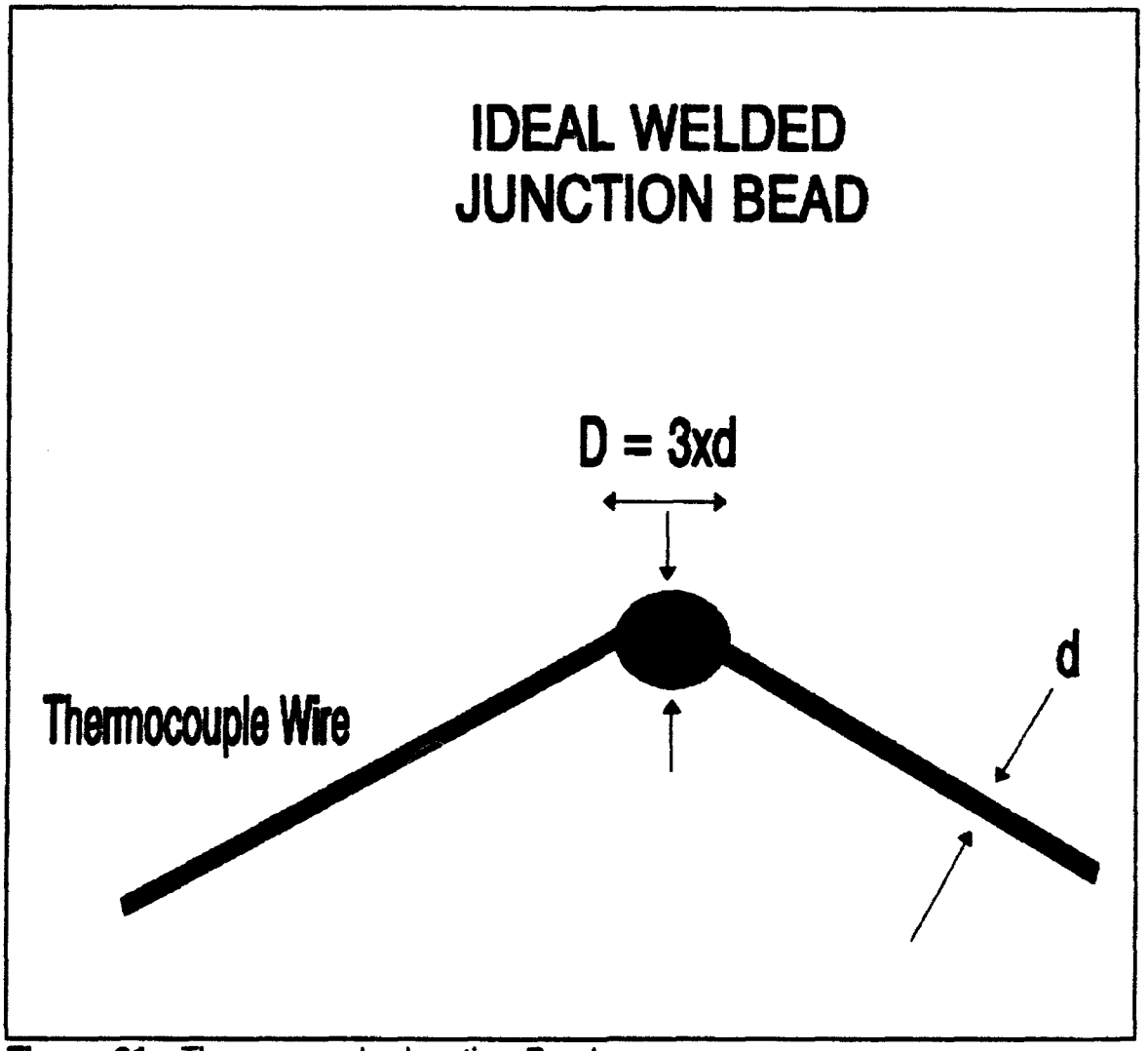


**Figure 21.** Thermocouple Junction Bead.

The geometry and mass of this welded junction bead give it different heat transfer characteristics than those of the cylindrical wire, and therefore, affect the true value of $\tau$. Moffat accounted for this difference by the expression

$$\frac{\tau}{\tau_0}=\left(\frac{D}{d}\right)^{0.375}, \tag{22}$$

where $\tau$ is the true characteristic time, $\tau_0$ is the characteristic time when the diameter of the junction bead and the diameter of the wire are the same (no weld effect), D is the diameter of the bead (assumed to be spherical), and d is the diameter of the probe wire. Moffat also emphasized that to ensure first order probe response, the diameter of the weld should not exceed the wire diameter by more than 10%. [Ref. 24:p. 566]

## 2. Thermocouple Characteristics

### *(1) Thermocouple Type*

The NPS differential thermosonde used thermocouple rather than resistance probes to simplify the electronic circuit. The smallest commercially available thermocouple was 12.4 $\mu$m in diameter, which was four times larger than those used by the Geophysics Directorate. The increased thermal mass reduced the high frequency response which had increasing importance in structure function measurements for small separations ($\sim$10 cm).

*(2) Material Properties*

The NPS Group used an ANSI Type E cylindrical wire thermocouple to make temperature measurements for all launches from July to November 1992. According to the specifications of the manufacturer, Omega Engineering, Inc., this chromel-constantan thermocouple was 12.4 $\mu$m in diameter. Its composition was 75% (Ni-10Cr) and 25% (Cu-43Ni) which gave it a specific heat capacity, c, of .4367 (J/g • K). Appendix C has more details on the thermocouple composition and characteristics. The NPS Group chose this thermocouple since it was the smallest available and because of its large thermoelectric response.

*(3) Thermocouple Geometry*

To ensure that all constants affecting the time constant were valid, we measured the diameter of the chromel-constantan thermocouple wire with a Cambridge 200, tungsten filament scanning electron microscope (SEM). The measured diameter of the cylindrical segment of the wire was 13.7 $\mu$m with an unspecified tolerance. This value was 10% higher than the manufacturer's specifications for the AWG no. 56 thermocouple wire. Since the SEM had not been calibrated recently and the operator's manual contained no specific measurement tolerances, we used the measurement as a verification of the general dimensions of the wire and to estimate the bead size [Ref. 25].

The "v"-shaped wire had a welded bead near the v, which according to the manufacturer, should have been spherically shaped and

approximately 3 times the wire diameter [Ref. 18:p. A-31]. The SEM measured the dimensions of the roughly cylindrical bead to be approximately 15.5 $\mu$m x 15.5 $\mu$m x 52.3 $\mu$m resulting in a volume of approximately 13,000 $\mu m^3$. Since the SEM only measured in 2 dimensions, it did not provide a value for the bead's height. Photograph's of the bead showed that the center segment of the bead appeared to be cylindrical; therefore, we assigned the bead a thickness of 15.5$\mu$m, the same value as the width. We used a spherical approximation because, ideally, this would be the shape of the weld bead according to manufacturer's specifications and as found in the examination of numerous other thermocouple wires. By approximating the shape of the bead as spherical and using the standard equation for the volume of a sphere,

$$V=\frac{1}{6}\pi D^3, \tag{23}$$

where D is the diameter of the sphere, the effective diameter of the bead became 29 $\mu$m. This diameter was ~2.3 times the wire diameter, in reasonable agreement with the 3:1 ratio given by the manufacturer. We calculated an adjusted value for the bead diameter due to the discrepancy between the manufacturer's specifications and the measured SEM values for the wire diameter. Since the SEM value was 10% higher than the manufacturer's value for diameter, its values for the bead dimensions should have been 10% higher as well. Factoring this adjustment into Eq. (23), yielded an adjusted bead

diameter of 26 $\mu$m. Using either the SEM or manufacturer's values, the ratio of the bead diameter to the wire diameter clearly exceeded the 10% allowance for first-order effects, therefore, higher-order effects would affect the probe response.

### 3. Theoretical Calculation of $\tau$

Figure 22 shows a plot of $\tau$ vs. altitude for the NPS 12.4 $\mu$m diameter wire thermocouple, uncorrected for a junction bead. The uncorrected $\tau$ for the 12.4 $\mu$m probe had a value of 4.2 ms at 0 km and 19.7 ms at 30 km. Figure 23 shows a plot of $\tau$ vs. altitude for the NPS 12.4 $\mu$m diameter wire thermocouple, corrected for a 26 $\mu$m junction bead. The time constant accounting for the bead was 5.8 ms at 0 km and 27.0 ms at 30 km. The effect of correcting for the bead yielded response times that were ~30% slower than for the calculations with no bead correction. Table IX summarizes these data.

**TABLE IX.** Calculated Thermocouple Probe Response vs. Altitude, for a 12.4 +/- 1.0 $\mu$m Chromel-Constantan Wire, with and without Correction for a 26 $\mu$m Junction Bead.

| d ($\mu$m) | 11.4 | 11.4 | 12.4 | 12.4 | 13.4 | 13.4 |
|---|---|---|---|---|---|---|
| ALT (km) | no bead | 26 $\mu$m bead | no bead | 26 $\mu$m bead | no bead | 26 $\mu$m bead |
| 0 | 3.7 | 5.0 | 4.2 | 5.6 | 4.8 | 6.2 |
| 10 | 6.2 | 8.4 | 7.1 | 9.4 | 8.1 | 10.4 |
| 20 | 10.5 | 14.3 | 12.1 | 15.9 | 13.8 | 17.6 |
| 30 | 17.1 | 23.3 | 19.7 | 26.0 | 22.5 | 28.8 |

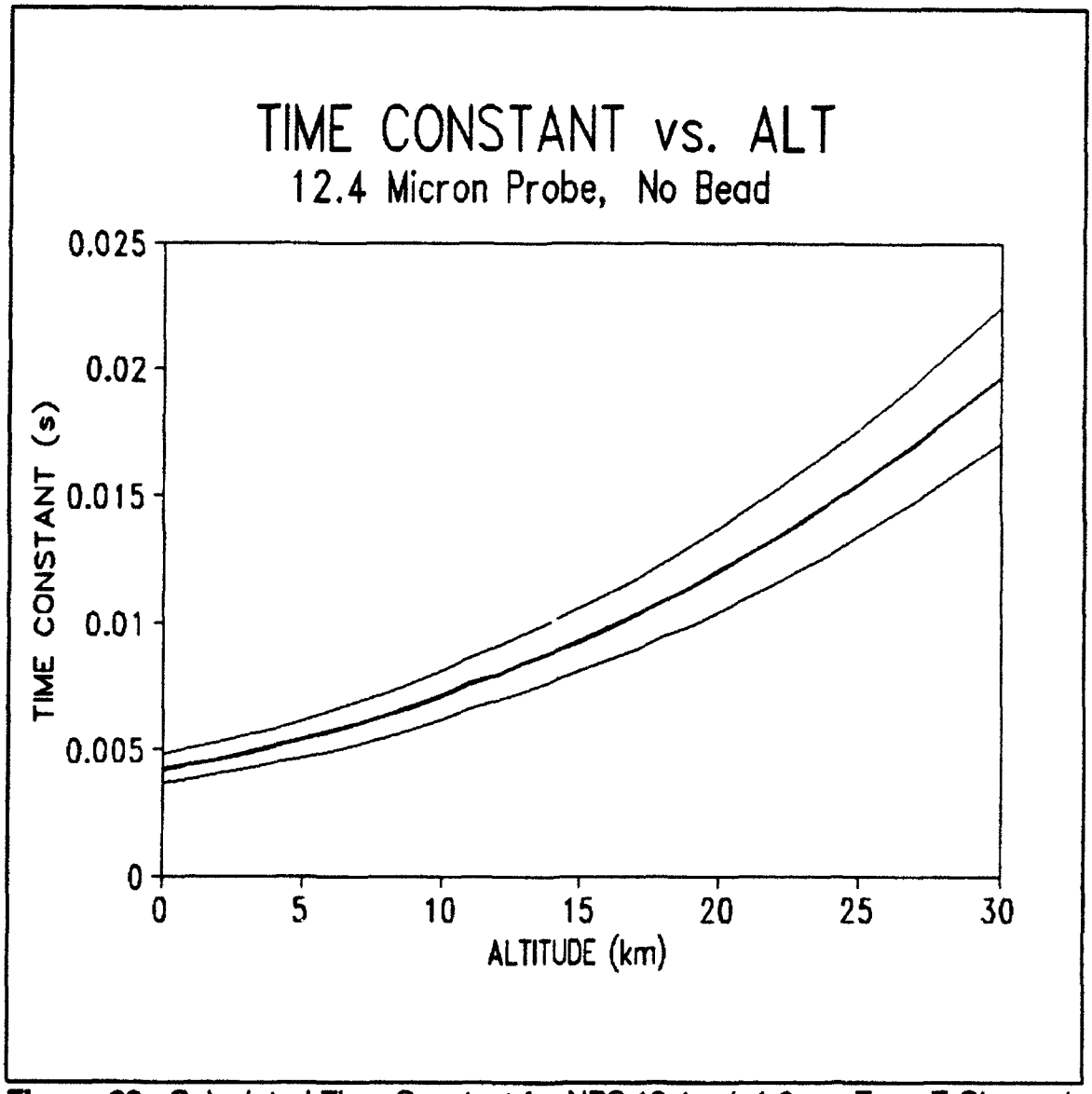


**Figure 22**. Calculated Time Constant for NPS 12.4 +/- 1.0 $\mu$m Type E Chromel-Constantan Thermocouple Probe with no Correction for a Junction Bead.

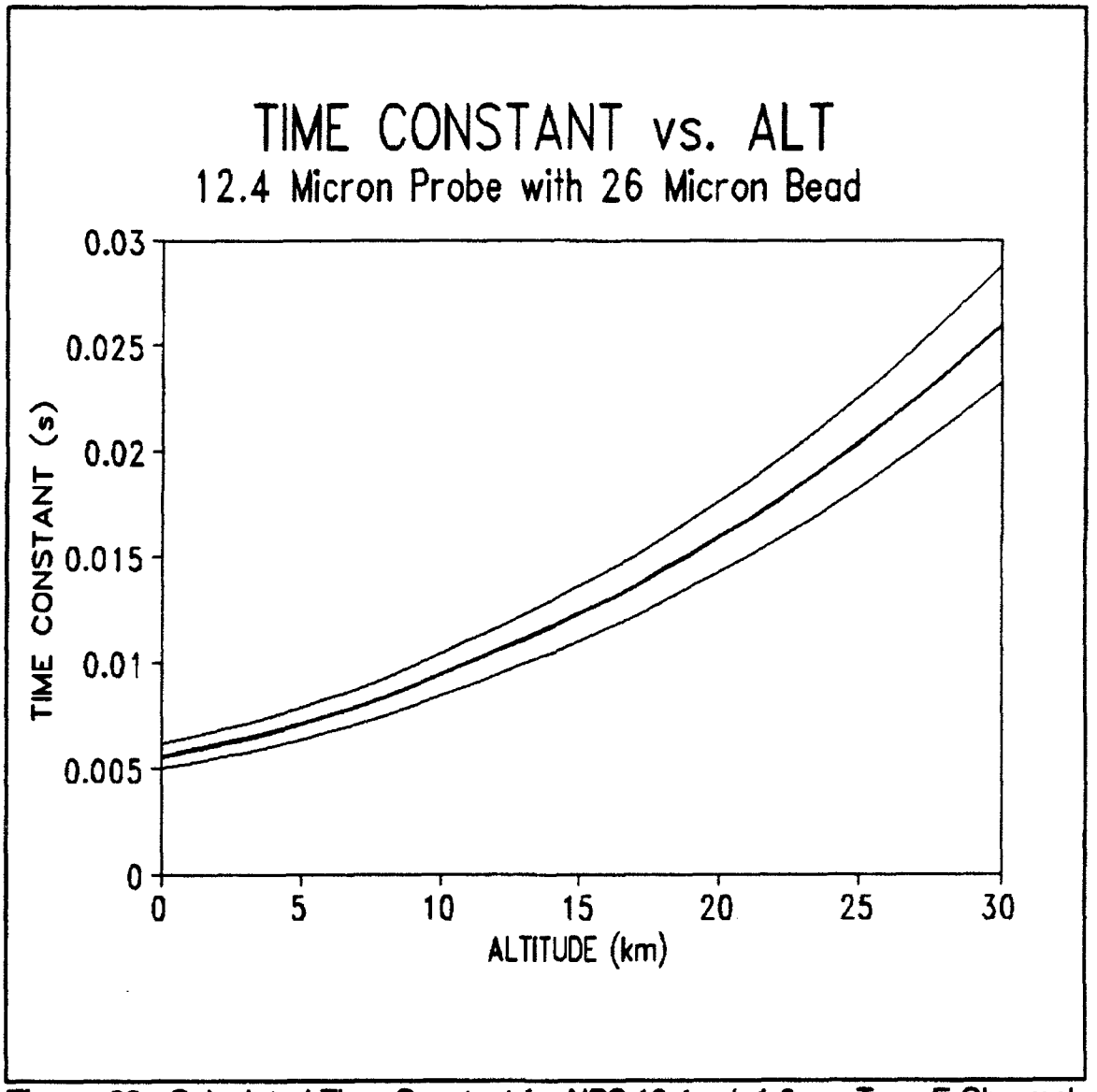


**Figure 23.** Calculated Time Constant for NPS 12.4 +/- 1.0 $\mu$m Type E Chromel-Constantan Thermocouple Probe with a Correction for a 26 $\mu$m Junction Bead.

## C. EXPERIMENTAL VERIFICATION OF PROBE RESPONSE TIME

### 1. Empirical Formula For Probe Thermal Response

When used to measure local gas temperature, a bare-wire thermocouple displays physical and thermodynamic behavior similar to that of a cold-wire anemometer. A cold-wire anemometer measures rapidly fluctuating flows such as the turbulent boundary layer surrounding an object (the probe). It consists of a fine wire mounted between two small probes. An empirical equation that relates the wire response time with the windspeed is

$$\frac{1}{\tau} = a + b\sqrt{v} \qquad (24)$$

where a and b are constants, a being the y-intercept of the plotted data and b being the slope of this data, plotted according to linear regression where $\tau$ is the response, and v is the wind velocity [Ref. 26:p. 13].

### 2. Wind Tunnel Test

We constructed a wind tunnel and subjected a 12.4 $\mu$m probe (not the same probe that we had SEM diameter measurements on) to cross-winds varying in speed from 0 to 4.4 meters-per-second. The maximum windspeed was 4.4 m/s because of the operating limit of the 24V DC fan that was the wind source. The 4.4 m/s windspeed approximated the average ascent velocity of a balloon which typically ranges from 4 to 6 m/s. While it was in the wind tunnel,

we illuminated the probe with an unfocused visible laser diode to provide a periodic instantaneous heating effect. This was to simulate the effect of an instantaneous change in air temperature as the probe moved through different air masses as it would throughout a flight. The control portion of this experiment was conducted at sea level conditions. The wind tunnel was built of styrofoam in order to minimize the influence of any external heat sources on the thermocouple. Figure 24 illustrates the experimental setup. Appendix C contains additional details of the experiment.

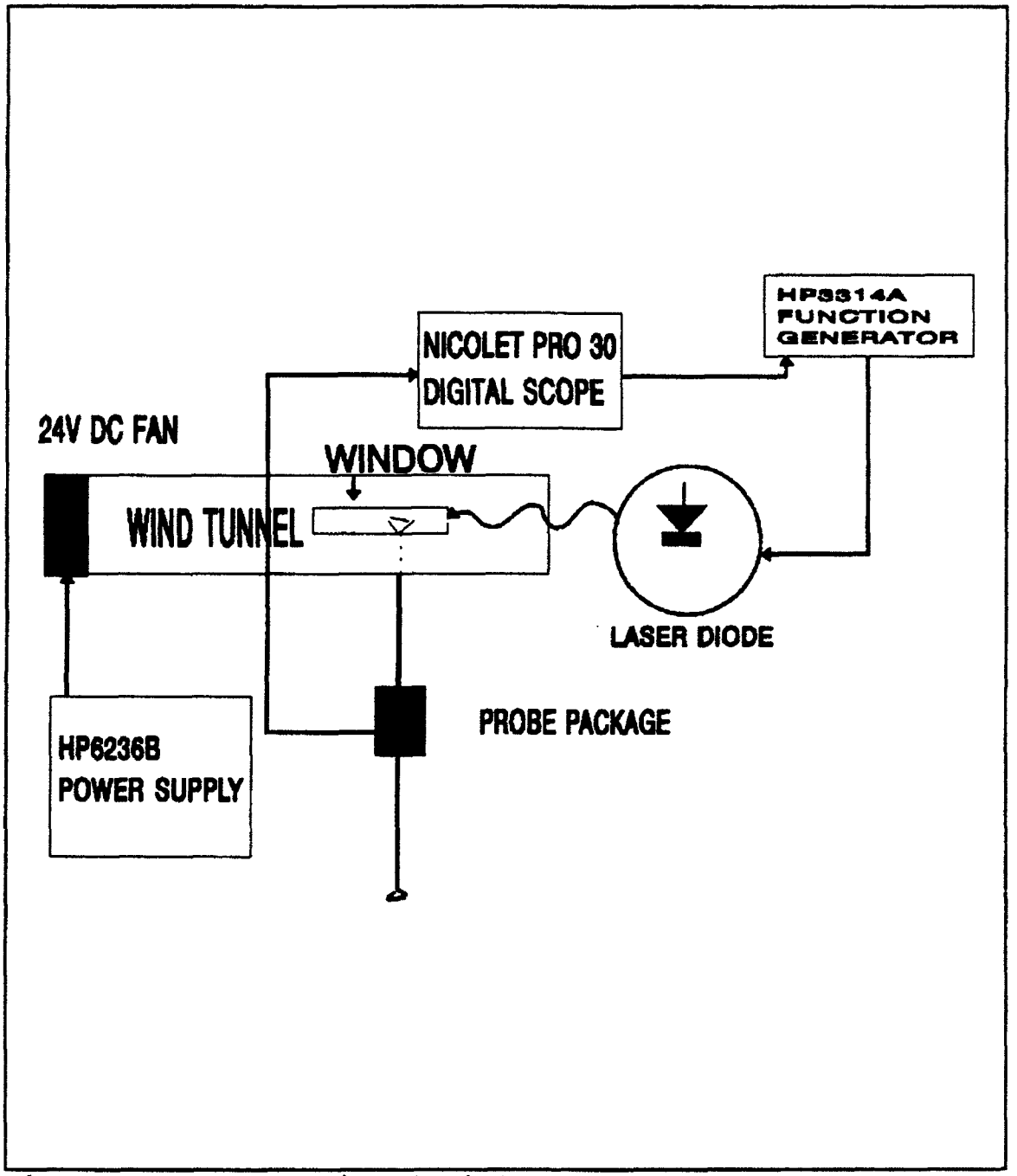


**Figure 24.** Schematic of Wind Tunnel Thermocouple Response Experiment Conducted in Monterey, CA at 0 km altitude and 25° C on 8 November 1992.

### 3. Experimental Results

The 12.4 $\mu$m probe had a measured time constant of 5.6 +/- 0.2 ms in a 4.4 m/s wind in the wind tunnel at 0 km altitude. Figure 25 is a plot of the probe response to the periodic laser pulse at this windspeed. It illustrates the rapid, but not instantaneous, response of the probe to an instantaneous temperature change. The horizontal distance along the x-axis between the instantaneous change and the time it takes the amplitude to reach the 1-1/e point is the time constant $\tau$. Appendix C contains plots of the results of performing this test on a 25 $\mu$m copper-constantan probe, a probe used frequently in previous experiments. Table X summarizes these data.

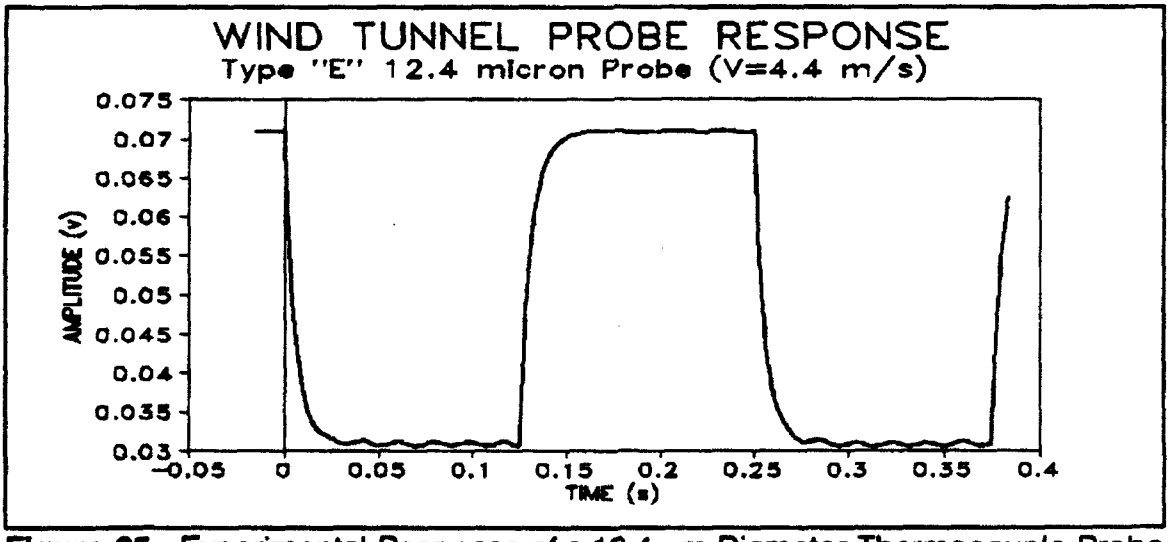


**Figure 25.** Experimental Response of a 12.4 $\mu$m Diameter Thermocouple Probe Illuminated by a Periodic Laser Diode in a 4.4 m/s Wind in the NPS Wind Tunnel Experiment of 2 November 1992. Time Constant Measured to be $\tau$ = 5.6 +/- 0.2 ms.

**TABLE X.** Measured Probe Response in Wind Tunnel for 12.4 and 25 $\mu$m Wires.

| Wind (m/s) | 12.4 $\mu$m Chrom-Const | 25 $\mu$m Copper-Const | Response Ratio (25$\mu$m/12.4$\mu$m) |
|---|---|---|---|
| 0 | 15.7 | 69 | 4.4 |
| 1.5 | 7.1 | 28.5 | 4.0 |
| 3.0 | 6.4 | 21 | 3.3 |
| 4.4 | 5.6 | 19.5 | 3.5 |

These results show a factor of four increase in probe response time for a factor of two increase in probe diameter. This shows the effect of the thermal mass slowing the response time. The quadratic diameter dependence arises from Eq. (21) because the $h_c$ term depends on d. Rearranging Eqs. (16), (17), and (20) yields an equation of the form C x ($d^2/d^n$) where C is a grouping of constants and n is an empirical constant equal to 0.33 for the Reynolds number regime of the 12.4 $\mu$m probe with a velocity of 4.4 m/s. The $d^2/d^n$ term then reduces to $d^{1.67}$ which accounts for the approximate $d^2$ ratio between the increase in the time constant based on a given change in probe diameter. Applying this same rationale to the spherical junction beads for the two different probe sizes should account for most of the remaining difference.

### 4. Comparison of Experiment vs. Theoretical Calculations

As previously shown, $h_c$, is a complicated function of numerous variables; therefore the characteristic time constant, $\tau$, is also a complicated

function that should change in a similar fashion. Table XI compares experimental response measurements with analytical model calculations for the 12.4 $\mu$m probe. Appendix C contains the experimental data and the results of the regression analysis. We did not include the plots for the 11.4 and 13.4 $\mu$m probes here because they would obscure the results and because their relationship to the response of the 12.4 $\mu$m probe is shown in Figures 22 and 23. Figure 26 plots the time constant at 0 km as a function of windspeed. This shows that at $v \geq$ 1.5 m/s windspeed, the analytical model closely approaches the wind tunnel experimental measurements for a 12.4 $\mu$m wire with a 26 $\mu$m bead. At v = 4.4 m/s, the average ascent velocity, the curves of the experimental regression data virtually overlay the modeled calculations. At $v \leq$ 1.5 m/s the plot shows the damping effect of the larger thermal mass. Figure 27 shows the same data using Eq. (24), the anemometer response expression.

**TABLE XI.** Time Constant Comparison: Experimental Measurements vs. Analytical Model for the NPS 12.4 +/- 1.0 $\mu$m Chromel-Constantan Thermocouple Probe.

| V (m/s) | EXPERIMENT Wind Tunnel | EXPERIMENT Curve fit | MODEL 12.4 $\mu$m No bead | MODEL 12.4 $\mu$m 26 $\mu$m bead |
|---|---|---|---|---|
| 0.01 | 15.7 | 15.0 | 14.7 | 19.4 |
| 1.5 | 7.1 | 7.5 | 6.0 | 7.9 |
| 3.0 | 6.4 | 6.2 | 4.8 | 6.3 |
| 4.4 * | 5.6 | 5.6 | 4.2 | 5.6 |

* Average ascent velocity

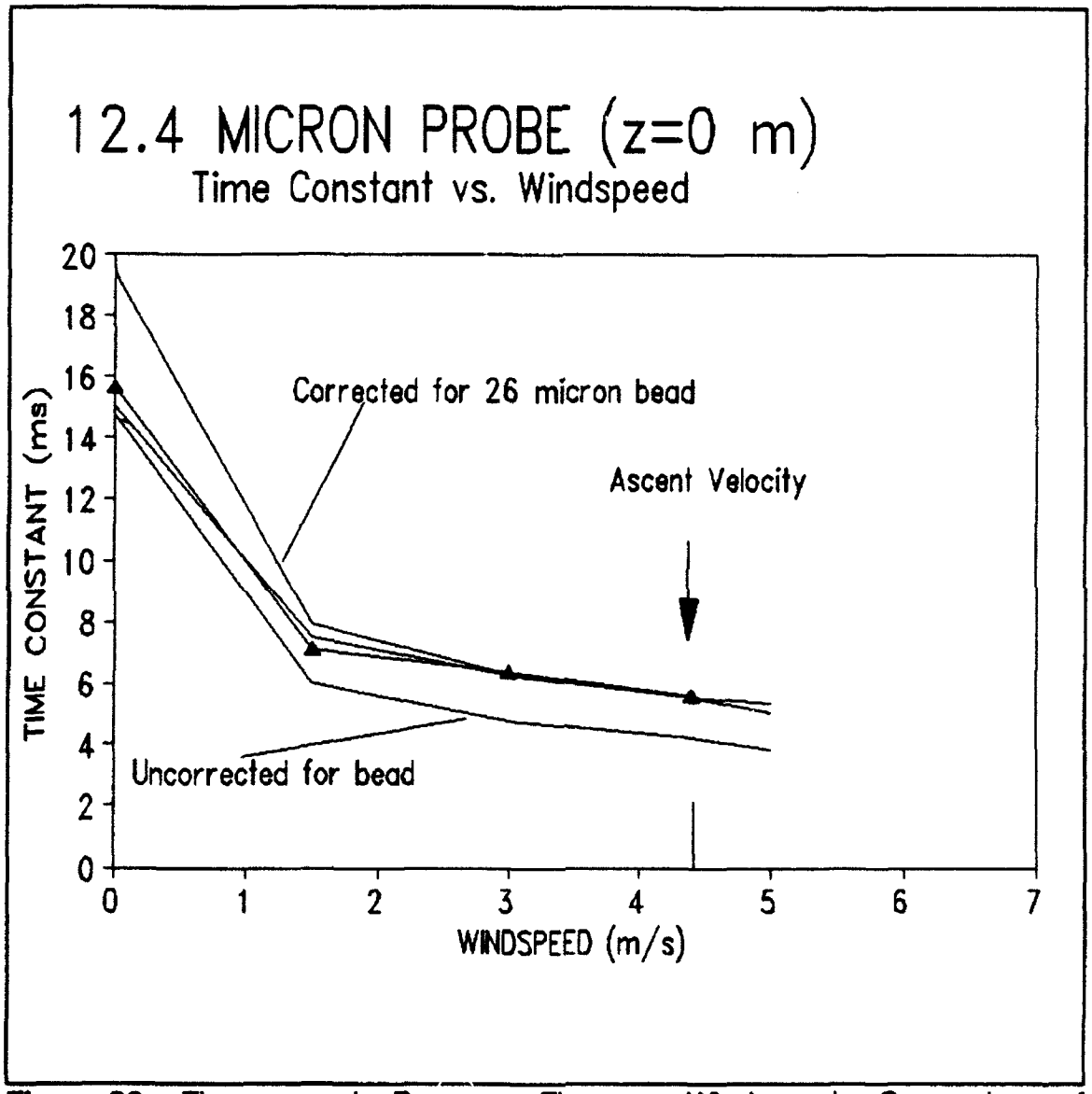


**Figure 26.** Thermocouple Response Times vs. Windspeed. Comparison of Experimental (Wind Tunnel) Measurements with Analytical Model Calculations for 12.4 +/- 1.0 $\mu$m Chromel-Constantan Wire, with and without Correction for 26 $\mu$m Junction Bead.

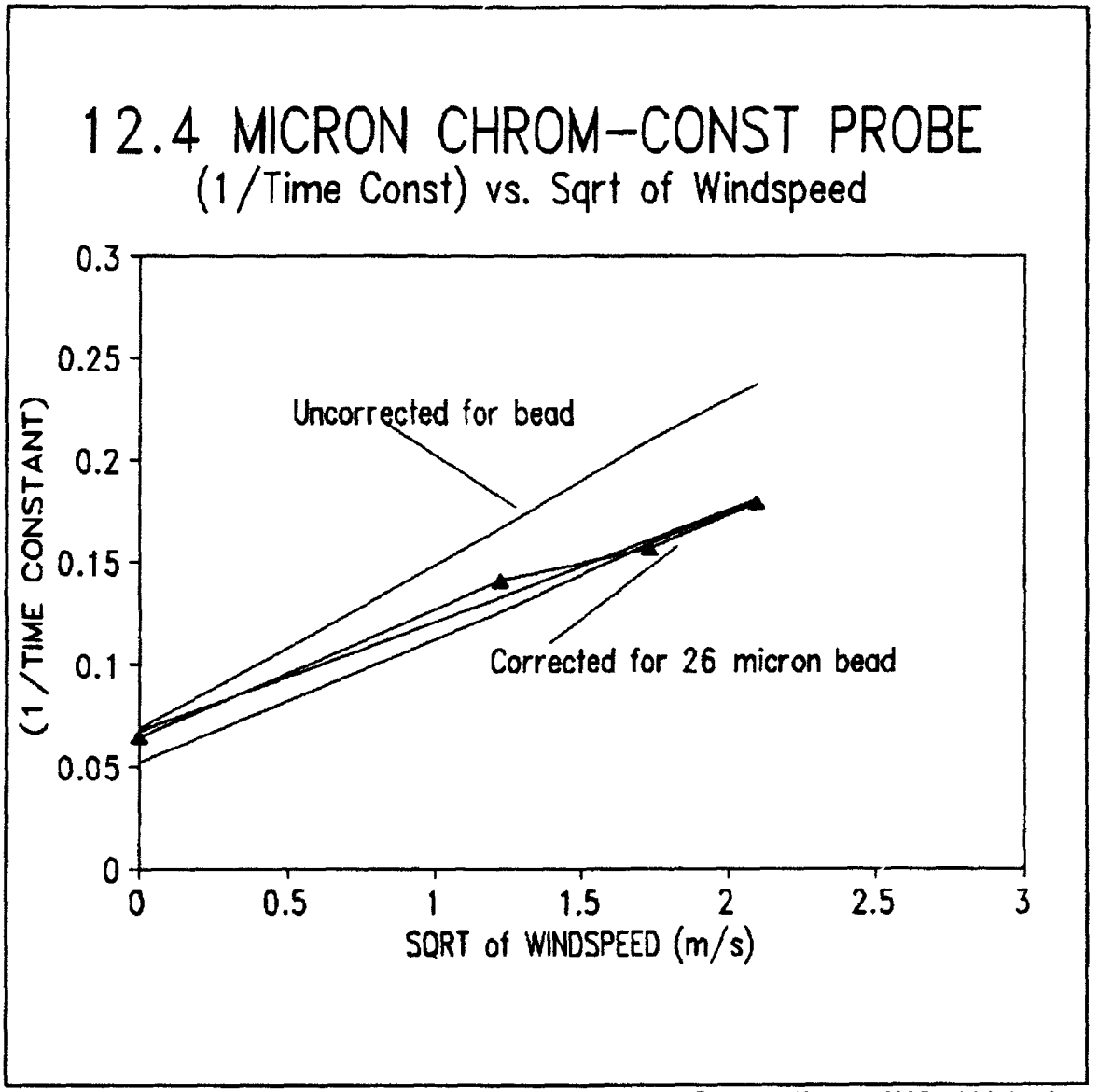


**Figure 27.** 1/e Thermocouple Probe Response vs. Square Root of Wind Velocity. Comparison of Wind Tunnel Measurements with Analytical Model for 12.4 +/- 1.0 $\mu$m Chromel-Constantan Wire, with and without Correction for 26 $\mu$m Junction Bead.

For a 12.4 $\mu$m probe, the analytical model overestimates the observed probe response by 29% when there is no correction factor for the bead. When a correction for the bead, assumed to be spherical and with a diameter of 26 $\mu$m, is made, the model is within 1% of the experimental probe response. It is not probable that the one correction made for bead diameter was sufficient to improve the model's accuracy by a factor of 30. Wind tunnel experimental biases such as uneven heating conditions, non-uniform windspeed, or other slight deviations from standard atmospheric conditions in the laboratory during measurements could have resulted in a larger difference between the model and experimental results. Coupled with this is the uncertainty in the exact dimensions of both the thermocouple wire and junction bead diameters. This uncertainty, although not insignificant, does not obscure the actual decrease in responsiveness, by a factor of approximately 4 (corresponding to the decrease in $h_c$ by the same factor), that occurs as the probe ascends from 0 to 30 km as shown in Figures 25 and 26. Figures 22 and 23 show that variations in the wire diameter, even within the manufacturer's specified tolerances, can alter response times by 22% under experimental conditions which equates to 2 ms at 10 km and 3 ms at 20 km. Table XII summarizes these data.

**TABLE XII.** Differences in Analytical Model Probe Response due to Tolerance in Wire Diameters as a Function of Altitude for the NPS 12.4 +/- 1.0 $\mu$m Thermocouple Probe.

| ALT (km) | Min $\tau$ (ms) | Max $\tau$ (ms) | $\Delta\tau$ (ms) |
|---|---|---|---|
| 0 | 5.0 | 6.2 | 1.2 |
| 10 | 8.4 | 10.4 | 2.0 |
| 20 | 14.3 | 17.6 | 3.3 |
| 30 | 23.3 | 28.8 | 5.5 |

## D. PROBE RESPONSE SUMMARY

The tolerance in the diameter of the 12.4 $\mu$m Type "E" chromel-constantan thermocouple wire and junction bead make analytical predictions of its true response uncertain to approximately 11% (5.6 +/- 0.6 ms at 0 km). Additionally, the 3:1 ratio of the bead to wire diameter results in higher-order response effects. The 12.4 $\mu$m chromel-constantan probe used by NPS is four times faster than the 25$\mu$m copper-constantan probe used extensively in previous experiments due to its relative mass to surface area ratio.

The effect of the spherical weld junction on the thermocouple wire was to slow the response time by 30%. Correcting for a spherical junction bead allowed the 12.4 $\mu$m probe to achieve a modeled performance within 11% of experimental wind tunnel results. A probe with uniform diameter and a spherical bead, or no

bead, would allow for even more precise extrapolations of modeled response calculations. A faster probe response would improve the vertical layer resolution as well as permit more precise structure function measurements at smaller probe spacings. A probe that optimizes response by minimizing its wire diameter, weld bead diameter, density, and/or its specific heat capacity would achieve this result. A thermocouple made of the 10 $\mu$m wire currently manufactured by Isabellenheutte Heusler, Gmbh, in Germany should be 60% faster than the 12.4 $\mu$m chromel-constantan probes used by NPS, assuming a proportionately sized junction bead of $\sim$21 $\mu$m.

# V. CONCLUSIONS AND RECOMMENDATIONS

## A. CONCLUSIONS

This thesis investigated two systematic error effects in balloon thermosonde systems used by both NPS and the U.S. Air Force Geophysics Directorate. It supports the existence of an order of magnitude solar contamination of all thermal probe daytime data above the tropopause. This most probably arises from a combination of package motion (rotation or pendulum-like oscillations producing a low frequency signal), and differential solar heating of the probes due to probe wire oscillation. The high correlation, 91%, observed for the temperature differences in the nighttime flight and the low correlation obtained during all daytime flights, ranging from 50% to 82%, particularly near the tropopause, support the hypothesis that the apparent order of magnitude increase in optical turbulence is a solar induced instrument effect.

This thesis also investigated the thermal response time of the thermocouple used in the NPS differential thermosonde. The relatively large size of the thermocouple made it imperative to reconcile its modeled response as a function of altitude with controlled laboratory tests. The inconsistencies in the diameter of the 12.4 $\mu$m type "E" chromel-constantan thermocouple wire and its spherical junction bead limit predictions of its true response to a precision of 11%. Additionally, the 3:1 ratio of the bead to wire diameter results in higher-order

response effects. Based upon calculated changes in atmospheric heat conductivity the thermal response time for the 12.4 $\mu$m chromel-constantan probe should be approximately 9-10 ms at altitudes of 10 km and roughly 15-17 ms at 20 km.

The geometric characteristics of the wire and the junction bead that govern probe response can vary for each probe. Measuring the time constant for a probe in a wind tunnel experiment, and then using the same probe in a launch, would have the effect of calibrating that probe against the model.

## B. RECOMMENDATIONS

To eliminate solar effects apparent in the daytime launches due to rotation and oscillation of the sonde, it is necessary to stabilize the sonde as much as possible. The most reliable and consistent data will occur when the probes maintain a consistent alignment with respect to the sun. Possible solutions to this may include the use of a gyro mechanism to stabilize the platform, vertical baffles or fin stabilizers, solar cells to determine relative solar angle, and weights or anchors to hold the apparatus steady. To reduce the effects of probe wire vibration, the tungsten wire probes must be attached straight across the probe supports rather than in a flexible configuration. This will involve a delicate compromise to avoid thermal stress and strain on the wire and its contacts and yet suppress any vibration.

Comparison of results from taut wire probes with those from the GP-type loose wire thermocouple should help clarify the issue of probe vibration. Calibrating a set of probes in a wind tunnel experiment prior to a launch should improve consistency in thermosonde temperature measurements.

A faster probe would improve measurement precision of the NPS system in the stratosphere. A probe that optimizes response by minimizing its size, density, and/or its specific heat capacity would achieve this result. Using a 10 $\mu$m thermocouple probe wire, available in Germany, should reduce the response time by a factor of about 1.6. Additionally, ensuring that thermocouple wire junction beads are geometrically uniform would allow for more precise extrapolation of experimental data to stratospheric data. Regardless of the probes used, thorough consistency checks should be built into subsequent experiments. Thermocouple probes from the same lot should be measured for wire diameter and both bead size and shape under a calibrated SEM. These same probes should then be tested for response in a wind tunnel experiment, varying the laser to illuminate both the wires and the junction beads. Finally, these probes should be launched in a thermosonde package that has redundant means of measurement at equal distances to establish an in-flight empirical database with which to resolve atmospheric structure functions.

## APPENDIX A

## DIURNAL VARIATION EXPERIMENT 2 DATA

Additional data from DVE 2 are shown below. The data contained in this appendix were used in the statistical summary shown in Table II and do not exhibit any atypical behavior. Figures 28 thru 33 show the results of the 4, 5, and 6 December 1990 flights. Figures 34 thru 37 show the averaged $C_n^2$ profiles for the 7 and 8 December flights.

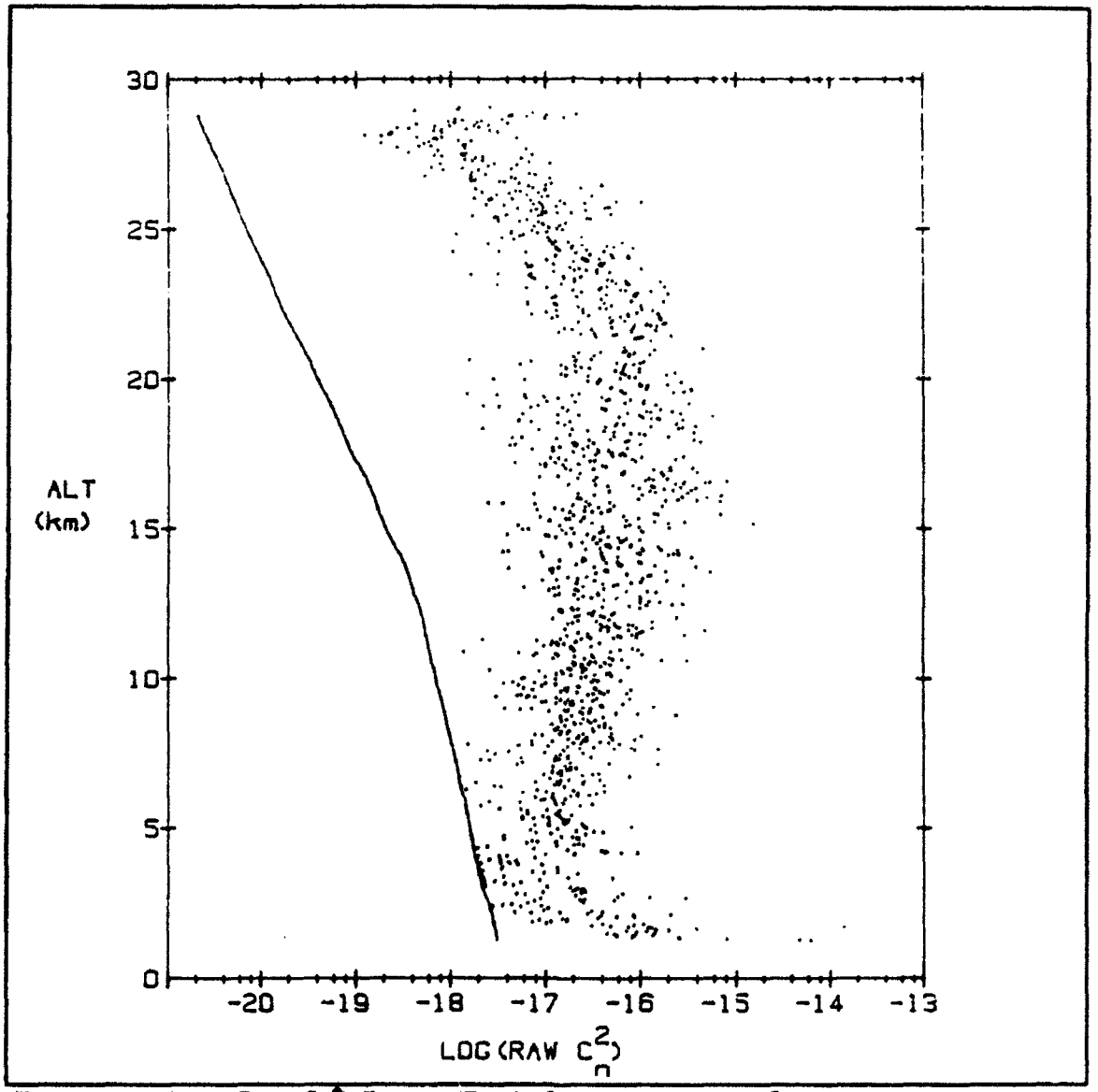


**Figure 28.** Log (Raw $C_n^2$) Profile (Day), Collected by the Geophysics Directorate, from 1.2 to 30 km, Holloman Air Force Base, NM, 4 December 1990 (Probe Set 1).

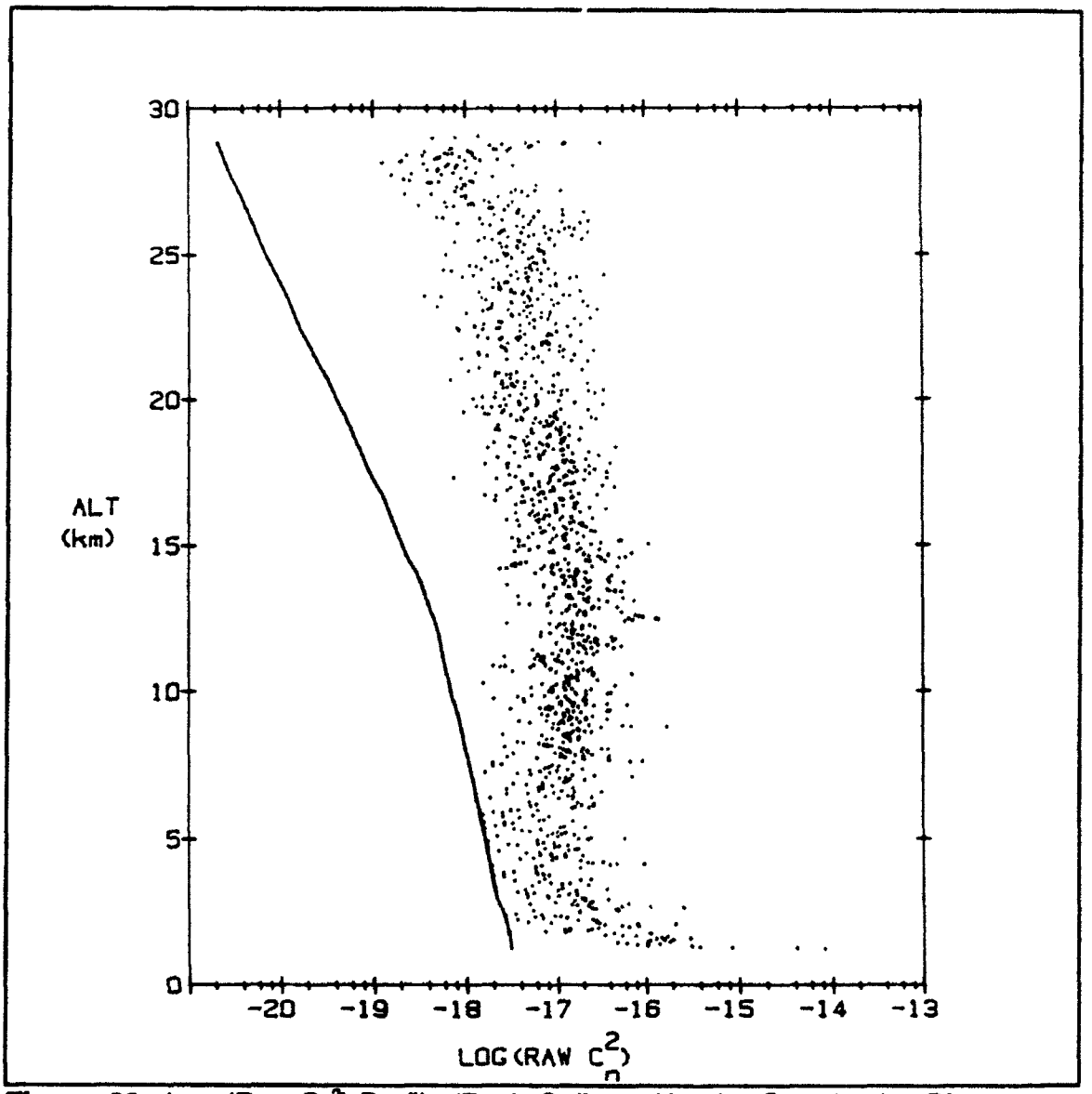


**Figure 29**. Log (Raw $C_n^2$) Profile (Day), Collected by the Geophysics Directorate, from 1.2 to 30 km, Holloman Air Force Base, NM, 4 December 1990 (Probe Set 2).

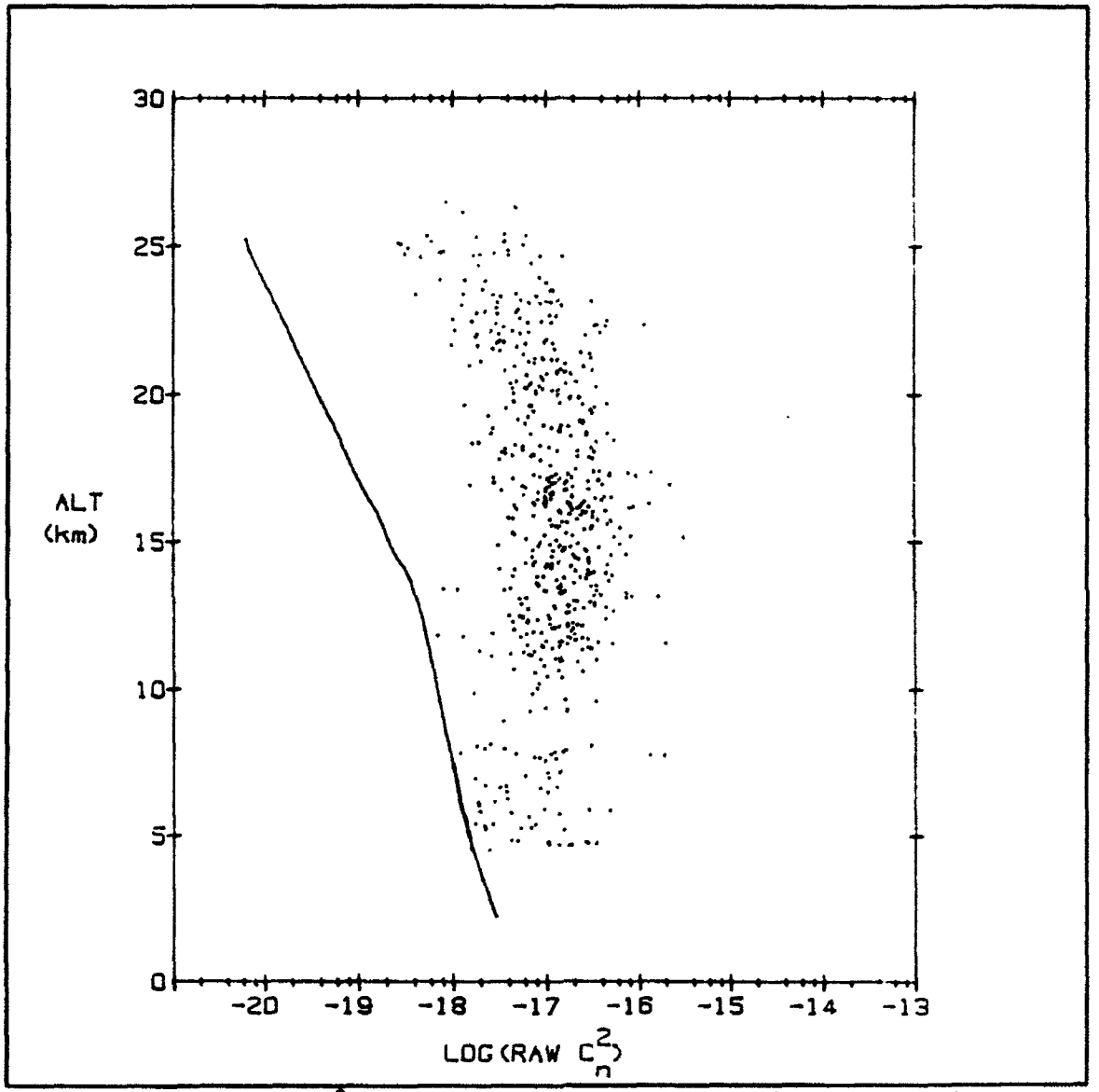


**Figure 30.** Log (Raw $C_n^2$) Profile (Day), Collected by the Geophysics Directorate, from 1.2 to 30 km, Holloman Air Force Base, NM, 5 December 1990 (Probe Set 1).

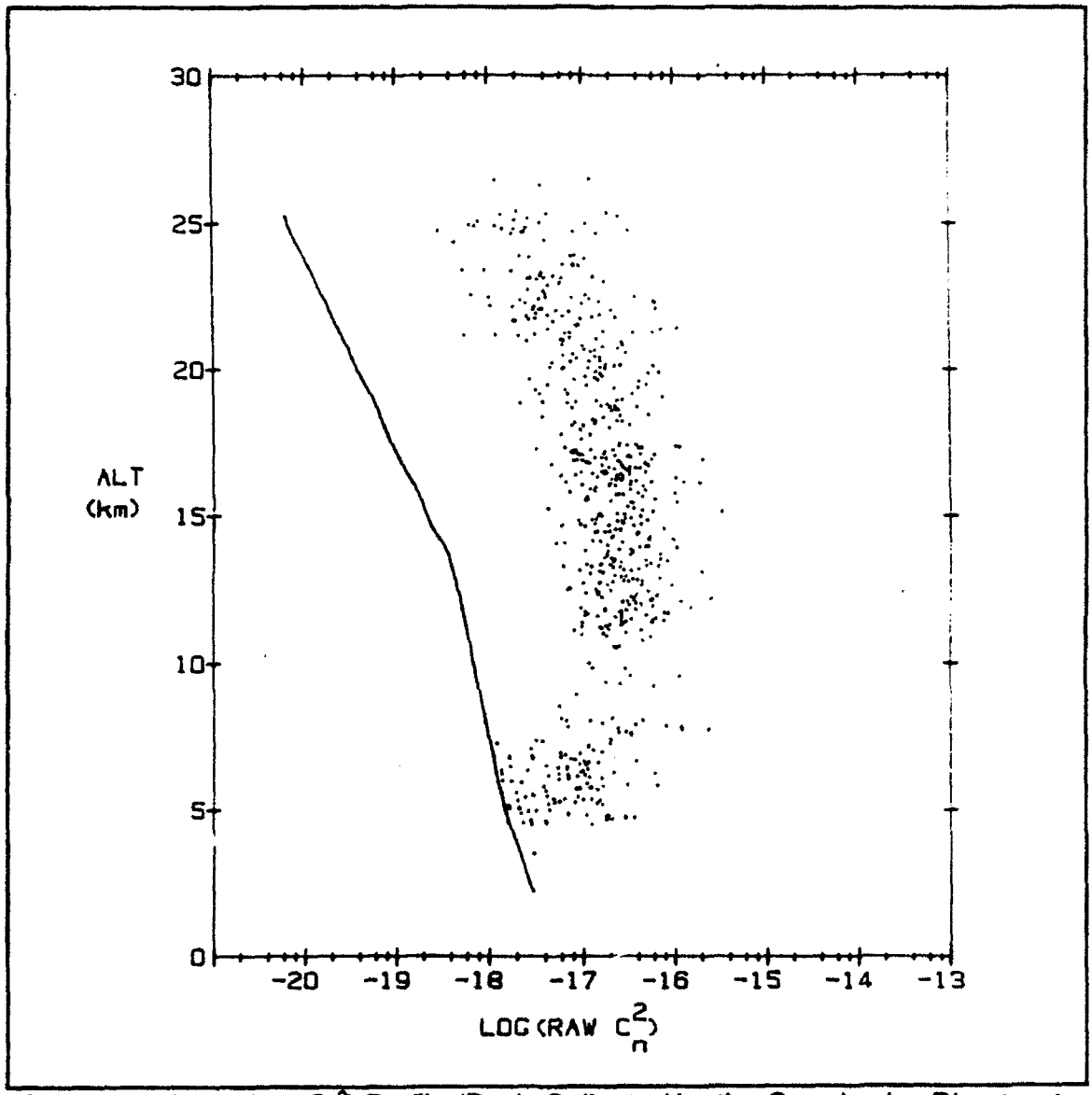


**Figure 31.** Log (Raw $C_n^2$) Profile (Day), Collected by the Geophysics Directorate, from 1.2 to 30 km, Holloman Air Force Base, NM, 5 December 1990 (Probe Set 2).

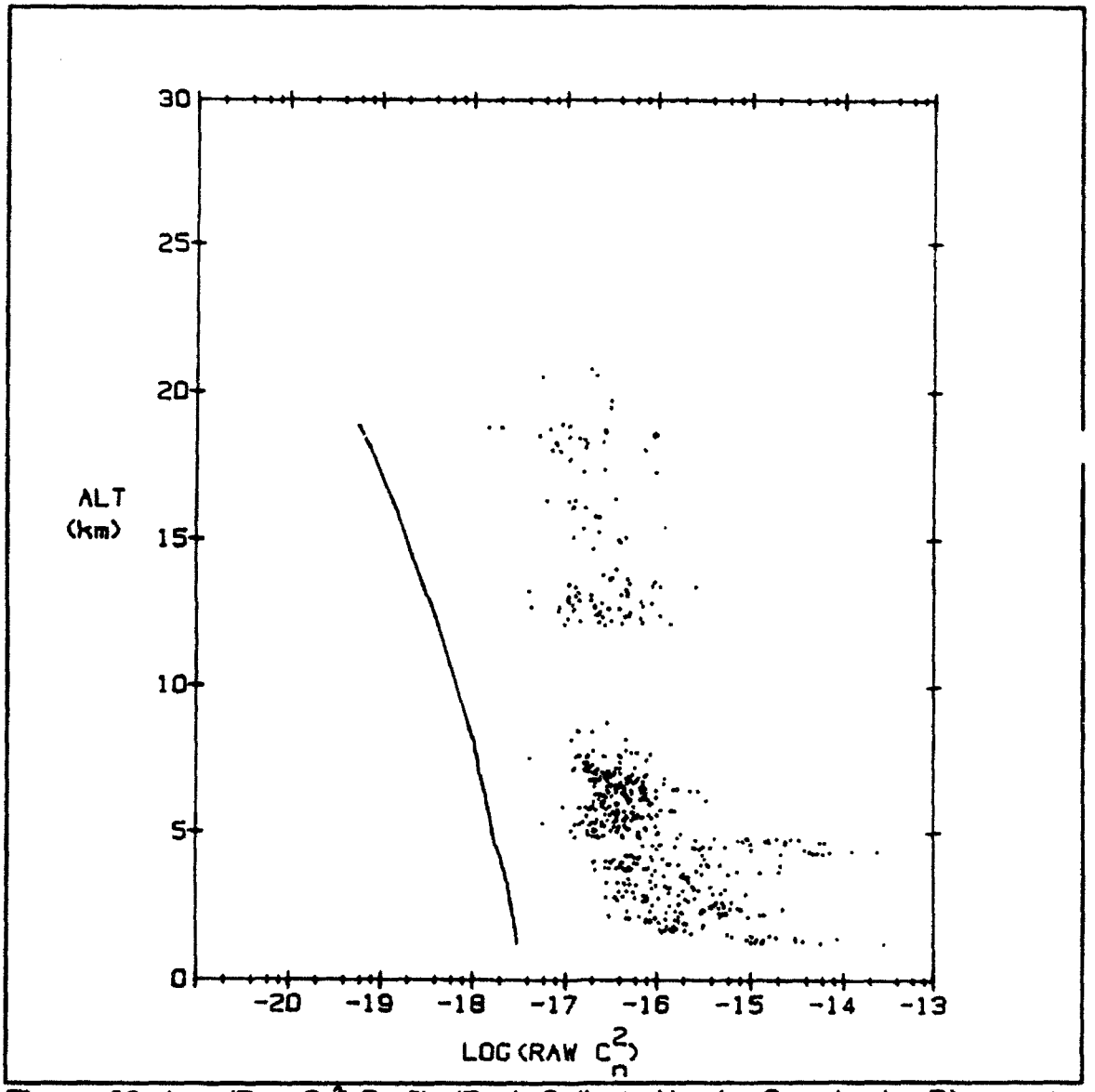


**Figure 32.** Log (Raw $C_n^2$) Profile (Day), Collected by the Geophysics Directorate, from 1.2 to 30 km, Holloman Air Force Base, NM, 6 December 1990 (Probe Set 1).

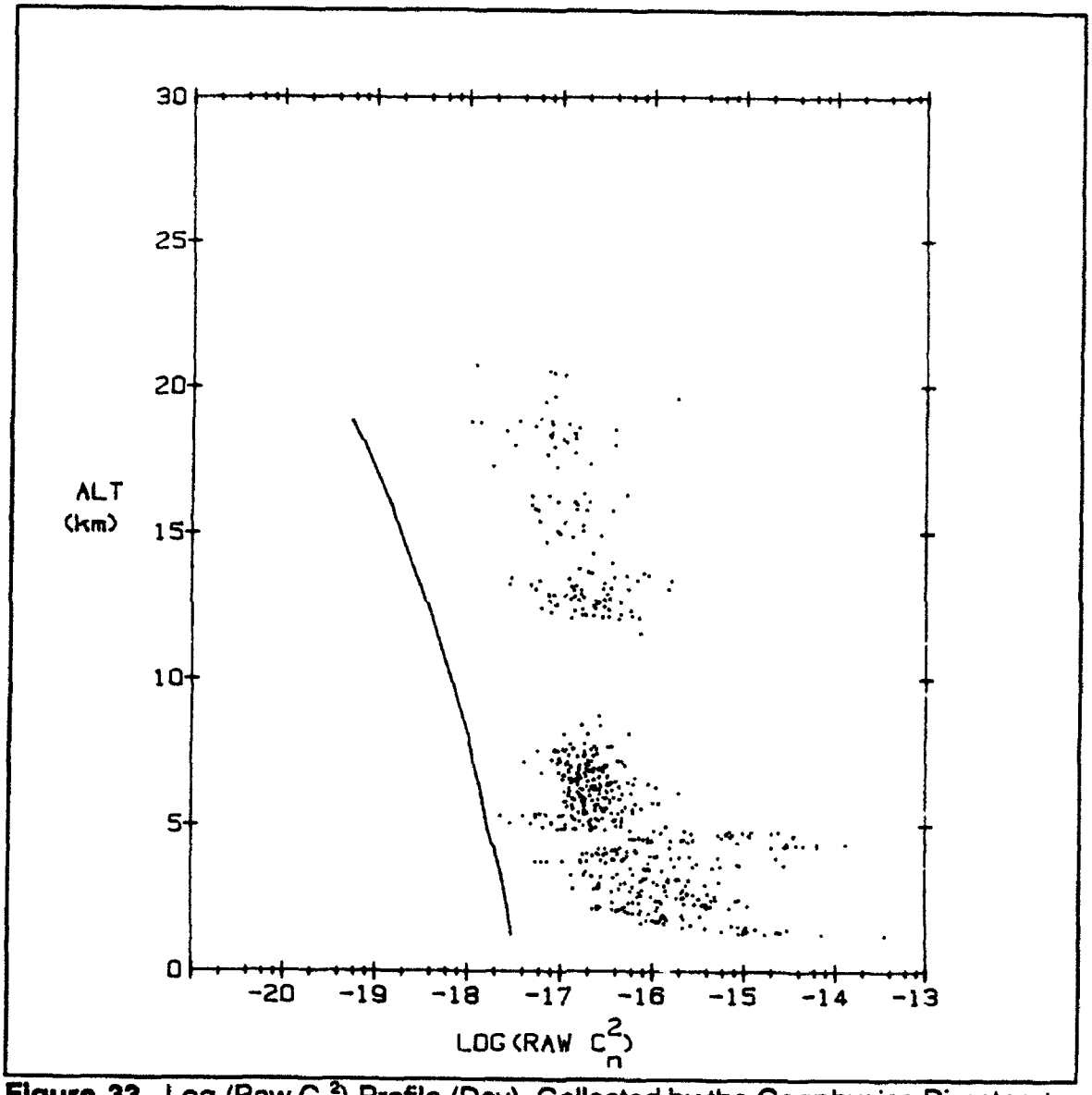


**Figure 33**. Log (Raw $C_n^2$) Profile (Day), Collected by the Geophysics Directorate, from 1.2 to 30 km, Holloman Air Force Base, NM, 6 December 1990 (Probe Set 2).

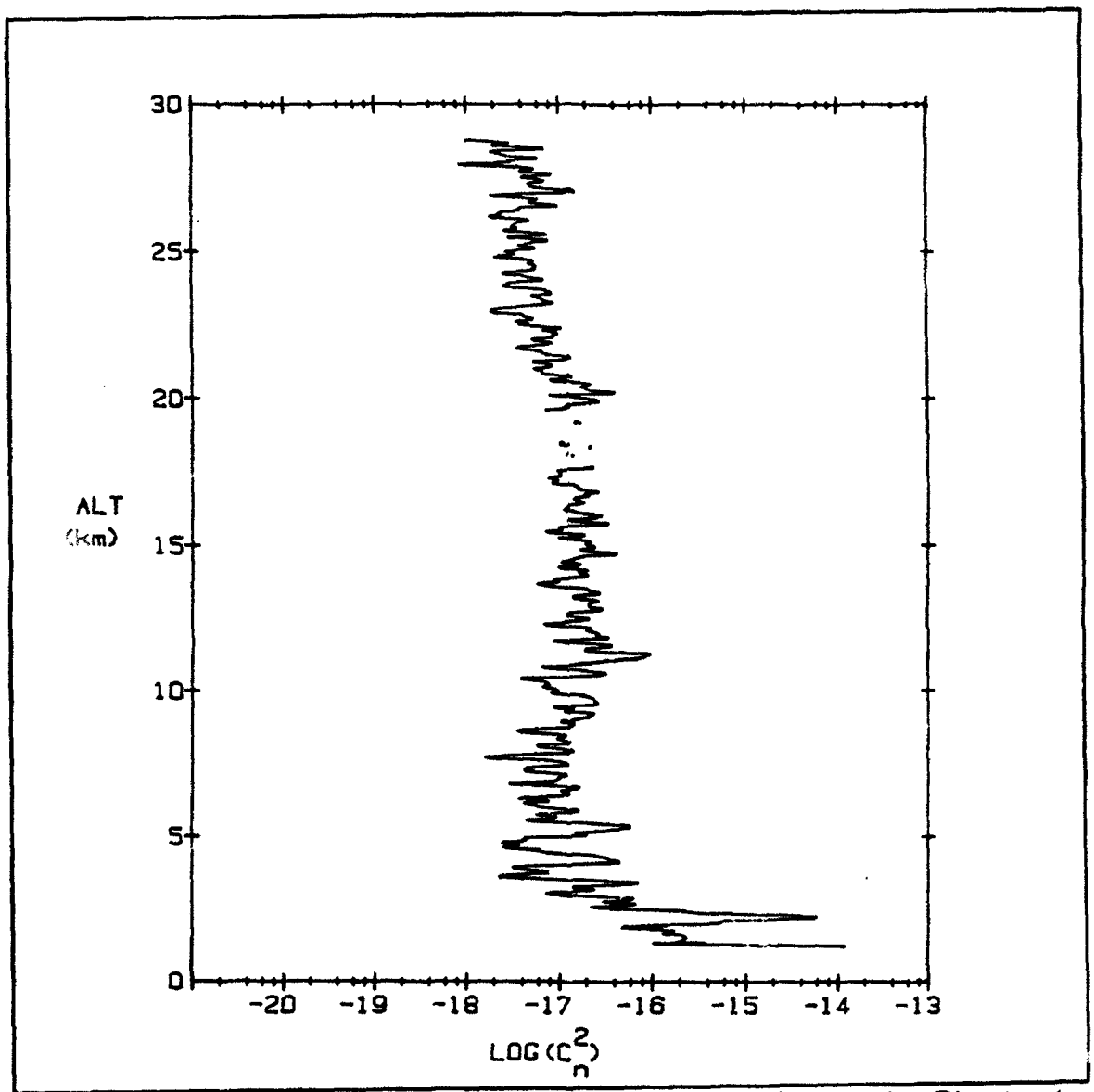


**Figure 34.** Averaged $C_n^2$ Profile (Day), Collected by the Geophysics Directorate, from 1.2 to 30 km, Holloman Air Force Base, NM, 7 December 1990 (Probe Set 1).

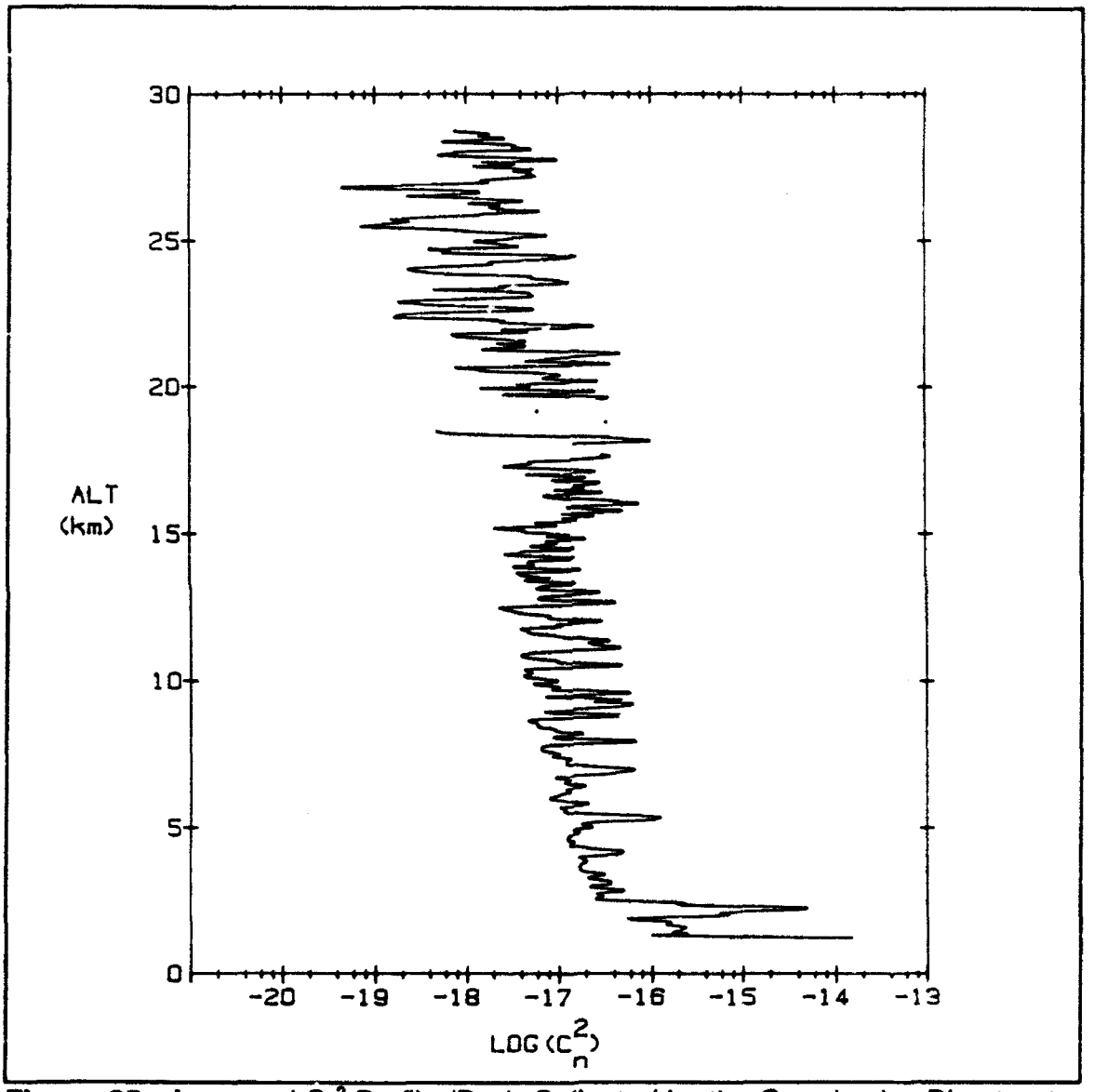


**Figure 35.** Averaged $C_n^2$ Profile (Day), Collected by the Geophysics Directorate, from 1.2 to 30 km, Holloman Air Force Base, NM, 7 December 1990 (Probe Set 2).

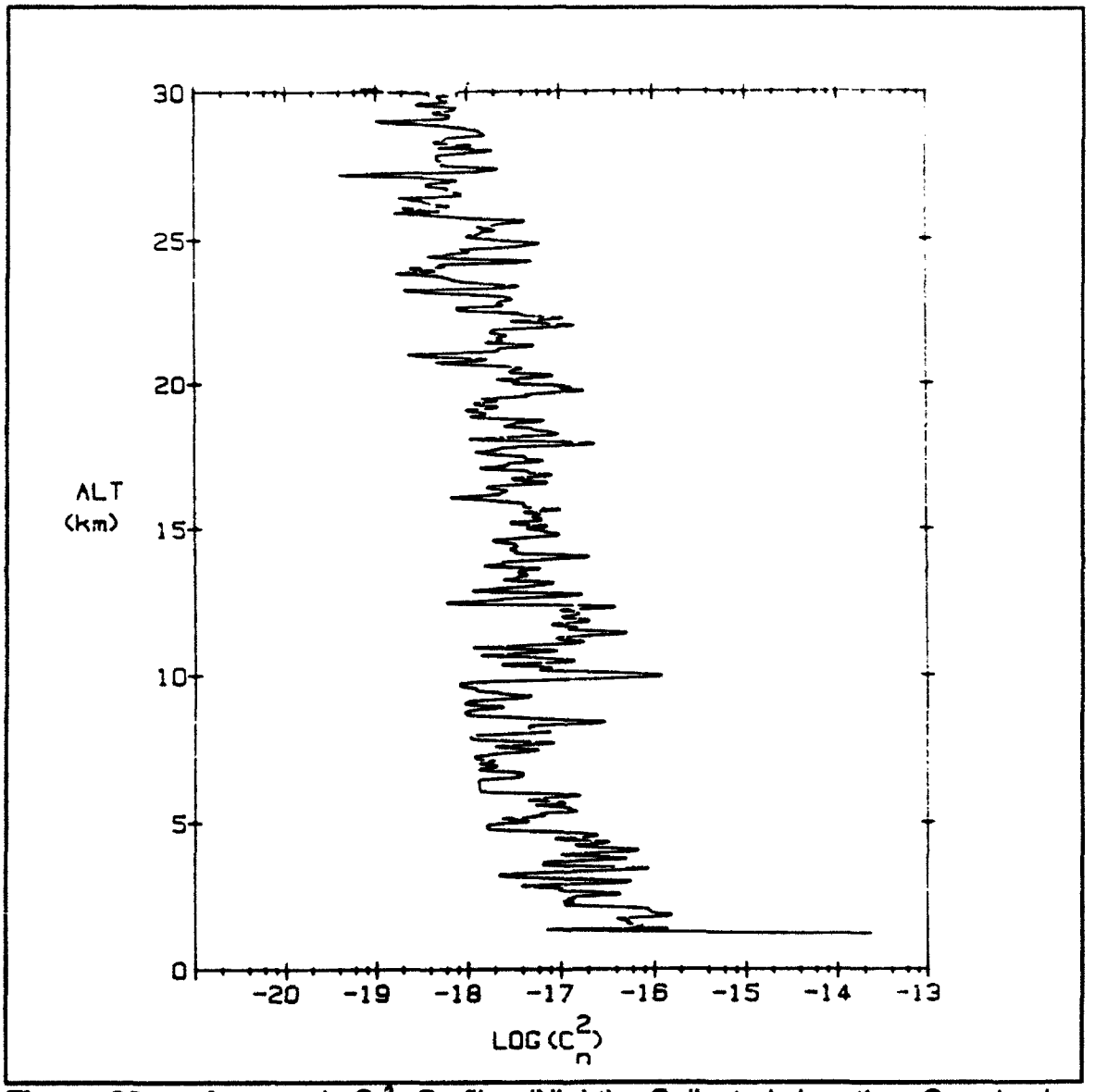


**Figure 36.** Averaged $C_n^2$ Profile (Night), Collected by the Geophysics Directorate, from 1.2 to 30 km, Holloman Air Force Base, NM, 8 December 1990 (Probe Set 1).

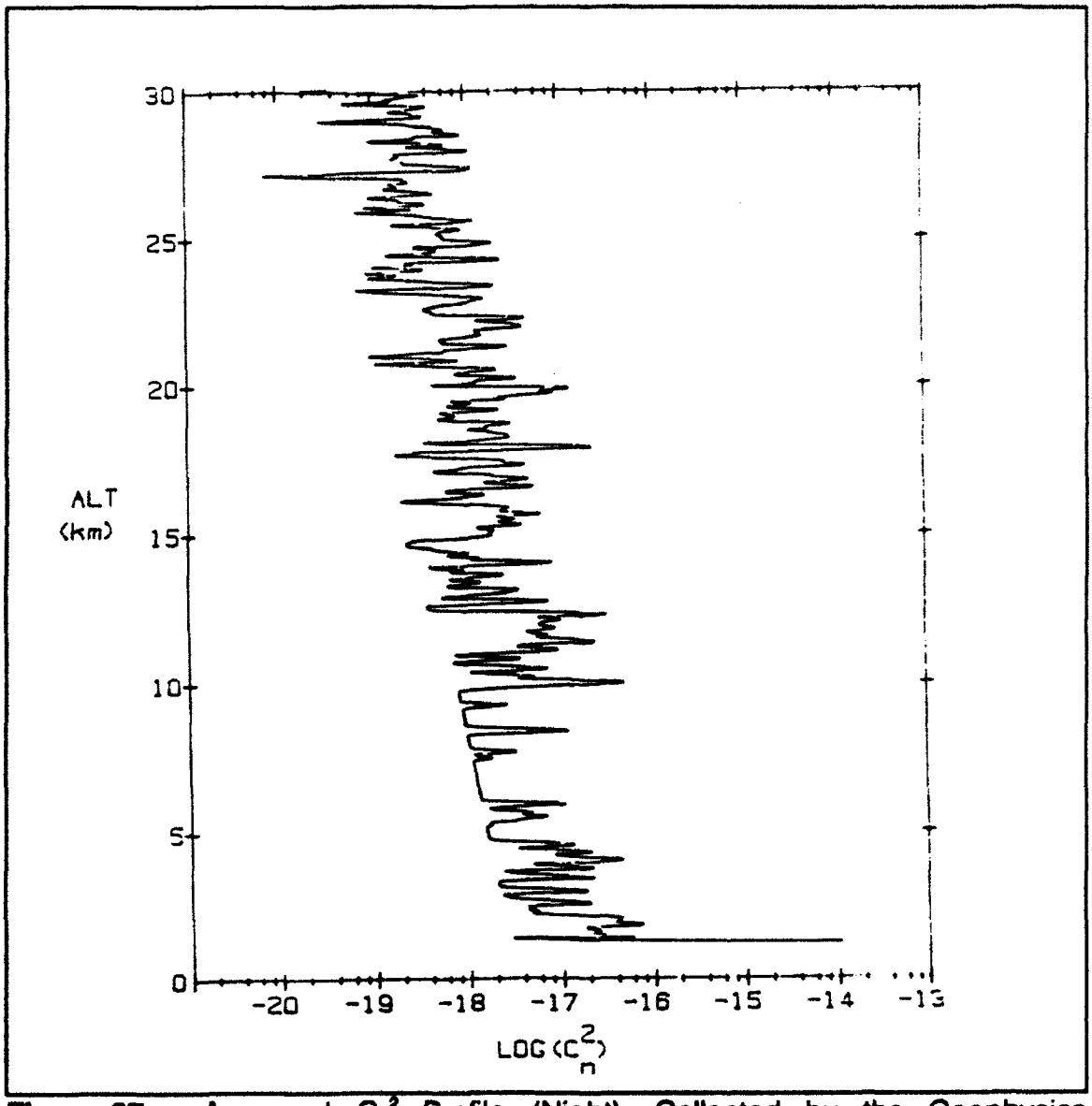


**Figure 37.** Averaged $C_n^2$ Profile (Night), Collected by the Geophysics Directorate, from 1.2 to 30 km, Holloman Air Force Base, NM, 8 December 1990 (Probe Set 2).

## APPENDIX B

## THERMOCOUPLE PROPERTIES

Table XIII shows the specific heat capacities of the materials that comprise the type E chromel-constantan probes [Ref. 18:p. 12-107]. Chromel-Constantan is 75% chromel and 25% constantan. Chromel is 90% nickel and 10% chromium. Constantan is 57% copper and 43% nickel [Ref. 27:p. 133]. Applying these percentages to the specific heat capacities in Table XIII results in a specific heat capacity of C=0.4367 (J/g·K) for the chromel-constantan thermocouple probe.

**TABLE XIII.** Type E Chromel-Constantan Thermocouple Material Specific Heat Capacity, C.

| | Nickel (Ni) C=0.106 | Chromium (Cr) C=0.110 | Copper (Cu) C=0.092 |
|---|---|---|---|
| Chromel | 90% | 10% | |
| Constantan | 43% | | 57% |

Specific heat capacity, C, is in (J/g·K).

## APPENDIX C

## WIND TUNNEL PROBE RESPONSE EXPERIMENT

Table XIV contains the wind tunnel measurements on the 12.4 $\mu$m probe.

**TABLE XIV.** Wind Tunnel Probe Response Measurements vs. Windspeed, 12.4 $\mu$m Chromel-Constantan Probe, 8 November 1992.

| V (m/s) | Measured $\tau$ (ms) | SQRT of V | $1/\tau$ |
|---|---|---|---|
| 0 | 15.7 | 0 | 0.06 |
| 1.5 | 7.1 | 1.22 | 0.14 |
| 3.0 | 6.4 | 1.73 | 0.16 |
| 4.4 | 5.6 | 2.1 | 0.18 |

Regression analysis on this data yielded values of a = 0.066 and b = 0.054 for the constants used in Eq. (24).

Figure 38 plots the response of a 25 $\mu$m copper-constantan probe in the wind tunnel in which the time constant was measured to be $\tau$ = 19.5 +/- 1.0 ms.

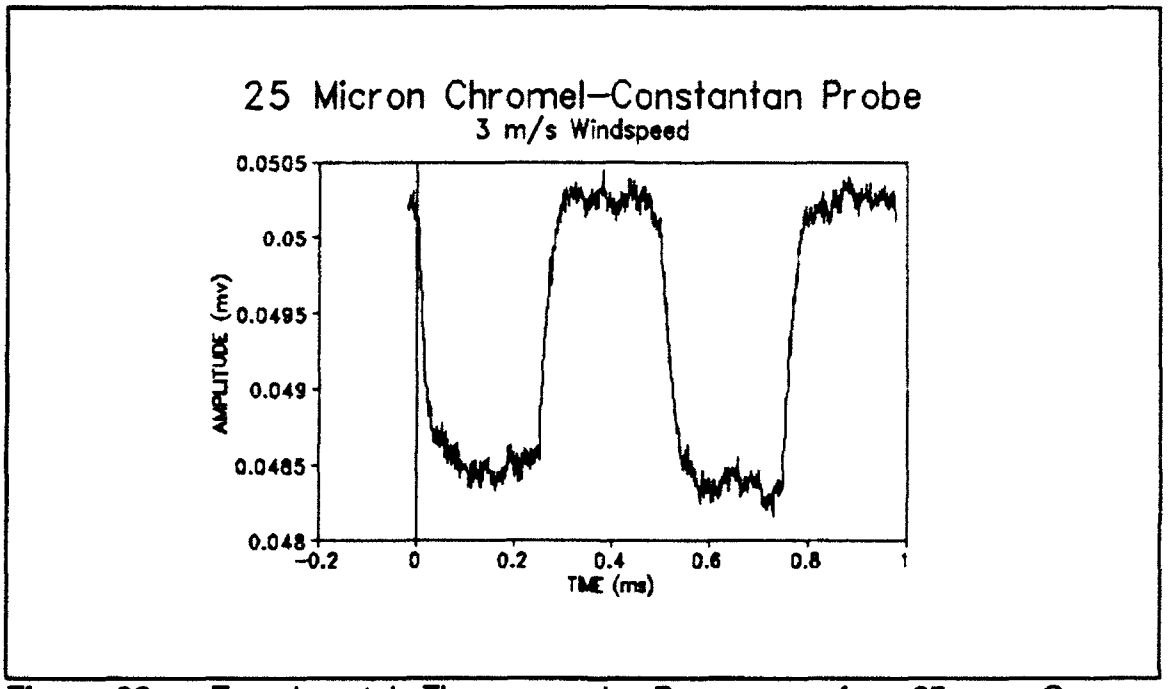


**Figure 38.** Experimental Thermocouple Response of a 25 $\mu$m Copper-Constantan Probe Illuminated by a Periodic Laser Diode Measured in a Wind Tunnel at v = 4.4 m/s in the NPS Wind Tunnel Experiment of 8 November 1992.

Table XV contains the instrument settings for each item of equipment used in the wind tunnel probe response experiment.

**TABLE XV**. Wind Tunnel Experiment Instrument Settings.

| NICOLET PRO 30 DIGITAL OSCILLOSCOPE | HP3314A FUNCTION GENERATOR | HP6236B POWER SUPPLY | LASER DIODE |
|---|---|---|---|
| switch time: 500 $\mu$sec | 2.02 hz | 0-24 V | ~ 15 cm from probe |
| 500 sweeps | 4.26 V Ampl. | | |
| 120 mv | 2.02 V Offset | | |

## LIST OF REFERENCES


1. Hufnagel, R.E., "Propagation Through Atmospheric Turbulence," in The Infrared Handbook, The Infrared Information Analysis Center, Environmental Research Institute of Michigan, 1989.

2. Brown, J.H. and others, Study of Possible Solar Heating Effects-Error Analysis, GL-TR-89-0178, Geophysics Laboratory, Hanscom Air Force Base, Massachusetts, July 1989.

3. Weitekamp, M. R., Investigation of the Source of Thermosonde Measured DiurnalVariation of Optical Turbulence, M.S. Thesis, Naval Postgraduate School, Monterey, California, December 1990.

4. Gast, V.J., Characterization of Atmospheric Turbulence For High Resolution Imaging and Laser Propagation , M.S. Thesis, Naval Postgraduate School, Monterey, California, December 1992.

5. Wilson, J. and Hawkes, J.F.B., Optoelectronics, An Introduction, Prentice Hall, 1989.

6. Krieth, Principles of Heat Transfer, International Textbook Company, 1968.

7. White, F.M., Fluid Mechanics, New York, McGraw Hill, 1979.

8. Tatarski, V.I., Wave Propagation in a Turbulent Medium, McGraw Hill, 1961.

9. Walters, D. L. and Kunkel, K. E., "Atmospheric Modulation Transfer Function For Desert and Mountain Locations: the Atmospheric Effects on $r_0$", Journal of the Optical Society of America, Volume 71, No. 4, April 1981.

10. Ochs, G.R. and others, "Laser-Beam Scintillation over Horizontal Paths from 5.5 to 145 Kilometers," in Journal of the Optical Society of America, Vol. 59, No. 2, February 1969.

11. Bauer, E., Atmospheric Effects on Airborne Lasers (ABL) for Tactical Missile Defense (TMD): Clouds and Turbulence Draft Report, IDA Log No.HQ 91-40634/1, Institute for Defense Analyses, Alexandria, Virginia, December 1991.

12. Brown, J.H. and others, Sonde Experiments for Comparative Measurements of Optical Turbulence, AFGL-TR-82-0079, ADA 118740, 24 February 1982.

13. Hummel, J.R. and Shettle, E.P., Effects of Solar Heating by Aerosols and Trace Gases on the Temperature Structure Constant, Scientific Report LTR90-009 written by Sparta, Inc. for Geophysics Laboratory, Hanscom AFB, Massachusetts (Report GL-TR-90-0349), 9 August 1990.

14. Beland, R., Experiment Plan for DVE2 (Diurnal Variation Experiment 2), internal Geophysics Laboratory memorandum, 23 November 1990.

15. Kiefer, D.A., Development of a Single Point Temperature Probe to Measure the Temperature Structure Parameter, M.S. Thesis, Naval Postgraduate School, Monterey, California, June 1990.

16. Holman, J.P., Heat Transfer, McGraw Hill Book Company, New York, 1990.

17. CRC Handbook of Chemistry and Physics, ed. Lide, David R., 71st Ed., 1991.

18. OMEGA Complete Temperature Measurement Handbook and Encyclopedia, vol.26, Omega Engineering, Stamford, Connecticut, 1988.

19. Handbook of Geophysics and the Space Environment, ed. A.S. Jursa, Air Force Geophysics Laboratory, 1985.

20. Telephone conversation between John S. Daley, of Omega Engineering, Inc., Quotations Engineering Department, and the author, 3 December 1992.

21. Kothandaraman, C.P. and Subramanyan, S., Heat and Mass Transfer Data Book, Halsted Press, New York, 1975.

22. Lunardini, V.J., Heat Transfer in Cold Climates, Van Nostrand Reinhold Company, New York, 1981.

23. Kacak, S. and others, Handbook of Single-Phase Convective Heat Transfer, John Wiley and Sons, New York, 1987.

24. Moffat, R.J., "Gas Temperature Measurement," in Temperature-Its Measurement and Control in Science and Industry, Vol. 3, Part 2, Rheinhold Publishing Company, New York, 1962.

25. StereoScan 200, TL2025-OM, Issue 3, April 85, Cambridge, England.

26. Hoover, C.R., Investigations of a Single Point Temperature Probe for Measurement of Atmospheric Turbulence, M.S. Thesis, Naval Postgraduate School, Monterey, California, December 1991.

27. Kinzie, P.A., Thermocouple Temperature Measurement, New York, John Wiley and Sons, 1973.

## INITIAL DISTRIBUTION LIST

| | | |
|---|---|---|
| 1. | Defense Technical Information Center<br>Cameron Station<br>Alexandria, VA 22304-6145 | 2 |
| 2. | Library, Code 52<br>Naval Postgraduate School<br>Monterey, CA 93943-5002 | 2 |
| 3. | Professor Karlheinz E. Woehler<br>Chairman, Department of Physics<br>Naval Postgraduate School (Code PHWh)<br>Monterey, CA 93943 | 1 |
| 4. | Professor Donald L. Walters<br>Naval Postgraduate School (Code PHWe)<br>Monterey, CA 93943 | 6 |
| 5. | U.S. Air Force Geophysics Directorate<br>Phillips Lab (GPOA)<br>ATTN: Bob Beland<br>Hanscom AFB, MA 01731-5000 | 2 |
| 6. | DCSOPS<br>Space and Special Weapons Directorate<br>ATTN: DAMO-SWS (CPT Roper)<br>Room 2C534, The Pentagon<br>Washington, DC 20310 | 2 |